DEVELOPMENT OF CELL CULTURE PLATFORMS BY ENZYMATIC FUNCTIONALIZATION OF REDOX-RESPONSIVE HYDROGELS

ワヒユ, ラマダン

DEVELOPMENT OF CELL CULTURE PLATFORMS BY ENZYMATIC FUNCTIONALIZATION OF REDOX-RESPONSIVE HYDROGELS

Wahyu Ramadhan

Department of Chemical Systems & Engineering
Faculty of Engineering
Kyushu University
2020

TABLE OF CONTENTS

CHAPTER 1 GENERAL INTRODUCTION

1.1 Hydrogel scaffold and the polymer choice

Untangling complex biological systems is still a major challenge for scientists despite over a hundred years of modern researches[1]. Mimicking a specific convoluted system is one of the best approaches to understand and valorize it for research purposes and applications benefitting a variety forms of life[2,3]. In recent years, bottom-up approaches including cellular scaffolding have been studied in tissue engineering, which could be the best path forward to initially mimicking the complexity of cellular environment. A rise in demand of this technology to treat chronic diseases is expected to drive a research, impelling the market growth through to 2027. Grand View Research Inc. has reported a perceived tendency of cell culture market in 2027. The world cell culture market value is forecasted to attain USD 3.2 billion, broadens at a compound annual growth rate of 11.3%[4].

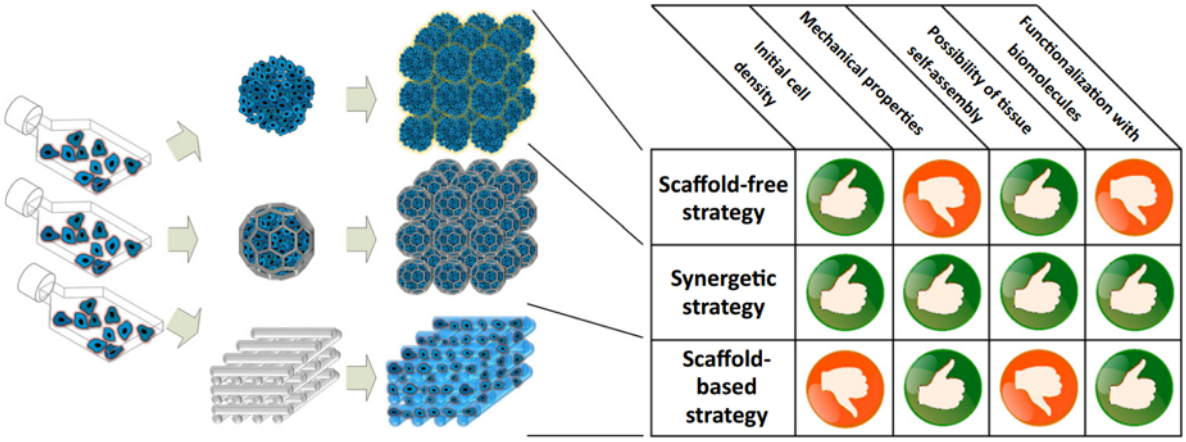

Fig. 1.1 Summary of different technological cell culture technology approaches. Reproduce by permission from ref[5] Copyright 2018 Elsevier.

Over the last decade, a variety of cell culture platforms have been developed to achieve versatile cell culture system as a research model, especially for the preclinical drug discovery and the development of tissue engineering itself. The cell culture technology was initiated by two-dimensional (2D) monolayer cell culture under

adherent conditions. At the same time, three-dimensional (3D) cell culture systems have been designed to sufficiently mimicking the physiological conditions of natural structures of the tissue. Current approaches in 3D cell culture platform are mainly represented by two strategies, scaffold-free and scaffold-based platform, where each having their advantages and posing intrinsic limitations (Fig 1.1). By integrating the lack of each system, it is desirable to constructively generate a smart scaffold while covering their drawbacks.

Today, one of promising smart scaffolds for cell culture is hydrogel, known as potential bio-based polymeric materials with dynamic chemical, physical, and structural properties[6,7]. Hydrogels have extensively studied by many researchers and recognized as the most popular scaffold in the past 30 years. The search for the words “hydrogel” and “hydrogel-cell culture” in the PubMed and Scopus database shows a significantly increase in the number of the issued articles (Fig 1.2).

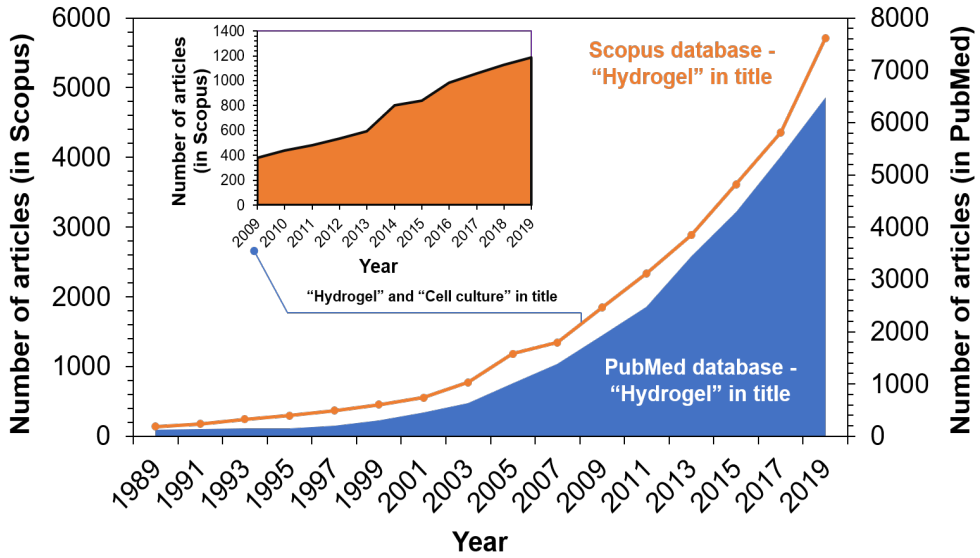

Fig. 1.2 The growing trend in published articles identified during the past 30 years with the keyword “hydrogel” and “hydrogel-cell culture” for the past 10 years.

Due to their unique three-dimensional (3D) hydrophilic network that is cross-linked and swollen, hydrogels serve as a wet environment or provide fluid to recapitulate and mimic the natural extracellular matrix (ECM) or many tissues in the body[8–10]. Therefore,

either hard or soft networks of hydrogels have shown an important class to have good compatibility. Hydrogels have been designed to create specific properties of biomaterial scaffolds for embedding bioactive molecules and other biological entities, particularly as a cell culture platform (Fig. 1.3).

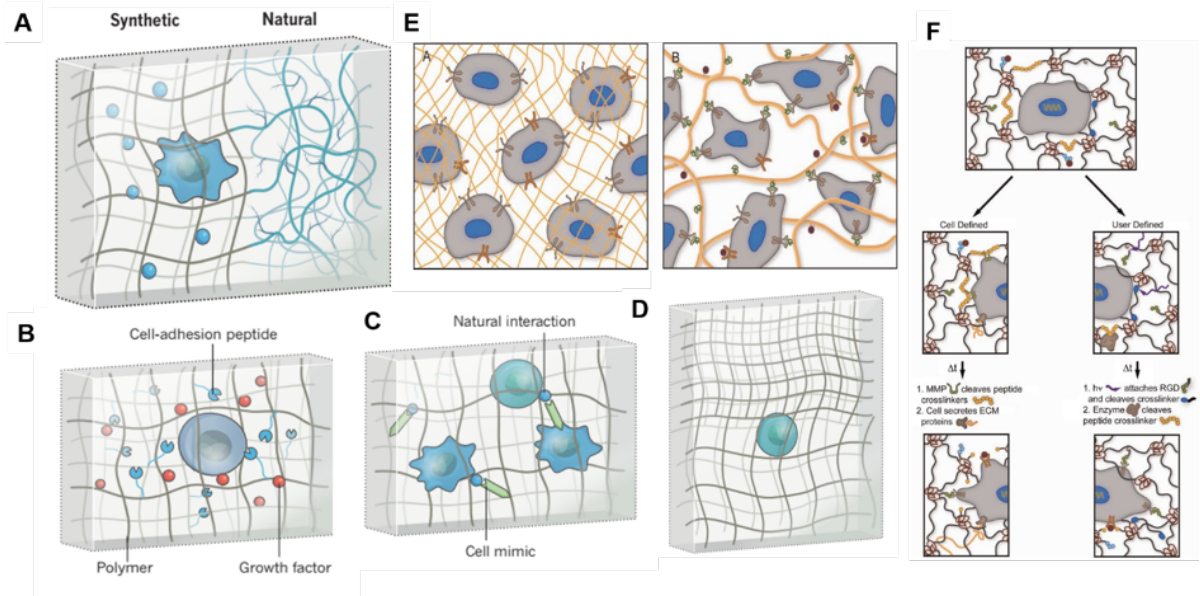

Fig. 1.3 Representation of the general strategies of hydrogel as a cell-laden scaffold. A. Synthetic polymer create and develop the environments that mimic tissues or natural structure. B. Hydrogel matrix able to alter with protein (such as cell adhesion peptide or growth factors) which is mimic properties of the ECM. C. Cells are live in communities, so the chemotaxis can be modified by attaching biochemical entities to a hydrogel that can mimic the natural interaction. D. The mechanical properties of hydrogel can be modified by controlling the cross-linking density and the ligand. E. Synthetic hydrogel (left; orange matrix) provide a 3D environment for cell culture scaffold but with a lack of activated integrins and receptors of cell (brown). Besides, hydrogel composed natural polymer (right) serve the growth factors (orange) and integrin sites (green) that can bind with the cell surface receptors. **F.** Engineered synthetic hydrogel that integrated and modified well-deveined natural compounds and chemical moieties. Fig. A-D are reproduced by permission from ref[6]. Copyright 2016 Springer Nature. Fig. E-F are reproduced by permission from ref[11]. Copyright 2009 John Wiley & Sons, Inc.

In the initial report of hydrogels, the scaffold was employed to encapsulate cells by natural polymers, such as fibrin, elastin, collagen, hyaluronic acid, gelatin, and other proteinaceous based polymer[12–15], namely natural hydrogel. Generally, natural hydrogel (biopolymer) can be categorized by constituents such as polysaccharide, protein, protein/polysaccharide hybrid polymers, DNA and decellularized matrices[16–18]. Several key class of natural hydrogel and their properties are described in Table 1.

Table 1. Key classes of natural compounds used as the main polymer of hydrogel fabrication, and their main advantages and drawback properties in the cell culturing.

Polymer	Class	Advantages	Disadvantages
Alginate	Polysaccharides	- Reactive handles for functionalization - Rapid gelation with divalent cations - Ease of use for 3D printing - Abundant	- Poorly adhesive - Cation leaching leads to dissolution - Non-biodegradable
Chitosan	Polysaccharides	- Adhesive and antimicrobial - Low immunogenicity - Abundant	- Poor solubility at neutral pH
HA	Polysaccharides	- Bioactive and biocompatible - Binds growth factors and cytokines - Reactive handles for functionalization	- Rapidly degraded in vivo - Low stability without cross-linking
Chondroitin Sulfate	Polysaccharides	- Bioactive and biocompatible - Binds growth factors and cytokines - Reactive handles for functionalization	- Low stability without cross-linking - Rapidly degraded in vivo
Collagen	Proteinaceous	- Adhesive and bioactive - Mimics native ECM - Abundant and biodegradable	- Contamination can lead to immunogenicity - Mechanical stability lost during processing - Assembly sensitive to modification
Gelatin	Proteinaceous	- Adhesive and bioactive - Tolerant of functionalization - Abundant and biodegradable	- Mechanically weak - Requires cross-linking - Contamination can lead to immunogenicity
Silk	Proteinaceous	- High mechanical strength and elasticity - Low immunogenicity - Adhesive	- Slow gelation
ELPs	Proteinaceous	- Tunable structure and sequence - Thermoresponsive (LCST) - Recombinant expression	- Low stability without cross-linking

As shown in Table 1, although the studies of natural hydrogels have been established early success in cell and tissue culture, the mechanical properties, gelation time, and degradation rate were difficult to control. Moreover, natural compounds have diverse contents, and batch-to-batch variability in compositions and biochemical properties lead to significant uncertainty in cellular experiments[20]. For these reasons, in recent years, synthetic materials possessing more tunable and well-

defined structures have been explored to create hydrogels for cell and tissue culture[7,21]. Synthetic polymers also show high gel strength, high capacity of water absorption, long shelf life and generally simpler well-defined structures than that of natural polymers, the introduction of cross-linking substrates is thus controllable. Eventually, synthetic polymers possessing in hydrogels fabrication can be exploited to generate the adjustable design especially in their degradation and functionalization properties for the advanced cell/tissue culture applications[19].

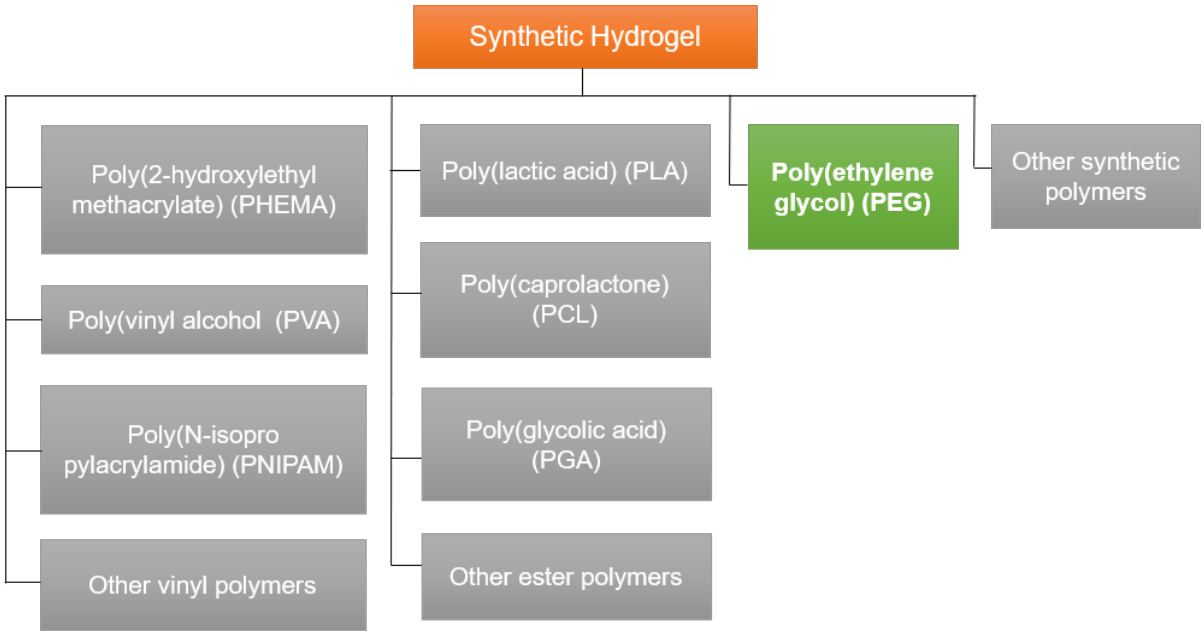

Fig. 1.4 Commonly used synthetic polymer as the hydrogel precursor for cell culture application.

In the class of synthetic material examined thus far[22–25], many polymers have been used as hydrogel precursors that can be classified by chemical entities such as polyvinyl, polyester, poly(ethylene oxide) and other synthetic polymer (Fig 1.4). One promising hydrogel's backbone is polyethylene glycol (PEG)[26,27]. PEG is the most commonly investigated polymer used to make synthetic hydrogels as an FDA-approved material. Its chemical and biological inertness, highly hydrophilic nature, controllable and homogenous microstructure as well as a wide range of polymer

architectures are attainable by synthetic chemistry[28,29]. Moreover, along with the ease of derivatization in which end-functionalization of PEG enable the inclusion of various chemical cues that can be applied for efficiently crosslinking reaction[19].

1.2 Methods of synthesis of hydrogels

Hydrogels are mostly constructed by the crosslinking reaction of polymeric matrix. Currently, the most attractive way to manipulate the shape, activity, and biocompatibility of a synthetic hydrogel is by altering the cross-linking site, either by physical or chemical means[30] (Fig .1.5). Physically cross-linked hydrogels are formed by weak and reversible intermolecular interactions, such as ionic cross-linking, hydrogen bonds, hydrophobic interactions of thermal inclusion mediated on upper Critical Solution Temperature (UCST)/Lower Critical Solution Temperature (LCST), and ultrasonication assisted formation of sol-to-gel phase transition[31,32]. The most important advantage of this system is its low cytotoxicity because of the absence of a chemical reaction. However, physical hydrogels have limited mechanical properties owing to the weak interaction involved in their cross-linking points.

On the contrary, chemical cross-linking is attained by covalent bond formation such as click chemistry[33], free-radical photopolymerization[34] and enzyme-mediated cross-linking[35]. The chemical crosslinking strategy serves higher stability and mechanical properties than that of the physical crosslinking methods; consequently, chemical hydrogels are more advisable for long-term cell culture and tissue engineering applications. However, from the viewpoint of cytocompatibility, there are a couple of shortcomings, including photoinitiators and irradiation used in photopolymerization, which are potentially detrimental to cell survival, causing tissue damage[36] and deactivating the incorporated proteins[37].

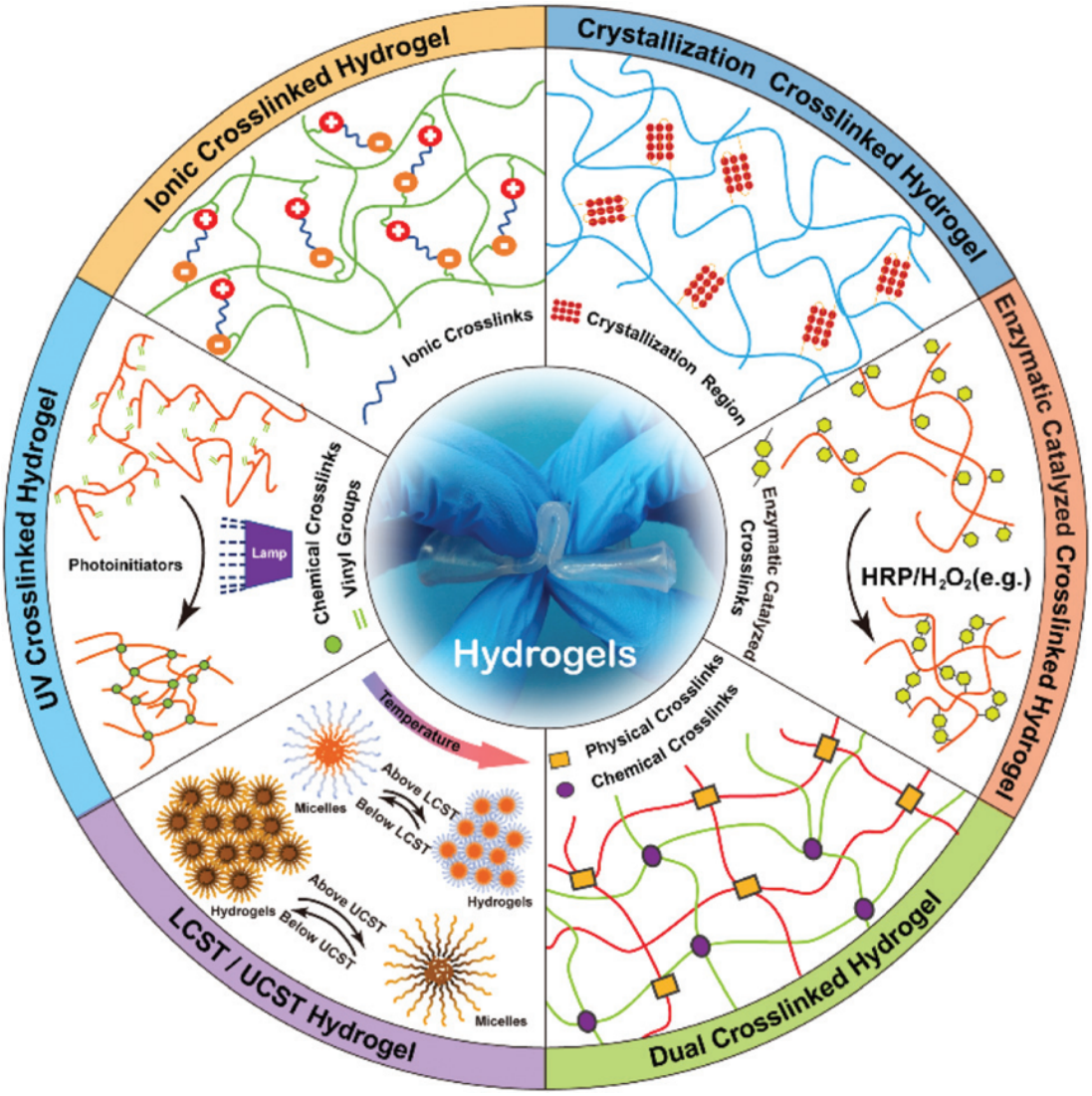

Fig. 1.5 The most widely used crosslinking strategies for hydrogel construction. Including crystallization crosslinked hydrogel, ionic crosslinking, UV crosslinking, LCST/UCST hydrogel, dual crosslinking and enzymatic catalyzed crosslinking. Reproduced with permission from ref[32]. Copyright 2019 The Royal Society of Chemistry.

Among these existing strategies, an emerging attractive approach for the rational and feasible design of hydrogels is enzyme-mediated hydrogelation. The enzyme-catalyzed hydrogelation realizes a mild cross-linking reaction, making it suitable with the incorporation of therapeutic proteins, drugs and typically for living cells[38–40]. The kinetic manipulation of hydrogel formation could be realized by controlling the catalytic behavior of enzymes in crosslinking reaction by adjusting reaction prameters. Despite hydrogel formation by an enzymatic reaction is a relatively recent concept, the interest

of an enzyme-based cross-linking is not only providing the strong and dynamic covalent bond but also exhibit the fast gelation under physiologically relevant and mild oxidative conditions.

So far, several enzymes have been studied for their abilities to control and provide advanced hydrogelation systems, such as lysyl oxidase[38], transglutaminase[41], sortase[42], laccase[43,44], phosphatases[45], ß-lactamase[46], plasma amine oxidase[47], thrombin[48], thermolysin[49], kinase/phosphatase[50,51], phosphopantetheinyl transferase[52], tyrosinase[53], α-chymotrypsin[54], and peroxidases[55]. Among these group of enzymes, peroxidases that catalyze a variety of oxidative transformations using hydrogen peroxide or other peroxides as oxidants[56], and horseradish peroxidase (HRP) extracted and isolated from horseradish roots is one of the most studied, favored and used enzymes in hydrogel fabrication[57–59]. HRP is widely applied as a biocatalyst due to the fast reaction kinetics, moderate substrate specificity, and ability to control the cross-linking density, that can be tailored by simply altering the precursor reactants[56,57,60–62]. In fact, another enzyme demonstrates weak mechanical properties, lower biorthogonality, less specific binding site and lack of immunogenicity. Conversely, because HRP is plant-based derived peroxidase that can offer relatively low immunogenicity risk, thus HRP has been authorized by the U.S. Food and Drug Administration (FDA) for biomedical applications[63] and commercially accessible. It was predicted that HRP could become the greatest enzyme for the next decade[64].

1.3 Designation of horseradish peroxidase (HRP)-catalyzed hydrogels

Hydrogels have transitioned from being a static and passive material to a dynamic, bio-based, and stimuli-responsive biomaterial for use in cell-seeding technology[65,66]. Recent advances towards such biologically active hydrogels have been directed to design biomaterials with superior feature for higher-order cell culture

than conventional 2D culture. As previously described, in the term of cellular scaffold development, HRP is promising biocatalyst because of its hydrogelation abilities. Thus, many HRP-mediated hydrogel systems have been proposed for 2D or 3D cellular scaffolds, which were deeply discussed in a recent review by Sakai and Nakahata[57], such as cell-laden microcapsules, solid- and hollow-core hydrogel fibers, approaching in single-cell hydrogel coating and biofabrication in 3D bioprinting.

1.3.1 Horseradish peroxidase (HRP)

HRP is an oxidoreductase comprising of 308 amino acid residues, 4 disulfide bonds between cysteine residues, a single heme group [iron(III) protoporphyrin IX] and two calcium ions (Fig 1.6-A)[67]. Basically, HRP-catalyzed reaction is described by the following equation, in which AH and AH_2 imply a radical product and its reducing substrate, respectively[67,68].

$$H_2O_2 + 2AH_2 \xrightarrow{HRP} 2H_2O + 2AH$$

The reaction cycle initiates from the binding of H_2O_2 to the vacant octahedral position on the iron atom of HRP (Fig. 1.6-A), and subsequently the oxidized HRP (compound I/II) oxidizes a reducing substrate and returns to its original form. Consequently, the created phenol radicals allow covalent bond formation within aromatic rings structure (Fig. 1.6-B)[68]. HRP recognizes indoles, sulfonates, phenylamines, and phenol as reducing substrates, which are converted to radicals to react with each other via a radical coupling reaction. These reducing substrates are introduced to polymers for the formation of hydrogels via cross-linking. Details of the HRP structure and its complex catalytic mechanism have been elegantly described in the recent literature[56,67,69–73].

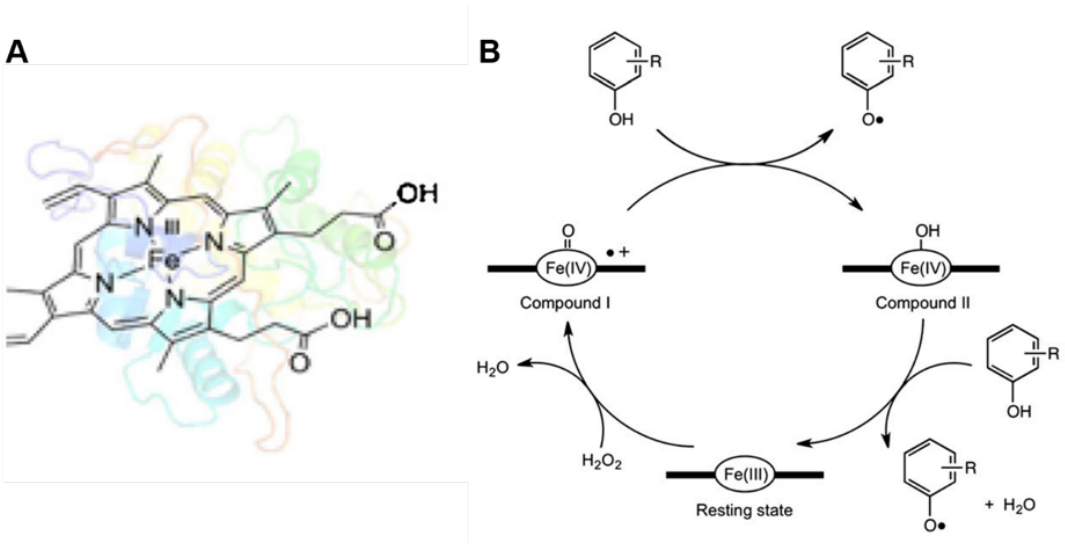

Fig.1.6 A. The heme as an active center of peroxidases structure. B. The catalytic cycle of horseradish peroxidase (HRP). A Reproduce from Refs.[73] with permission from Elsevier 2019. B. Reproduce from ref[68] with permission from John Wiley & Sons, Ltd. 2014

1.3.2 Horseradish peroxidase (HRP)-mediated hydrogel formation through cross-linking between phenol groups

The crosslinkable substrate is one of the most important considerations to increase the stability of polymer crosslinking through HRP-catalyzed hydrogelation. In fact, despite many functional groups, for instance phenolic acids, aromatic phenols, and amines can be applied as the reducing substrate[67]. Currently, the introduction of phenolic groups is the most commonly used method to improve HRP-mediated hydrogelation in many polymers[63] because it is a common form of industrial waste[68]. Various phenol derivatives are introduced to the backbone of hydrogels such as tyrosine[74], tyramine[75], phenylalanine, 4-hydroxyhneyl acetic acid[76] and hydroxyphenyl propionic acid[77,78] to form cross-linking in the hydrogels.

Precursor that works in phenol-mediated cross-linking has wide range of polymer type, either natural or synthetic moieties could be conjugated and modified through its sites[63]. Conjugation of phenol moieties in hydrogel network can be selected according to the chemical cues of each polymer. Generally, water soluble carbodiimide hydrochloride (WSDC) is utilized in the reaction between carboxyl group and a primary amine (e.g. tyramine)[79] (Fig. 1.7-A). An alternative method is also using WSDC within the reaction of polymer consisting amine group and propionic acid (Fig. 1.7-B).

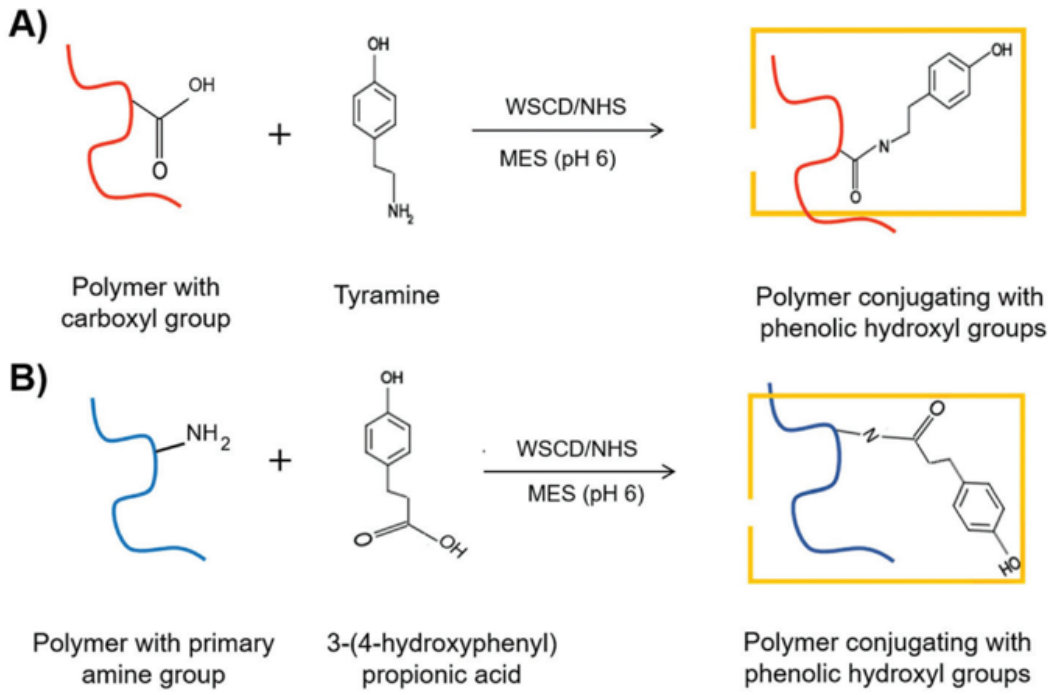

Fig. 1.7. Schematics illustration of synthesis of phenol polymer using water soluble carbodiimide hydrochloride (WSDC/NHS). Reproduce from ref[79] with permission from Royal Chemistry Society 2018.

From the viewpoint of the compatibility of the main polymer, the bound phenol moieties in HRP system work in many types of polymers because of the reasonable design and substrate specificity of HRP. Natural compounds for instance collagen[80], hyaluronic acid[81], gelatin[82], chitosan[83], silk[84], chondroitin sulfate[85], dextran[86], alginate[87], and various combinations among them have been used as compatible substrates polymer in HRP-mediated hydrogelation. However, as described in the

previous section due to the low mechanical properties of natural-based polymer, it will predict limits of the application on the biomedical field where the mechanical aspect is crucial. To overcome the limitation, the synthetic polymer has been obtained to construct hydrogel backbone, and among all the synthetic material, functionalized polyethylene glycol (PEG) is widely involved as a base polymer for HRP-mediated hydrogelation due to highly controllable and homogenous microstructure[28,29].

1.3.3 Timeline and research evolution of the HRP-mediated hydrogelation as a cell culture scaffold

Historically, the first report of the valorization of an HRP-catalyzed oxidation in a hydrogel system was reported by Kaplan *et al.* in 2002, where they demonstrated the fabrication of poly(aspartic acid) modified with phenol as a gel precursor using an HRP catalysis system[55]. Since then, many researchers have followed the same concept to construct hydrogels based on HRP catalysis either using natural polymer or synthetic polymer[22,23,87–96,24,55,80–85].

A significant improvement was reported by Kurisawa and coworkers in 2005[76] in the application of a hyaluronic acid-tyramine conjugate to produce an injectable hydrogel, where HRP induced oxidative coupling, resulting in hydrogelation. In their report, the classical HRP cycle could interact with hydrogen peroxide (H_2O_2) to form highly intermediate product as oxidants. The results show HRP mediated hydrogelation can support the injection of hydrogel as a minimally invasive technique. However, in general, these development of HRP-mediated hydrogelation systems involves H_2O_2 in the equal ratio as HRP amount to the fabrication of cell-laden hydrogel scaffold (Fig. 1.8).

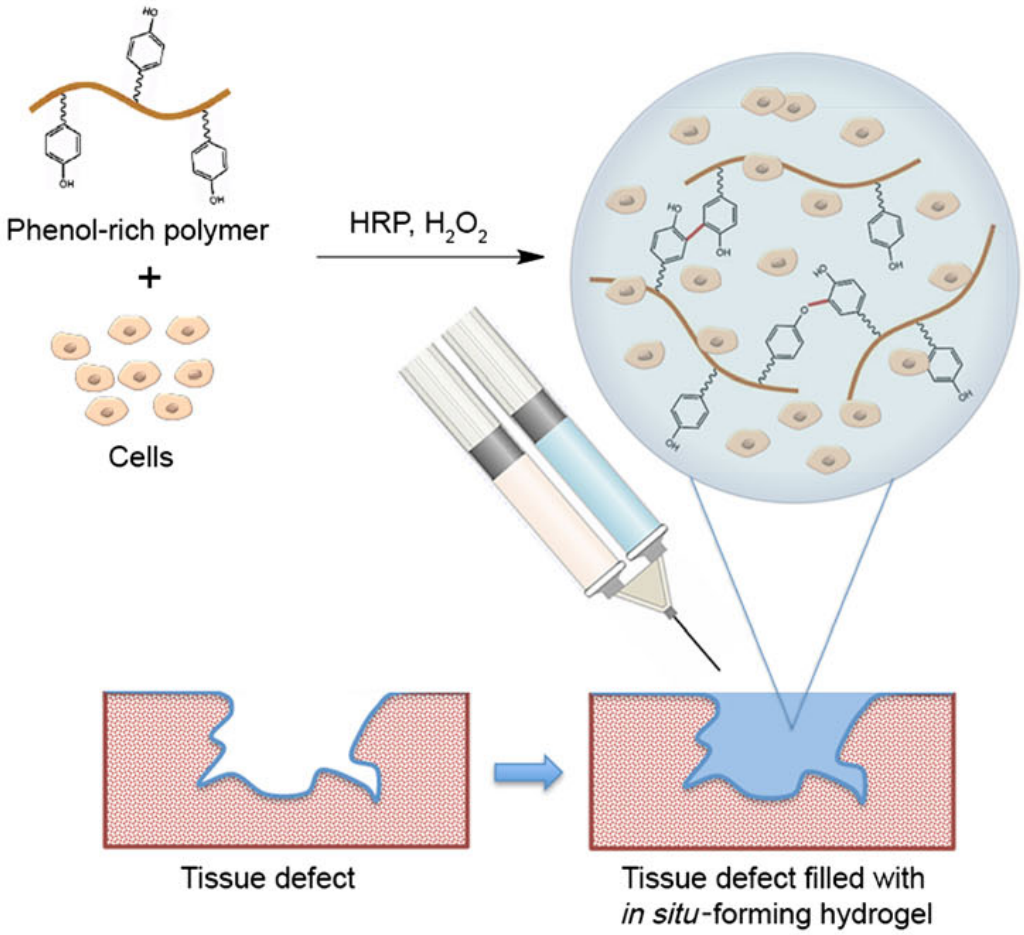

Fig.1.8. HRP-catalyzed crosslinking reaction with phenol-rich polymer and H_2O_2 as a common cell encapsulation strategy in the fabrication of hydrogel in the tissue engineering field. Reproduce from ref[68] with permission from John Wiley & Sons, Ltd. 2014.

It should be pointed out that HRP-catalyzed cross-linking of several reaction type has been reported and discussed in thousands of research papers in various points of view[56,57,70,73,79]. However, from the viewpoint of cytotoxicity, removal of residual H_2O_2 in the HRP-mediated hydrogelation system for mild conditions to cells and increase in the cytocompatibility of hydrogel system are required.

Despite the development of HRP-mediated preparation hydrogel has been conducted since more than twenty years ago, the trend of published paper during 2000 to 2010 certainly reveals that the study and progress of HRP-hydrogels are still at an early development phase, against with the considerably steps taken to totally remove the use of H_2O_2 in its system (Fig 1.9). The continuous work has been settled to adapt

and integrate the facile HRP preparation system with the another chemical/biological entity as well as the significantly effort to advance the different compartment in cell culture application.

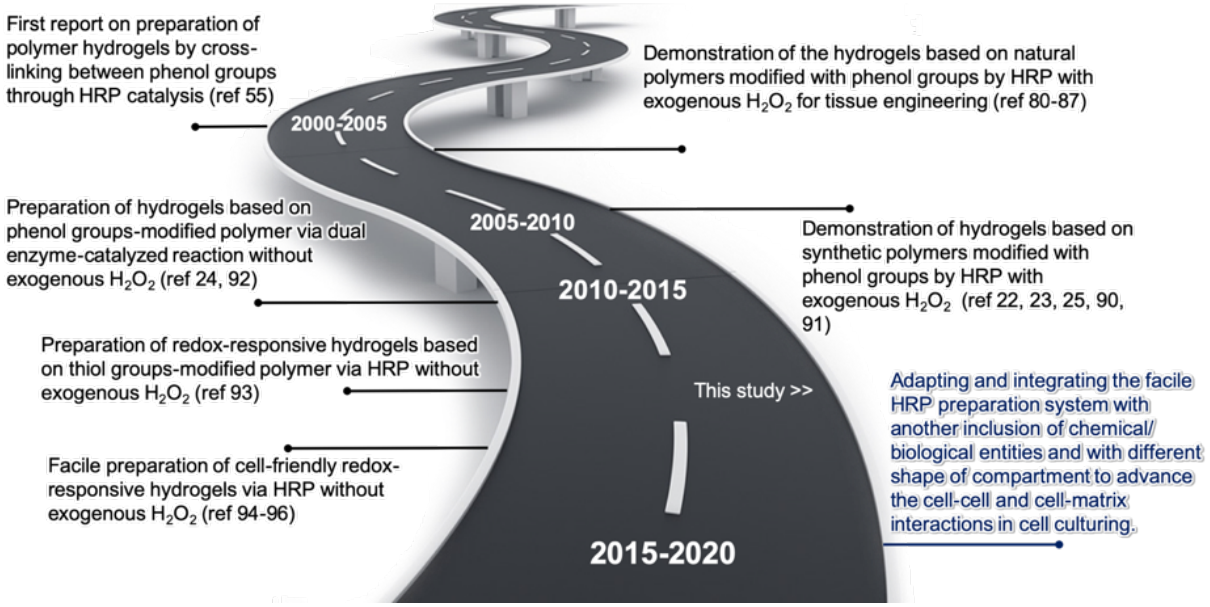

Fig 1.9. Timeline chart of the evolution of HRP-mediated preparation of hydrogels based on natural and synthetic polymers and the current goal of this study. Reproduced and redrawn from ref[64] with permission from the Springer Nature 2020.

In the previous section, it was discussed that H_2O_2 is necessary in the HRP-mediated hydrogelation. However, the amount of H_2O_2 is crucial concern for harsh impact in cytocompatibility, thus the consumption of H_2O_2 amount should be decreased. However, the low H_2O_2 dosage and the short cell exposure time to H_2O_2 may not provide milder condition especially when the system uses as the cellular scaffold. The further approach to solve the problem is using glucose oxidase (GOx), where oxidizing glucose to glucono-δ-lactone by consuming oxygen could suppress the high concentration of H_2O_2[92]. Nevertheless, the remaining GOx in the system might still produce H_2O_2 and react with glucose, thus predict gives negative impact to the cell. Indicating in the *in vivo* application this technique may face potential problem, as the glucose is a common molecule in ECM, GOx in the hydrogel will subsequently oxidize the excess of glucose molecules and create undesired H_2O_2.

Another important report came from Singh and colleagues, where they found that the thiol groups incorporated into the polymer promoted hydrogelation induced by HRP, without recruitment of H_2O_2[93]. Under aerobic condition, mixture of HRP and thiol can generate hydrogelation reaction of phenol compound via autooxidation in the redox sensitive hydrogel. This basic gelation concept is in the presence of thiol, thinly radical was dimerized to form disulfides or interact with the disulfide radicals after reacting with oxygen. However, in this system the hydrogelation condition occurs in the pH 8.5, which may not suitable with the physiological condition in ECM. Moreover, the gelation time of the polymer solution was also slow (41-110 min), even at high HRP concentration and high concentration of polymeric substrates.

To date, the next impactful research developed from our group, where the dramatic improvement of the HRP-catalyzed hydrogelation of thiolated polymers is realized[94]. The main concept of the gelation system was the improvement of phenolic compounds as the substrates for HRP catalysis. The rate of second-order constant of HRP compound II with the general thiol substrate cysteine is < 50 M^{-1} s^{-1} [97], while that with phenolic compounds is usually in the range of 10^3–10^7 M^{-1} s^{-1} [98], indicating that the inclusion of thiolated polymers as an HRP substrate would lead to much slower gelation kinetics than phenolated ones. Nevertheless, in the incorporation of phenolic substrates, radical exchange between the phenol radicals produced by HRP catalysis and thiols occurs with a rate constant at pH 7.15 is reportedly 10^6 M^{-1} s^{-1}. Therefore, in the HRP-cycle, the presence of single electron oxidation from thiol occurs when generated the phenol radicals and that thiols radical then transformed to disulfides after interacting with the oxygen. Eventually, the resultant phenolic compounds should accelerate the HRP-mediated fabrication of disulfide-crosslinked hydrogels without exogenous H_2O_2[64] (Fig. 1.10).

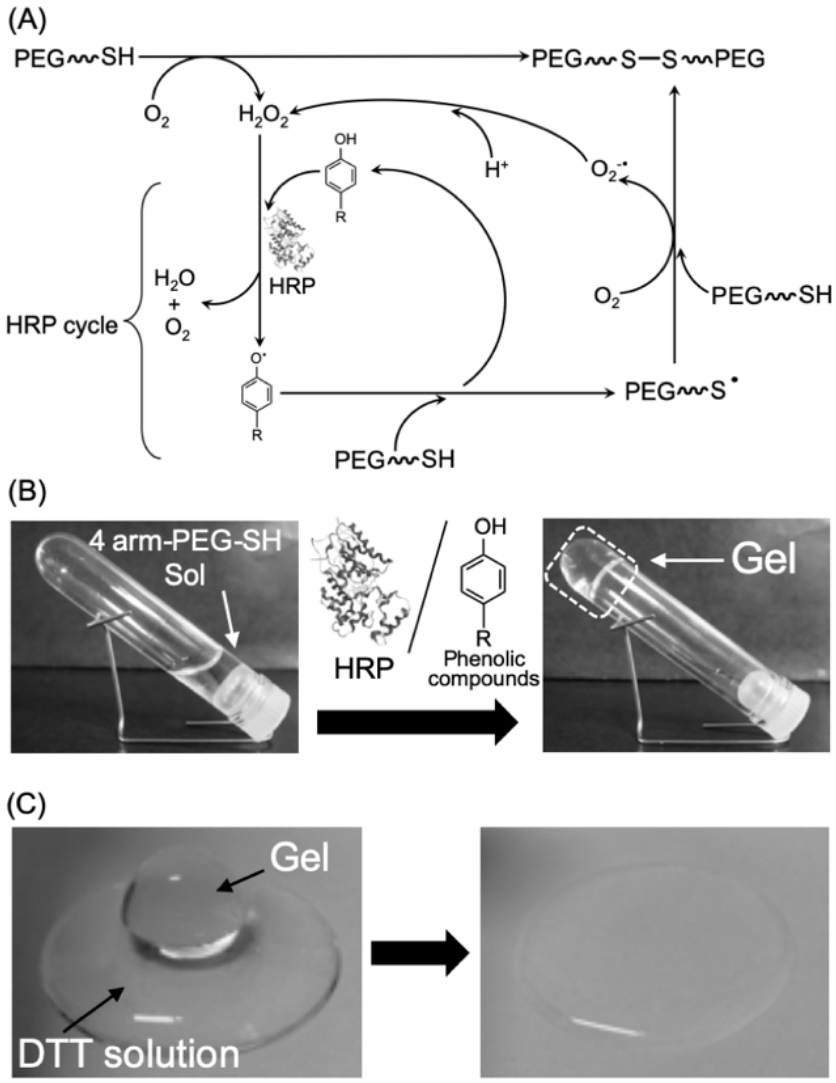

Fig. 1.10. HRP-mediated hydrogel system without exogenous H_2O_2 using thiolated polymers. (A) Proposed scheme of hydrogelation in the presence of a phenolic compound as a direct HRP substrate. (B) Hydrogel formation using 4-arm-PEG-SH, HRP, and tyramine at pH 7.4. (C) Degradation of the redox-responsive hydrogel by soaking in DTT solution for 15 min. Reproduced from ref[64] with permission from the Springer Nature 2020.

This strategy was the first report of disulfide-cross-linked hydrogels prepared by HRP catalysis at neutral pH without the addition of exogenous H_2O_2. In this HRP hydrogelation system, the inclusion of phenolic compound is aid and amplify the autooxidation of the thiol groups. Indicating this phenolic compound plays a significant and crucial role as the direct substrate in the HRP catalytic cycle and in the preparation of the redox-responsive disulfide-cross-linked hydrogels. Obviously, the design of formation and degradation of the disulfide cross-linking in this system can effectively

encapsulate and release living cells, which might be highly beneficial for the development of cell culture platform[64].

1.4 Aim and outline of the thesis

The aim of this research is to integrate and develop the facile HRP preparation system in redox responsive hydrogel with the inclusion of chemical/biological entities and with different shapes of compartment to advance the cell-cell and cell-matrix interactions in cell culturing.

In Chapter 1, a general introduction was described on the development of scaffold to better mimic the natural life form and the increase of hydrogel research as a cell culture platform in history which constructed based on the variety of polymer. A brief review of the polymer choice and the crosslinking strategy for precious hydrogelation in hydrogel was included as well. The designation of HRP as the selected biocatalyst in hydrogelation and their improvement year by year as the cellular friendly scaffold was also discussed.

In Chapter 2, the feasibility of using HRP hydrogelation system in the PEG-based hydrogel as the main polymer was discussed with functionalized gelatin and heparin. By varying the gelatin type and heparin concentration, the capture of growth factors in hydrogel system and cell adherence as well as the rapid fabrication of cell sheet on the redox responsive hydrogel were studied.

In Chapter 3, the performance of obtained cell sheet on the redox responsive hydrogel is utilized to wrap and encapsulate other cells and biological entities to form heterogeneous of multicellular structure. Cell sheet detachment from hydrogel and their wrapping behavior induced by cysteine were studied. By changing the density of cell or the number of carcinoma spheroids, the cell number of endothelial cell and the collagen beads number, the properties and the resultant of heterogenous 3D cellular

structure were investigated.

In Chapter 4, functionalized gelatin in facile HRP-mediated preparation was adapted to transform the liquid marble system to hydrogel marble as a scaffold for 3D cell culture. With this new hydrogel marble system, the carcinoma spheroid fabrication process was described.

Finally, in **Chapter 5** the findings of this research are outlined and discussed further research direction related to the next development of HRP hydrogels as a scaffold and their prospect in medical application and tissue engineering fields.

1.5 References

1. Ma'ayan, A. Complex systems biology. *J. R. Soc. Interface* **14**, (2017).
2. Raman, R. & Bashir, R. Biomimicry, Biofabrication, and Biohybrid Systems: The Emergence and Evolution of Biological Design. *Adv. Healthc. Mater.* **6**, 1–20 (2017).
3. Patterson, J., Martino, M. M. & Hubbell, J. A. Biomimetic materials in tissue engineering. *Mater. Today* **13**, 14–22 (2010).
4. Grand View Research. *Three-dimensional Cell Culture Market Size, Share & Trends Analysis Report by Technology (Scaffold Based, Scaffold Free, Bioreactors), by Application (Cancer, Drug Development), by End Use, by Region, and Segment Forecasts, 2020 – 2027.* (2020).
5. Ovsianikov, A., Khademhosseini, A. & Mironov, V. The Synergy of Scaffold-Based and Scaffold-Free Tissue Engineering Strategies. *Trends Biotechnol.* **36**, 348–357 (2018).
6. Green, J. J. & Elisseeff, J. H. Mimicking biological functionality with polymers for biomedical applications. *Nature* **540**, 386–394 (2016).
7. Lee, S. C., Kwon, I. K. & Park, K. Hydrogels for delivery of bioactive agents: A historical perspective. *Adv. Drug Deliv. Rev.* **65**, 17–20 (2013).
8. Kopeček, J. Swell gels. *Nature* **417**, 389–391 (2002).
9. Hoffman, A. S. Hydrogels for biomedical applications. *Adv. Drug Deliv. Rev.* **54**, 3–12 (2002).

10. Kang, D. H., Kim, D., Wang, S., Song, D. & Yoon, M. H. Water-insoluble, nanocrystalline, and hydrogel fibrillar scaffolds for biomedical applications. *Polym. J.* **50**, 637–647 (2018).
11. Tibbitt, M. W. & Anseth, K. S. Hydrogels as extracellular matrix mimics for 3D cell culture. *Biotechnol. Bioeng.* **103**, 655–663 (2009).
12. Schneider-Barthold, C., Baganz, S., Wilhelmi, M., Scheper, T. & Pepelanova, I. Hydrogels based on collagen and fibrin - Frontiers and applications. *BioNanoMaterials* **17**, 3–12 (2016).
13. Janmey, P. A., Winer, J. P. & Weisel, J. W. Fibrin gels and their clinical and bioengineering applications. *J. R. Soc. Interface* **6**, 1–10 (2009).
14. Chen, Y. Front-matter. *Hydrogels Based Nat. Polym.* i–iii (2020). doi:10.1016/b978-0-12-816421-1.00018-5
15. Hughes, C. S., Postovit, L. M. & Lajoie, G. A. Matrigel: a complex protein mixture required for optimal growth of cell culture. *Proteomics* **10**, 1886–1890 (2010).
16. Catoira, M. C., Fusaro, L., Di Francesco, D., Ramella, M. & Boccafoschi, F. Overview of natural hydrogels for regenerative medicine applications. *J. Mater. Sci. Mater. Med.* **30**, (2019).
17. Kirchmajer, D. M., Gorkin, R. & In Het Panhuis, M. An overview of the suitability of hydrogel-forming polymers for extrusion-based 3D-printing. *J. Mater. Chem. B* **3**, 4105–4117 (2015).
18. Varghese, S. A., Rangappa, S. M., Siengchin, S. & Parameswaranpillai, J. *Natural polymers and the hydrogels prepared from them*. *Hydrogels Based on Natural Polymers* (Elsevier Inc., 2019). doi:10.1016/B978-0-12-816421-1.00002-1
19. Spicer, C. D. Hydrogel scaffolds for tissue engineering: The importance of polymer choice. *Polym. Chem.* **11**, 184–219 (2020).
20. Caliari, S. R. & Burdick, J. A. A practical guide to hydrogels for cell culture. *Nat. Methods* **13**, 405–414 (2016).
21. McKinnon, D. D., Kloxin, A. M. & Anseth, K. S. Synthetic hydrogel platform for three-dimensional culture of embryonic stem cell-derived motor neurons. *Biomater. Sci.* **1**, 460–469 (2013).
22. Park, K. M., Shin, Y. M., Joung, Y. K., Shin, H. & Park, K. D. In situ forming hydrogels based on tyramine conjugated 4-Arm-PPO-PEO via enzymatic oxidative reaction. *Biomacromolecules* **11**, 706–712 (2010).
23. Lee, S. H. *et al.* Enzyme-mediated cross-linking of Pluronic copolymer micelles for

injectable and in situ forming hydrogels. *Acta Biomater.* **7**, 1468–1476 (2011).

24. Sakai, S. *et al.* Polyvinyl alcohol-based hydrogel dressing gellable on-wound via a co-enzymatic reaction triggered by glucose in the wound exudate. *J. Mater. Chem. B* **1**, 5067–5075 (2013).
25. Sun, Y., Deng, Z., Tian, Y. & Lin, C. Horseradish peroxidase-mediated in situ forming hydrogels from degradable tyramine-based poly(amido amine)s. *J. Appl. Polym. Sci.* **127**, 40–48 (2013).
26. Tan, H. & Marra, K. G. Injectable, biodegradable hydrogels for tissue engineering applications. *Materials (Basel).* **3**, 1746–1767 (2010).
27. Patel, G. & Dalwadi, C. Recent Patents on Stimuli Responsive Hydrogel Drug Delivery System. *Recent Pat. Drug Deliv. Formul.* **7**, 206–215 (2013).
28. Macdougall, L. J., Pérez-Madrigal, M. M., Arno, M. C. & Dove, A. P. Nonswelling Thiol-Yne Cross-Linked Hydrogel Materials as Cytocompatible Soft Tissue Scaffolds. *Biomacromolecules* **19**, 1378–1388 (2018).
29. Ulery, B. D., Nair, L. S. & Laurencin, C. T. Biomedical applications of biodegradable polymers. *J. Polym. Sci. Part B Polym. Phys.* **49**, 832–864 (2011).
30. Buwalda, S. J. *et al.* Hydrogels in a historical perspective: From simple networks to smart materials. *J. Control. Release* **190**, 254–273 (2014).
31. Kuo, C. K. & Ma, P. X. Ionically crosslinked alginate hydrogels as scaffolds for tissue engineering: Part 1. Structure, gelation rate and mechanical properties. *Biomaterials* **22**, 511–521 (2001).
32. Hu, W., Wang, Z., Xiao, Y., Zhang, S. & Wang, J. Advances in crosslinking strategies of biomedical hydrogels. *Biomater. Sci.* **7**, 843–855 (2019).
33. Crescenzi, V., Cornelio, L., Di Meo, C., Nardecchia, S. & Lamanna, R. Novel hydrogels via click chemistry: Synthesis and potential biomedical applications. *Biomacromolecules* **8**, 1844–1850 (2007).
34. Choi, J. R., Yong, K. W., Choi, J. Y. & Cowie, A. C. Recent advances in photo-crosslinkable hydrogels for biomedical applications. *Biotechniques* **66**, 40–53 (2019).
35. Hu, B. H. & Messersmith, P. B. Rational Design of Transglutaminase Substrate Peptides for Rapid Enzymatic Formation of Hydrogels. *J. Am. Chem. Soc.* **125**, 14298–14299 (2003).
36. Mironi-Harpaz, I., Wang, D. Y., Venkatraman, S. & Seliktar, D. Photopolymerization of cell-encapsulating hydrogels: Crosslinking efficiency

versus cytotoxicity. *Acta Biomater.* **8**, 1838–1848 (2012).

37. Steinhilber, D. & Haag, R. Multifunctional Dendritic Polyglycerol Nano- and Microgels for Encapsulation and Release of Functional Biomacromolecules. **20**, 7545 (2011).
38. Moreira Teixeira, L. S., Feijen, J., van Blitterswijk, C. A., Dijkstra, P. J. & Karperien, M. Enzyme-catalyzed crosslinkable hydrogels: Emerging strategies for tissue engineering. *Biomaterials* **33**, 1281–1290 (2012).
39. Buwalda, S. J., Vermonden, T. & Hennink, W. E. Hydrogels for Therapeutic Delivery: Current Developments and Future Directions. *Biomacromolecules* **18**, 316–330 (2017).
40. Kurisawa, M., Chung, J. E., Yang, Y. Y., Gao, S. J. & Uyama, H. Injectable biodegradable hydrogels composed of hyaluronic acid-tyramine conjugates for drug delivery and tissue engineering. *Chem. Commun.* 4312–4314 (2005). doi:10.1039/b506989k
41. Yung, C. W., Bentley, W. E. & Barbari, T. A. Diffusion of interleukin-2 from cells overlaid with cytocompatible enzyme-crosslinked gelatin hydrogels. *J. Biomed. Mater. Res. - Part A* **95**, 25–32 (2010).
42. Cambria, E. *et al.* Covalent Modification of Synthetic Hydrogels with Bioactive Proteins via Sortase-Mediated Ligation. *Biomacromolecules* **16**, 2316–2326 (2015).
43. Huber, D. *et al.* Anti-inflammatory and anti-oxidant properties of laccase-synthesized phenolic-O-carboxymethyl chitosan hydrogels. *N. Biotechnol.* **40**, 236–244 (2018).
44. Huber, D. *et al.* Chitosan hydrogel formation using laccase activated phenolics as cross-linkers. *Carbohydr. Polym.* **157**, 814–822 (2017).
45. Yang, Z. *et al.* Enzymatic formation of supramolecular hydrogels. *Adv. Mater.* **16**, (2004).
46. Yang, Z. *et al.* Using β-lactamase to trigger supramolecular hydrogelation. *J. Am. Chem. Soc.* **129**, 266–267 (2007).
47. Bakota, E. L., Aulisa, L., Galler, K. M. & Hartgerink, J. D. Enzymatic cross-linking of a nanofibrous peptide hydrogel. *Biomacromolecules* **12**, 82–87 (2011).
48. Rowe, S. L., Lee, S. Y. & Stegemann, J. P. Influence of thrombin concentration on the mechanical and morphological properties of cell-seeded fibrin hydrogels. *Acta Biomater.* **3**, 59–67 (2007).

49. Toledano, S., Williams, R. J., Jayawarna, V. & Ulijn, R. V. Enzyme-triggered self-assembly of peptide hydrogels via reversed hydrolysis. *J. Am. Chem. Soc.* **128**, 1070–1071 (2006).
50. Hai, Z., Li, J., Wu, J., Xu, J. & Liang, G. Alkaline Phosphatase-Triggered Simultaneous Hydrogelation and Chemiluminescence. *J. Am. Chem. Soc.* **139**, 1041–1044 (2017).
51. Yang, Z., Liang, G., Wang, L. & Xu, B. Using a kinase/phosphatase switch to regulate a supramolecular hydrogel and forming the supramolecular hydrogel in vivo. *J. Am. Chem. Soc.* **128**, 3038–3043 (2006).
52. Mosiewicz, K. A., Johnsson, K. & Lutolf, M. P. Phosphopantetheinyl transferase-catalyzed formation of bioactive hydrogels for tissue engineering. *J. Am. Chem. Soc.* **132**, 5972–5974 (2010).
53. Kim, E. H., Lim, S., Kim, T. E., Jeon, I. O. & Choi, Y. S. Preparation of in situ Injectable Chitosan/Gelatin Hydrogel Using an Acid-tolerant Tyrosinase. *Biotechnol. Bioprocess Eng.* **23**, 500–506 (2018).
54. Xie, Y. *et al.* Enzyme-substrate interactions promote the self-assembly of amino acid derivatives into supramolecular hydrogels. *J. Mater. Chem. B* **4**, 844–851 (2016).
55. Sofia, S. J., Singh, A. & Kaplan, D. L. Peroxidase-catalyzed crosslinking of functionalized polyaspartic acid polymers. *J. Macromol. Sci. - Pure Appl. Chem.* **39 A**, 1151–1181 (2002).
56. Lopes, G. R., Pinto, D. C. G. A. & Silva, A. M. S. Horseradish peroxidase (HRP) as a tool in green chemistry. *RSC Adv.* **4**, 37244–37265 (2014).
57. Sakai, S. & Nakahata, M. Horseradish Peroxidase Catalyzed Hydrogelation for Biomedical, Biopharmaceutical, and Biofabrication Applications. *Chem. - An Asian J.* **12**, 3098–3109 (2017).
58. Bae, J. W., Choi, J. H., Lee, Y. & Park, K. D. Horseradish peroxidase-catalysed in situ -forming hydrogels for tissue-engineering applications. *J. Tissue Eng. Regen. Med.* **9**, 1225–1232 (2015).
59. Guebitz, G. M. & Nyanhongo, G. S. Enzymes as Green Catalysts and Interactive Biomolecules in Wound Dressing Hydrogels. *Trends Biotechnol.* **36**, 1040–1053 (2018).
60. Lee, F., Bae, K. H. & Kurisawa, M. Injectable hydrogel systems crosslinked by horseradish peroxidase. *Biomed. Mater.* **11**, 14101 (2015).

61. Shakya, A. K. & Nandakumar, K. S. An update on smart biocatalysts for industrial and biomedical applications. *J. R. Soc. Interface* **15**, (2018).
62. Krainer, F. W. & Glieder, A. An updated view on horseradish peroxidases: recombinant production and biotechnological applications. *Appl. Microbiol. Biotechnol.* **99**, 1611–1625 (2015).
63. Guebitz, G. M. & Nyanhongo, G. S. Enzymes as Green Catalysts and Interactive Biomolecules in Wound Dressing Hydrogels. *Trends Biotechnol.* **36**, 1040–1053 (2018).
64. Wakabayashi, R., Ramadhan, W., Moriyama, K., Goto, M. & Kamiya, N. Poly(ethylene glycol)-based biofunctional hydrogels mediated by peroxidase-catalyzed cross-linking reactions. *Polym. J.* (2020). doi:10.1038/s41428-020-0344-7
65. Ohya, Y. Temperature-responsive biodegradable injectable polymer systems with conveniently controllable properties. *Polym. J.* **51**, 997–1005 (2019).
66. Kambe, Y., Tokushige, T., Mahara, A., Iwasaki, Y. & Yamaoka, T. Cardiac differentiation of induced pluripotent stem cells on elastin-like protein-based hydrogels presenting a single-cell adhesion sequence. *Polym. J.* **51**, 97–105 (2019).
67. Veitch, N. C. Horseradish peroxidase: A modern view of a classic enzyme. *Phytochemistry* **65**, 249–259 (2004).
68. Bae, J. W., Choi, J. H., Lee, Y. & Park, K. D. Horseradish peroxidase-catalysed in situ -forming hydrogels for tissue-engineering applications. *J. Tissue Eng. Regen. Med.* **9**, 1225–1232 (2014).
69. Rodríguez-López, J. N. *et al.* Mechanism of reaction of hydrogen peroxide with horseradish peroxidase: Identification of intermediates in the catalytic cycle. *J. Am. Chem. Soc.* **123**, 11838–11847 (2001).
70. Zakharova, G. S., Uporov, I. V. & Tishkov, V. I. Horseradish peroxidase: Modulation of properties by chemical modification of protein and heme. *Biochem.* **76**, 1391–1401 (2011).
71. Kobayashi, S., Uyama, H. & Kimura, S. Enzymatic Polymerization. *Chem. Rev.* **101**, 3793–3818 (2001).
72. Wang, L. S., Chung, J. E. & Lee, F. (12) Patent Application Publication (10) Pub. No.: US 2010/0074956 A1. **1**, (2010).
73. Hoang Thi, T. T., Lee, Y., Le Thi, P. & Park, K. D. Engineered horseradish

peroxidase-catalyzed hydrogels with high tissue adhesiveness for biomedical applications. *J. Ind. Eng. Chem.* **78**, 34–52 (2019).

74. Ulery, B. D., Nair, L. S. & Laurencin, C. T. Biomedical applications of biodegradable polymers. *J. Polym. Sci. Part B Polym. Phys.* **49**, 832–864 (2011).
75. Lim, K. S. *et al.* Promoting Cell Survival and Proliferation in Degradable Poly(vinyl alcohol)-Tyramine Hydrogels. *Macromol. Biosci.* **15**, 1423–1432 (2015).
76. Kurisawa, M., Chung, J. E., Yang, Y. Y., Gao, S. J. & Uyama, H. Injectable biodegradable hydrogels composed of hyaluronic acid-tyramine conjugates for drug delivery and tissue engineering. *Chem. Commun.* 4312–4314 (2005). doi:10.1039/b506989k
77. Zaviskova, K. *et al.* Injectable hydroxyphenyl derivative of hyaluronic acid hydrogel modified with RGD as scaffold for spinal cord injury repair. *J. Biomed. Mater. Res. - Part A* **106**, 1129–1140 (2018).
78. Sgambato, A., Cipolla, L. & Russo, L. Bioresponsive Hydrogels: Chemical Strategies and Perspectives in Tissue Engineering. *Gels* **2**, 28 (2016).
79. Khanmohammadi, M. *et al.* Horseradish peroxidase-catalyzed hydrogelation for biomedical applications. *Biomater. Sci.* **6**, 1286–1298 (2018).
80. Kuo, K. C. *et al.* Bioengineering vascularized tissue constructs using an injectable cell-laden enzymatically crosslinked collagen hydrogel derived from dermal extracellular matrix. *Acta Biomater.* **27**, 151–166 (2015).
81. Raia, N. R. *et al.* Enzymatically crosslinked silk-hyaluronic acid hydrogels. *Biomaterials* **131**, 58–67 (2017).
82. Sakai, S., Hirose, K., Taguchi, K., Ogushi, Y. & Kawakami, K. An injectable, in situ enzymatically gellable, gelatin derivative for drug delivery and tissue engineering. *Biomaterials* **30**, 3371–3377 (2009).
83. Sakai, S., Yamada, Y., Zenke, T. & Kawakami, K. Novel chitosan derivative soluble at neutral pH and in-situ gellable via peroxidase-catalyzed enzymatic reaction. *J. Mater. Chem.* **19**, 230–235 (2009).
84. Zhou, B. *et al.* Self-Crosslinking of Silk Fibroin Using H2O2-Horseradish Peroxidase System and the Characteristics of the Resulting Fibroin Membranes. *Appl. Biochem. Biotechnol.* **182**, 1548–1563 (2017).
85. Chen, F. *et al.* An Injectable Enzymatically Crosslinked Carboxymethylated Pullulan/Chondroitin Sulfate Hydrogel for Cartilage Tissue Engineering. *Sci. Rep.* **6**, 1–12 (2016).

86. Jin, R., Hiemstra, C., Zhong, Z. & Feijen, J. Enzyme-mediated fast in situ formation of hydrogels from dextran-tyramine conjugates. *Biomaterials* **28**, 2791–2800 (2007).
87. Sakai, S. & Kawakami, K. Synthesis and characterization of both ionically and enzymatically cross-linkable alginate. *Acta Biomater.* **3**, 495–501 (2007).
88. Kim, Y. J. & Uyama, H. Biocompatible hydrogel formation of gelatin from cold water fish via enzymatic networking. *Polym. J.* **39**, 1040–1046 (2007).
89. Sun, Y., Deng, Z., Tian, Y. & Lin, C. Horseradish peroxidase-mediated in situ forming hydrogels from degradable tyramine-based poly(amido amine)s. *J. Appl. Polym. Sci.* **127**, 40–48 (2013).
90. Moriyama, K., Minamihata, K., Wakabayashi, R., Goto, M. & Kamiya, N. Enzymatic preparation of streptavidin-immobilized hydrogel using a phenolated linear poly(ethylene glycol). *Biochem. Eng. J.* **76**, 37–42 (2013).
91. Moriyama, K., Wakabayashi, R., Goto, M. & Kamiya, N. Characterization of enzymatically gellable, phenolated linear poly(ethylene glycol) with different molecular weights for encapsulating living cells. *Biochem. Eng. J.* **93**, 25–30 (2014).
92. Sakai, S., Komatani, K. & Taya, M. Glucose-triggered co-enzymatic hydrogelation of aqueous polymer solutions. *RSC Adv.* **2**, 1502–1507 (2012).
93. Singh, S., Topuz, F., Hahn, K., Albrecht, K. & Groll, J. Embedding of active proteins and living cells in redox-sensitive hydrogels and nanogels through enzymatic cross-linking. *Angew. Chemie - Int. Ed.* **52**, 3000–3003 (2013).
94. Moriyama, K., Minamihata, K., Wakabayashi, R., Goto, M. & Kamiya, N. Enzymatic preparation of a redox-responsive hydrogel for encapsulating and releasing living cells. *Chem. Commun.* **50**, 5895–5898 (2014).
95. Moriyama, K., Wakabayashi, R., Goto, M. & Kamiya, N. Enzyme-mediated preparation of hydrogels composed of poly(ethylene glycol) and gelatin as cell culture platforms. *RSC Adv.* **5**, 3070–3073 (2015).
96. Moriyama, K., Naito, S., Wakabayashi, R., Goto, M. & Kamiya, N. Enzymatically prepared redox-responsive hydrogels as potent matrices for hepatocellular carcinoma cell spheroid formation. *Biotechnol. J.* **11**, 1452–1460 (2016).
97. Obinger, C., Burner, U. & Ebermann, R. Generation of Hydrogen Peroxide by Plant Peroxidases Mediated Thiol Oxidation. *Phyt. - Ann. Rei Bot.* **37**, 219–226 (1997).

98. Dunford, H. B. & Adeniran, A. J. Hammett ϱσ correlation for reactions of horseradish peroxidase compound II with phenols. *Arch. Biochem. Biophys.* **251**, 536–542 (1986).

CHAPTER 2 ENZYMATICALLY PREPARED DUAL FUNCTIONALIZED HYDROGELS WITH GELATIN AND HEPARIN TO FACILITATE CELLULAR ATTACHMENT AND PROLIFERATION

2.1 Introduction

Mimicking the structure and function of natural extracellular matrices by synthetic materials is of great interest to promote the field of biomaterial scaffolds for tissue engineering and numerous studies have shown the potential of hydrogels as cell culture platforms[1]. The most attractive feature of synthetic hydrogels is that their physicochemical properties can be manipulated by altering the chemical components of the water-swollen three-dimensional (3D) polymeric network[2]. Many different approaches have been proposed to prepare biologically active hydrogels[3]. A major obstacle in the fabrication of engineered hydrogels is development of methods for *in situ* crosslinking of gel precursors without impairing bioactive agents. Enzyme-mediated hydrogelation is a recent popular approach for this purpose because of the mild crosslinking reaction conditions and compatibility with drugs, therapeutic proteins, and living cells[4,5]. As a relatively recent concept, several enzymes have been found to perform advanced hydrogelation in scaffold design[6]. Because horseradish peroxidase (HRP)-mediated crosslinking provides mild gelation conditions (e.g., physiological conditions), it is one of the best studied enzymes to trigger hydrogelation in a variety of biomedical applications including tissue engineering[7,8] and a range of natural and synthetic polymers have been designed for HRP-mediated crosslinking[9].

Properly functionalized 4-arm polyethylene glycol (PEG) is widely employed as a base polymer for hydrogelation[10]. The incorporation of bioactive factors into scaffolds should facilitate cells to adhere and grow[11]. Recently, our group developed an HRP-catalyzed gelation system to prepare a redox-responsive PEG-based hydrogel

consisting of a thiolated synthetic polymer. Formation of the disulfide bonds proceeds by simply mixing thiolated 4-arm PEG (PEG-SH), HRP, and small phenolic compounds without exogenous addition of H_2O_2[12]. This hydrogelation system is cytocompatible and could prepare 3D spheroids of human liver cancer (HepG2) cell line[13] or fabricate a 2D cell monolayer (i.e., cell sheet[14]) of fibroblast (L929) cells using the bioactive hydrogel co-crosslinked with PEG-SH and thiolated gelatin (Gela-SH)[15]. Gelatin-based materials are an excellent bioactive compound to support the proliferation of cells with correct biological signals for cellular activity[16]. Gelatin is also suitable to sustain cellular adhesion and proliferation, because it contains the cellular binding motif Arg-Gly-Asp (RGD)[17]. Gelatin itself, has been extensively studied and widely used in a range of hydrogel scaffolds because of their biocompatibility and biodegradability[18]. In addition, chemically modified gelatin was employed to tune mechanical properties of hydrogel[19]. Nevertheless, the incorporation of bioactive signaling compounds into hydrogel networks to mimic an ECM should expand the properties of this simple HRP-mediated hydrogelation system to the formation of engineered tissues[20].

In addition to the increase in cellular adhesion that is closely related to cell-cell and cell-matrix interactions, growth factors (GFs) influence cell behaviors markedly. In well-established cell culture techniques, because of the fast degradation of signaling compounds, which reduces their stimulation, periodic addition of GFs to culture medium is mandatory[21]. However, GFs solely in medium can reduce their bioactivities because of the difficulty in conserving their native state and controlling the orientation for adequate interaction with target receptors. However, immobilization of GFs on a substrate for direct contact to the cell surface is presumed to decrease downregulation of cell receptors and support intracellular signal transduction[22]. A simple method to

provide biomimetic functionality in a PEG-SH-based hydrogel is to introduce another polymeric component that accommodates GFs in the hydrogel network. Heparin is a highly sulfated, anionic polysaccharide of repeating disaccharide (1,4)-linked glucosamine and uronic acid residues and know to bind GFs[23]. Importantly, it protects GFs from denaturation and enzymatic degradation *in vivo.* I thus selected heparin as a bioactive component to capture basic fibroblast growth factor (bFGF), because it accelerates the regeneration of several tissues such as skin, bone, cartilage, and nerves. bFGF is also a potent mitogen and chemotactic factor for human fibroblasts[24]. The first report on the heparin immobilization into hydrogel by Tae and coworkers[25] was followed by a broad-spectrum of studies[26,27]. The incorporation of heparin was accomplished either via covalent conjugation or via non-covalent interaction to the polymeric network in hydrogel[25,28].

As shown above, both gelatin and heparin have been actively incorporated in hydrogels to acquire the superior intrinsic feature such as cellular adhesiveness and immobilization of bioactive molecules. However, only a specific combination of gelatin and heparin has been used so far (for example, type-A gelatin and heparin[29] or type-B gelatin and heparin[30]). To the best of our knowledge scientific and systematic comparison has not been available on the combined use of gelatin and heparin in HRP-mediated preparation of PEG-based hydrogels.

In this manuscript, our goal was to develop a simple but effective method to manufacture PEG-SH-based hydrogels functionalized with various biochemical properties, cellular attachment (Gela-SH), and a GF-capturing ability (Hepa-SH) to enhance cellular adhesiveness and proliferation. The gelatin type that can maintain physical and biological properties of hydrogel is explored. I also hypothesize that thiolation chemistry via HRP-mediated hydrogelation allows the stable incorporation

of gelatin and heparin into hydrogels, leading to accelerate formation of higher order cellular aggregates.

Here, the effect of combined incorporation of different type of Gela-SH and Hepa-SH into PEG-based hydrogels on adherent cell culture is systematically evaluated. Evidently, the type of gelatin strongly affected the biological activity of hydrogels. Specifically, thiolated type-B gelatin had much higher compatibility with Hepa-SH compared with thiolated type-A gelatin, resulting in a shorter gelation time and higher storage modulus of hydrogels observed in physicochemical characterization. Finally, incorporation of GFs into dual functionalized hydrogels under optimized conditions was validated by the proliferation and morphological change of NIH-3T3 cells and HUVECs seeded on the hydrogels and accelerated formation of 2D cellular sheets for cell sheet-based tissue engineering.

2.2 Experimental

2.2.1 Materials.

PTE-200 SH (Sunbright®) {4arm PEG, -$[(CH_2)_2$-SH$]_4$, MW 20 kDa} was purchased from NOF Corporation (Tokyo, Japan). Glycyl-L tyrosine hydrate and 1-ethyl-3-(3 dimethyl aminopropyl) carbodiimide (EDC) were purchased from Tokyo Chemical Industry (Tokyo, Japan). HRP (100 U/mg), 1,4-dithiothreitol (DTT), and heparin sodium salt (200 U/mg, MW 15 kDa) were purchased from Wako Pure Chemical Industries (Osaka, Japan). 1-Hydroxybenzotriazole (HOBt) was purchased from Watanabe Chemical Industry (Hiroshima, Japan). Gelatin from porcine skin (type A, acid-treated gelatin) and gelatin from bovine skin (type B, alkaline-treated gelatin) were purchased from Sigma Aldrich. 5,5′-Dithiobis (2-nitrobenzoic acid) (DTNB) and a Cellstain-double staining kit were purchased from Dojindo (Kumamoto, Japan).

NIH3T3 mouse fibroblasts was obtained from the Riken Cell Bank (Tsukuba, Japan), and human umbilical vein endothelial cells (HUVECs) was purchased from KURABO (Osaka, Tokyo). Recombinant human basic fibroblast growth factor (bFGF, RSD) was acquired from Funakoshi (Tokyo, Japan). Trypan blue (0.4%), minimum essential medium (MEM), GlutaMAX™-I, and 10% fetal bovine serum (FBS) were purchased from Thermo Fisher Scientific (Waltham, USA). Cysteamine (2-mercaptoethylamine hydrochloride), cystamine, 1% antibiotic-antimycotic, trypsin 0.25%/1 mM EDTA, and Dulbecco's phosphate buffered saline [D-PBS (-)] were purchased from Nacalai Tesque (Kyoto, Japan). EGM-2 supplemented with FBS, hydrocortisone, growth factors, such as bFGF, VEGF, R3-IGF-1, and hEGF, ascorbic acid, and GA-1000 was supplied by Lonza (Walkersville, USA). Human FGF DuoSet ELISA kit was acquired from R&D systems (Minneapolis, USA). Milli-Q® water was used in experiments.

2.2.2 Synthesis of Hepa-SH and Gela-SH.

Briefly, heparin was dissolved in Milli-Q water at 10 mg/mL, and then EDC and HOBt were added. The molar ratio of reactants was 1:1:1:2 (heparin:HOBt:EDC: cysteamine)[25,31]. The pH of the reaction mixture was adjusted to 6.8 with 0.1 M NaOH and/or HCl solutions, and the reaction was allowed to continue for 5 h with stirring at room temperature. Then, a 10-fold molar excess of DTT (moles per COOH of heparin) was added to reduce the disulfide groups and generate free thiol groups. The reaction was performed for 3 h at pH 7.5 that was adjusted to pH 3.5 by addition of 1 N HCl. The solution was dialyzed against HCl (pH 3.5) containing 100 mM NaCl, followed by lyophilization. Gela-SH was prepared by following the protocol in our previous study[15]. Free thiol groups in gelatin samples were measured by Ellman's reagent assay. DTNB reacted with a free sulfhydryl group to yield a mixed disulfide and 2-nitro-5-thiobenzoic acid (TNB). The absorbance of Gela-SH samples was measured with a microplate

reader (Power Wave X, Bio-Tec Instruments Inc., USA) at 412 nm. A cysteine solution was used to estimate free thiols. A calibration curve to quantify free thiol groups was obtained by measuring the absorbance of known concentrations of cysteine solutions (Fig. 2.1). Hereafter, Gela-SH samples obtained from type A and B gelatin are abbreviated as Gela(A)-SH and Gela(B)-SH, respectively.

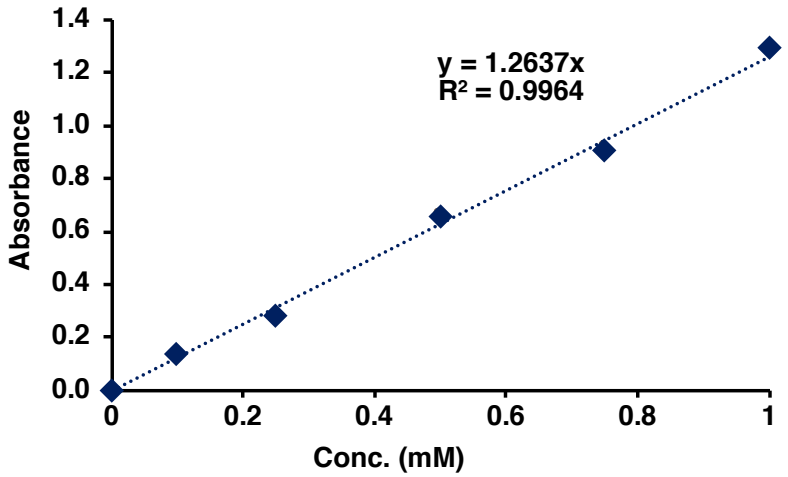

Fig. 2.1. Calibration curve obtained by measuring the absorbance of the cysteine solution.

2.2.3 Arginine density of gelatin.

The amount of free arginine side chains is measured using a fluorometric technique adapted from previous studies[33,34]. The arginine density in Gel-SH (from bovine or porcine gelatin) was quantified by reacting arginine groups with 9,10-phenanthrenequinone to produce a fluorescent compound. Several diketo compounds, such as 2-amino-1*H*-phenanthrol[9,10-*d*] imidazole and 9,10-phenanthrenequinone, form a stable fluorescent compound upon reaction with arginine. 9,10-phenanthrenequinone has been shown to react with arginine and related compounds containing quanidinium groups. Briefly, 1 mg/mL gelatin or gel-SH was mixed with 300 µL of an ethanol solution of 9,10-phenanthrenequinone (150 µM) and 50 µL of an NaOH aqueous solution (2 N). The mixture was incubated at 60 °C in the dark for 3 h. Then, 200 µL of the gelatin solution was mixed with 200 µL HCl (1.2

N), and the mixture was allowed to stand at room temperature in the dark for 1 h. Fluorescence emission of the mixture was measured at 355 nm with an excitation wavelength of 312 nm by a LS-55 spectrofluorometer (Perkin Elmer, USA).

2.2.4 Heparin loading amount in hydrogel system.

The incorporation of Hepa-SH in the hydrogels was evaluated by using Toluidine blue O (TBO) assay[35]. After hydrogelation and incubation for 6 h at 37^{o}C, PEG/Gela/Hepa hydrogels were washed twice in phosphate buffered saline PBS (PBS) for five minutes each. After the second wash, 10 mM of Cys were added to PEG/Gela/Hepa_hydrogels and incubate for 30 min. Subsequently, the sol solutions were recovered for the further TBO assay (0-day samples). While, other PEG/Gela/Hepa_hydrogels were immersed in PBS for 24 h at 37^{o}C and after one day of incubation, the hydrogels were degraded with 10 mM Cys for 30 min at 37^{o}C. The recovery solutions were collected for the further TBO assay (1-day samples). The incorporation of Hepa-SH in hydrogel system at the 0-day and after one day incubation (1-day) were evaluated by TBO assay. The final results of Hepa-SH grafting efficiency were evaluated by comparing the Hepa-SH density ($\mu g/cm^2$) at 0 and 1 day to initial amount of Hepa-SH in hydrogel system.

Detailed procedure of Hepa-SH detection by Toluidine blue assay as follow.

Briefly, 0.04 wt.% TBO solution was prepared by dissolving the TBO powder in aqueous 0.01 M HCl/0.2 wt.% NaCl, and then the samples were incubated in 5 ml TBO solution under static conditions at 37 ^{o}C for 4 h and rinsed three times with UP water. Subsequently, the Hepa–TBO complex that formed on sample surface was eluted and dissolved in 5 ml 80% ethanol/0.1 M NaOH mixture (4/1 v/v) solution. Ultimately 150 μl of the supernatant was transferred to a 96-well plate and the

absorbance was measured at 530 nm by a microplate reader and the Hepa-SH density on the sample surface was evaluated using a calibration standard curve.

For standard curve preparation, 2 ml 0.04 wt.% TBO was first added to 2 ml of a known concentration Hep solution (0.0001%-0.1% of Hepa-SH) and incubated at 37 ^{o}C with gentle shaking for 4 h, the Hepa-SH--TBO complex spontaneously formed and precipitated in the mixture. Then the mixture was centrifuged at 3500 rpm for 10 min, the supernatant was removed, and the precipitate was carefully rinsed twice with aqueous 0.01 M HCl/0.2 wt.% NaCl. Finally, 5 ml 80% ethanol/ 0.1 M NaOH mixture (4/1 v/v) solution was added to dissolve the precipitate and the absorbance was measured at 530 nm.

2.2.5 Fabrication of hydrogels.

The hydrogel was prepared by HRP-mediated crosslinking of thiolated polymers with a slight modification[13,15]. In brief, 4-arm PEG-SH (5%, w/v), Gela(A)-SH, or Gela(B)-SH (0.1%, w/v) and Gly-Tyr (5 mM) were dissolved in phosphate buffered saline (PBS) (pH 7.4). Hepa-SH (0–0.1%, w/v) and bFGF (1–100 ng/mL) were mixed, and then the solution was added to the above solution. Subsequently, the aqueous solution of HRP (5 U/mL) was added to the mixture, followed immediately by gentle pipette mixing. The reaction and hydrogelation proceeded by incubation at 37 °C for 6 h. Hydrogels are abbreviated as follows: PEG_hydrogel is the base PEG-SH hydrogel; PEG/Gela_hydrogel is the PEG-SH hydrogel with Gela-SH; PEG/Gela/Hepa_hydrogel is the dual functionalized PEG-SH hydrogel with both Gela-SH and Hepa-SH.

The physical properties of hydrogels formed using different types of Gela-SH were evaluated. The hydrogels contained PEG-SH (5%), Gly-Tyr (5 mM), HRP (5 U/mL), Hepa-SH (0.01, 0.05%, and 1%), and different types of gelatin [Gela(A)-SH or Gela(B)-

SH] at a fixed concentration (0.1%). The concentrations of Hepa-SH and Gela-SH were optimized. The gelation time, fibroblast proliferation, and immobilization of bFGF were evaluated. The hydrogel was fabricated by addition of Hepa-SH (0–1%) and bFGF (1, 10, and 100 ng/mL), and cell morphology assessment was performed.

2.2.6 Measurement of gelation time and rheological properties.

The gelation time of the hydrogel precursor solution was determined by a stirring magnet bar method[12,36]. Each sample was dissolved in PBS (pH 7.4). The polymer solution was transferred into a 48-well plate (Iwaki, Tokyo, Japan) at 200 μL/well, and the mixtures were stirred at 200 rpm using magnetic stirrer bars (length: 7 mm; width: 3 mm). The effects of the different Gela-SH types and Hepa-SH concentrations were evaluated at constant concentrations of Gly-Tyr (5 mM) and HRP (5 U/mL). Finally, the sol-gel transition time when a stirrer bar in the gel did not move was recorded as the gelation time.

Viscoelastic properties of the hydrogels were evaluated by rheological measurements on a MCR302 rheometer (Anton Paar, Graz, Austria) using a cone plate (diameter: 25 mm; 2.003°) in the oscillatory mode (EMS/TEK 500 disposable dishes). First, 1500 μL of the hydrogel solution was poured onto rheometer stage (PP50-SN31036). After the hydrogelation by incubation at 37 °C for 6 h. the measurement was started. The frequency and strain were set at 0.1 Hz and 0.1%, respectively. The measurement was allowed to proceed until the storage modulus (*G'*) reached the equilibrium value.

2.2.7 Swelling behavior of PEG/Gela/Hepa_hydrogels.

The hydrogels contained PEG-SH, Gela-SH, Gly-Tyr, and HRP at 5% (w/v), 0.1% (w/v), 5 mM, and 5 U/mL, respectively. Gela(A)-SH and Gela(B)-SH were used. The hydrogels were shaped into a disk (diameter: ~1.5 cm; thickness: 3 mm) and incubated

in 10 mL PBS (pH 7.4) at 37 °C for 4 days to reach equilibrium. The mass of the hydrogels was measured after swelling (M_S). The hydrogels were then dried in an oven and their dry masses (M_D) were measured. The equilibrium swelling ratio (Q_M) was calculated after excluding the effect of the weight of solutes in PBS according to Eq[37].

2.2.8 ζ-potential measurements.

The ζ-potentials of gelatin and heparin in Milli-Q water were estimated using a Zetasizer Nano ZSP (Malvern Instruments Ltd., Worcestershire, UK). The heparin and gelatin concentration were 0.1%, temperature was set at 25 °C, and the ζ-potential was measured at pH 7.4 using a DTS1070 folded capillary cell.

2.2.9 Adhesion and proliferation of cells on hydrogels.

Cell adhesion was measured to evaluate the effect of Gela-SH in the PEG-SH-based hydrogel. The polymer solution (250 μL) was prepared in a 24-well culture plate. The hydrogel was supplied with minimum essential medium (MEM) containing 10% fetal bovine serum (FBS) and a 1% antibiotic-antimycotic solution. Then, the cells were seeded on the hydrogel sheets at 5×10^4 cells/cm^2 to evaluate cell adhesiveness after 6 h. To this end, the cells were rinsed with 500 μL D-PBS(-) and recovered by trypsin treatment (200 μL). The number of adherent cells was then determined. The proliferation assay was performed in a 24-well culture plate. The cells were seeded on hydrogel sheets at 5×10^3 cells/cm^2. The medium was changed after 1 day of incubation, and the number of cells was evaluated after 3 days of incubation. Cell viability on the hydrogel was determined by a trypan blue counting method. The cells were collected by trypsin treatment (5 min) and stained with 0.4% trypan blue and live cells were determined by an automated cell counter (Bio-Rad, USA).

Cellular proliferation on PEG/Gela_hydrogel with or without Hepa-SH was evaluated using NIH3T3 cells. First, we evaluated the effect of the Gela-SH type in the

presence of Hepa-SH on cell proliferation, the proliferation of NIH3T3 cells was determined by the trypan blue counting method. Various concentrations (0, 0.01%, 0.05%, and 0.1%) of Hepa-SH in hydrogels were used in the absence of bFGF. The effect of Hepa-SH was evaluated in the presence of bFGF, concentrations of Hepa-SH were 0.00001%–1% with 10 ng/mL bFGF. Then, the effect of the bFGF concentration (1, 10, and 100 ng/mL) on cell proliferation was evaluated under the optimized concentration of Hepa-SH (0.01%) using a WST-8 assay for 7 days of culture.

Live/dead staining was performed to evaluate cell viability in hydrogels using a Cellstain Double Staining Kit (Dojindo Laboratories, Tokyo, Japan). After 1 and 7 days of culture, the cell-laden hydrogel disks were washed with PBS and incubated in serum-free medium containing calcein-AM (2 μM) and propidium iodide (4 μM) for 15 min. Then, the live and dead cells in the interior areas of hydrogels were observed under a fluorescence microscope (BZ-9000, Keyence, Osaka, Japan). To characterize cell morphology, cells were stained with calcein-AM. Then, the cell length and area were quantified by NIH Image Software (Free software for Mac OS X, National Institutes of Health, Bethesda, Maryland)[38]. Results were obtained from 100 cells.

2.2.10 Immobilization strategies of growth factors.

GFs were added to hydrogels by two strategies. NIH3T3 cells and HUVECs (5×10^3 cells/cm^2) were used to validate the strategies. The first strategy was in situ immobilization of GFs in the PEG/Gela/Hepa_hydrogel, where GFs were immobilized in the hydrogel (strategy I). The second strategy was surface immobilization by physical adsorption of GFs into the PEG/Gela/Hepa_hydrogel, where GFs were added to the hydrogel surface before seeding cells (strategy II). Details of the two strategies are shown below (Fig 2.2).

Strategy I: The hydrogel consisted of PEG-SH (5%), Gly-Tyr (5 mM), HRP (5 U/mL), Hepa-SH (0.01%), Gela(B)-SH) (0.1%), and 10 ng/mL GF(s) with a final volume of 250 μL/well. In NIH3T3 cell culture, bFGF was used as the single GF. bFGF (25 μL) was added and then mixed into the hydrogel before gelation. In HUVEC culture, 25 μL of GFs including bFGF, VEGF, R3-IGF-1, and hEGF were incorporated into the hydrogel at a ratio of 4:1:1:1, respectively. Then, other supplements (hydrocortisone, ascorbic acid, and GA-1000) were dispersed in endothelial basal medium-2.

Strategy II: After hydrogelation, 25 μL GF was mixed with 75 μL PBS and immobilized on the hydrogel surface by 4 h of incubation at 4 °C. Then, NIH3T3 cells and HUVECs at the same density were seeded on the hydrogel.

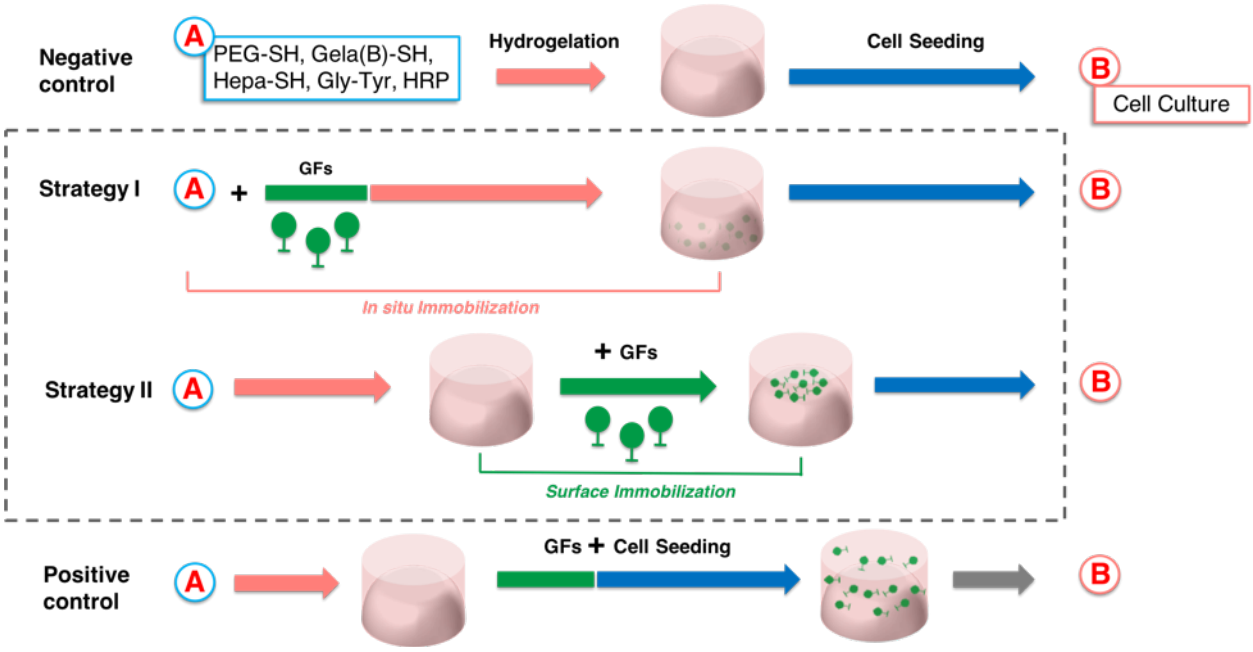

Fig 2.2 Schematic illustration of growth factor immobilization strategies. Reproduce with permission from ref[32].Copyright 2019 American Chemical Society.

In positive control experiments, we used the conventional method for cell culture[39]. The soluble forms of GFs were dissolved in the basal medium. The medium was changed on the second day. In negative control experiments, cell seeding on hydrogels without GFs was performed. Cell number evaluation for 7 days of culture

was conducted to evaluate GF immobilization in the hydrogel-based cell culture system. The loading amount and release profile of bFGF from PEG/Gela/Hepa_hydrogel was evaluated by an ELISA for 7 days.

2.2.11 Antiproliferative effects of native heparin and Hepa-SH.

Heparin inhibition was evaluated by comparing fibroblast proliferation on hydrogels with different heparin concentrations by the initial cell number on a hydrogel without heparin incorporation. The hydrogels consisted of PEG-SH, Gly-Tyr, Gela(B)-SH, Hepa-SH, and HRP. The concentrations of Hepa-SH were 0.00001%–1% (w/v) (AT). All materials were mixed and added to a 96-well plate, followed by incubation for 6 h. Cells were then seeded at 1×10^4 cells/well. Serum-free medium was used for cell culturing. Three days later, fibroblasts were counted by an automated cell counter TC 20 (Bio-Rad, Singapore) using a dual chamber counting slide and trypan blue staining (0.4%) (Gibco, USA). Experiments were performed in triplicate. Additionally, the cell number on a hydrogel without heparin was evaluated as a control treatment (A0). The percentage of proliferation inhibition was calculated by the following equation:

$$\% \text{ Inhibition of cell proliferation} = (A0 - AT)/A0 \times 100\%$$

2.2.12 Effect of various Hepa-SH concentrations on the numbers of NIH3T3 cells treated with exogenous bFGF.

To confirm the effect of the different Hepa-SH concentration on cell proliferation with growth factor (GF) immobilization, 0.1% Gel(B)-SH and 10 ng/mL bFGF were loaded into the hydrogel system with NIHT3T cells ($5\times10^3/cm^2$). The hydrogel was prepared with PEG-SH, Gly-Tyr, Gela-SH, Hepa-SH, and HRP. The concentration of Hepa-SH ranged from 0.00001% to 1% (w/v).

2.2.13 Measurement of the loading capacity of bFGF on PEG/Gela/Hepa_ hydrogels and the release profile of bFGF from the loaded hydrogels.

The amount of bFGF loaded in PEG/Gela/Hepa_hydrogel was measured by ELISA according to a standard protocol provided by the manufacturer. Hydrogel was fabricated by using strategy I and II as mentioned in experimental section. Hydrogels obtained were washed twice with PBS, then an aqueous solution of 10 mM Cys was added. After 1 h, hydrogels were degraded, and the recovered solution was used for ELISA assay. The loading capacity of bFGF (%) was calculated by comparing the amount of bFGF in the recovered solution with the initial amount of bFGF in PEG/Gela/Hepa_hydrogel.

To check the release profile of bFGF, the amount of bFGF in medium at 0, 1, 2, 3, 6, 24, 48, 72, 96, 120, 144 and 168 h culture time (7 days) are measured. The amount of bFGF in medium (MEM) was compared with the initial amount of bFGF loaded in the hydrogel.

2.2.14 Statistical analysis.

GraphPad Prism 6 (GraphPad Software, La Jolla, CA, USA) was used for statistical analysis and the data expressed as a mean±standard deviation (SD). One-way analysis of variance was used to assess the gelatin type or heparin concentration in terms of hydrogel properties. Significant differences were analyzed by the Tukey's HSD post-hoc test for multiple comparisons.

2.3 Results and discussion

2.3.1 Synthesis and characterization of dual functionalized hydrogels

Because cellular adhesiveness is affected by the chemical and physical properties of hydrogels[40], basic characteristics of the PEG/Gela_hydrogels were evaluated by

varying the type of gelatin, (Gela(A)-SH or Gela(B)-SH). In addition, the effect of Hepa-SH in PEG/Gela_hydrogels on gelation time, charge compatibility, storage modulus, and equilibrium swelling ratios of hydrogels are assessed.

First, Hepa-SH and Gela-SH were synthesized by EDC chemistry. To prepare Hepa-SH, the molar ratio of heparin (-COOH), HOBt, EDC, and cysteamine was set at 1:1:1:2 according to a previous report showing that the resultant Hepa-SH has sufficient fibrinogen adsorption and anticoagulant activity[27]. The incorporation of Hepa-SH in the hydrogels by using Toluidine blue O (TBO) assay was confirmed. The incorporation of Hepa-SH in hydrogel system at the 0-day and after one day incubation (1-day) were evaluated by TBO assay. The results of Hepa-SH grafting efficiency were evaluated by comparing the Hepa-SH density (μg/cm^2) at 0 and 1 day to initial amount of Hepa-SH in hydrogel system (Fig. 2.3).

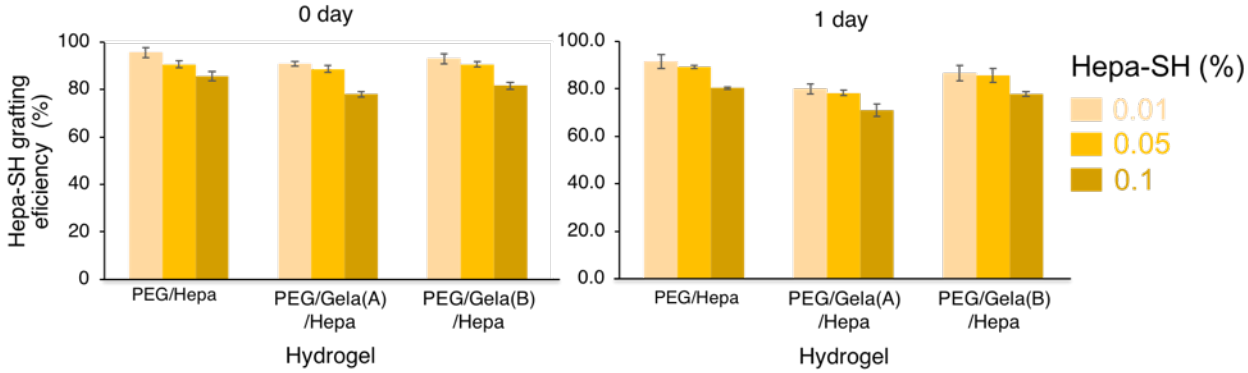

Fig. 2.3. Hepa-SH grafting efficiency profile on different concentration of Hepa-SH and gelatin type by TBO assay evaluation (mean ± SD, *N=4*).

From the Fig.2.3, more than 90% of heparin was incorporated to all the hydrogel at the 0.1% Hepa-SH after hydrogelation (i.e. at 0 day). Even after 1-day incubation, PEG/Gela(B)/Hepa_hydrogel retained more than 90% of the initial heparin loaded.

To prepare Gela-SH, two types of gelatin, acid-treated porcine gelatin and alkaline-treated bovine gelatin were used. The amounts of thiol groups modified in porcine gelatin [Gela(A)-SH] and bovine gelatin [Gela(B)-SH] were *ca.* 0.39 and 0.50 mmol-

SH/g-gelatin, respectively (Fig. 2.2). The results were comparable with those obtained in our previous report[15]. In addition, regardless of the type of gelatin, the chemical modification with thiol groups showed little change in arginine contents (Fig. 2.4).

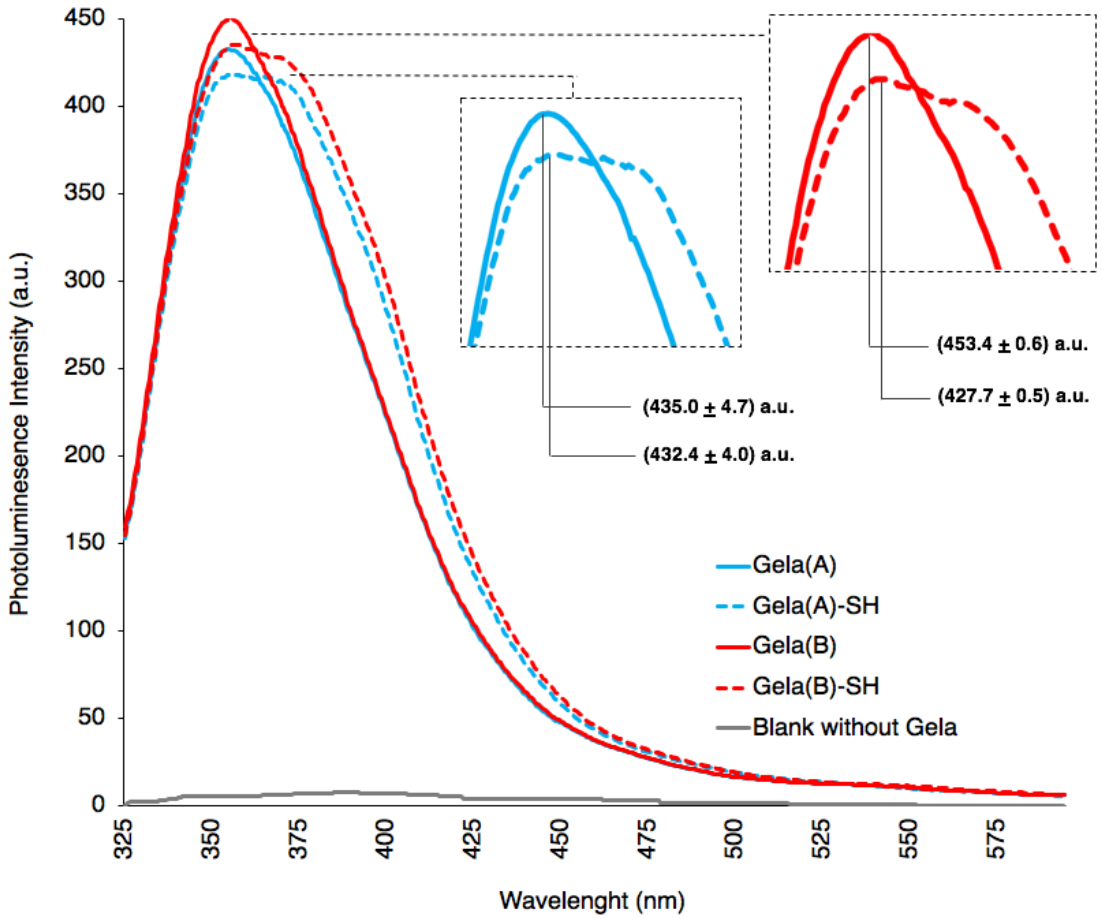

Fig. 2.4. Arginine density-photoluminescence spectra of 9,10-phenanthrenequinone after reacting with native gelatin and thiolate gelatin. Reproduce with permission from ref[32]. Copyright 2019 American Chemical Society.

The circular dichroism (CD) spectroscopy to characterize the secondary structure and compare Gela(A), Gela(B) and the thiolated forms (Gela(A)-SH and Gela(B)-SH) were conducted (Fig 2.5). The CD spectra of Gela(A) and Gela(B) showed different peaks, a negative peak at 208 nm (Gela(A)) and 213 nm (Gela(B)) which would have the different random coil conformations between the gelatin type. After thiolation, Gela(A)-SH and Gela(B)-SH revealed the altered spectral shape with different peak positions at 214 nm and 218 nm, respectively.

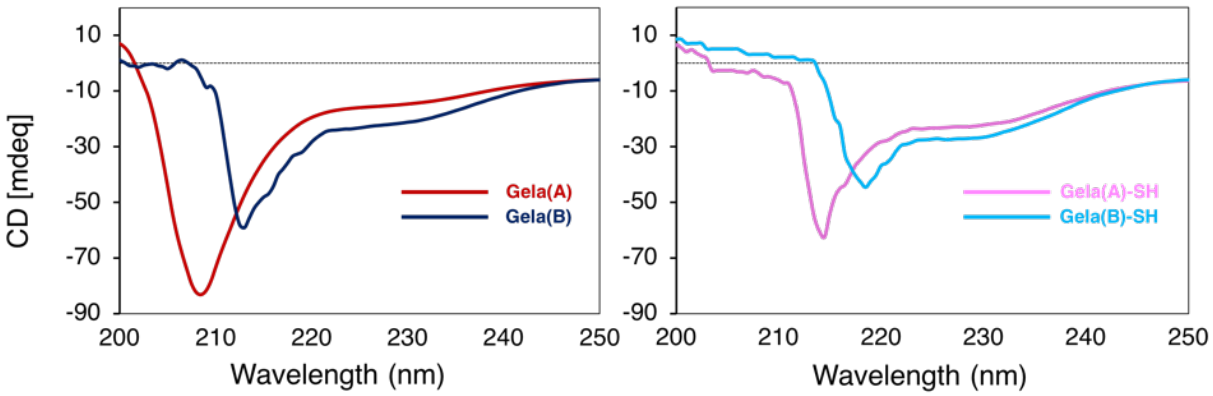

Fig. 2.5. Effect of thiolation on different gelatin type by circular dichroism (CD) profile in the wavelength region from 200-250 nm. All gelatin concentrations were 0.1 (% wt).

Gelation time of PEG_hydrogels was significantly decreased in the presence of Gela-SH (Fig. 2.6-A). PEG/Gela(B)_hydrogels exhibited the shortest gelation time (23.3 ± 0.8 min). This result might be due to the difference in the thiol groups number of Gela(A)-SH and Gela(B)-SH. In particular, Gela(B)-SH, which has higher thiol groups contents, which mainly contributes to the stability of network formation and increasing cross linking density, resulting in a shorter gelation time of hydrogels.

The gelation time was significantly increased when dual functionalized PEG/Gela/Hepa_hydrogels were prepared with 0.1% Gela(A)-SH and 0.05% Hepa-SH (Fig. 2.6-B). In contrast, the effect of Hepa-SH on the gelation time was not significantly altered and increased slightly at 33–45 min when combined with Gela(B)-SH.

The ζ-potential measurements showed that Hepa-SH was negatively charged (-18.8 ± 0.6 mV), whereas Gela(A)-SH and Gela(B)-SH had slightly positive (3.8 ± 0.7 mV) and negative (-5.5 ± 0.7 mV) charges, respectively. These results indicated that electrostatic complexation between Hepa-SH and Gela(A)-SH in the aqueous mixture[41].

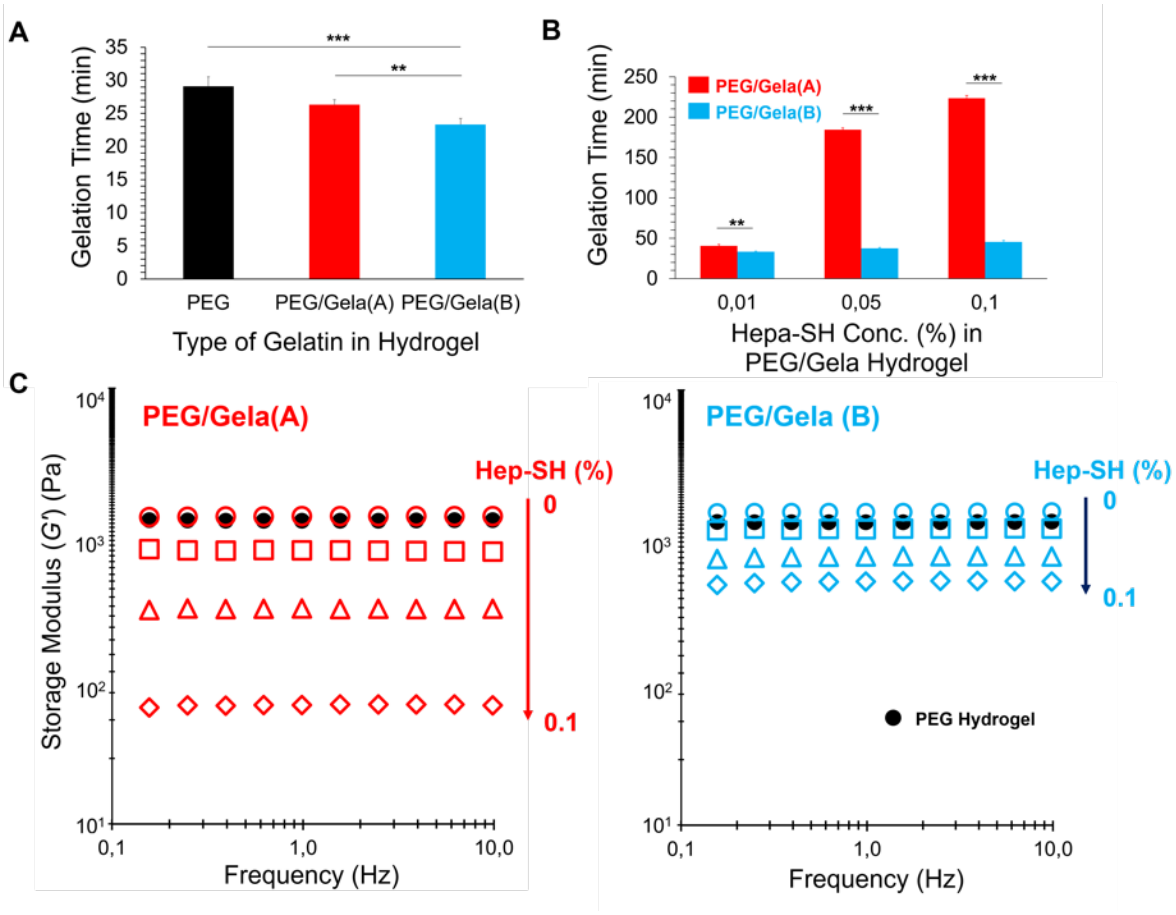

Fig 2.6. (A) Gelation time of the PEG_hydrogel and PEG/Gela_hydrogels with different types of Gela-SH (0.1%); (B) Effect of the Hepa-SH concentration on gelation time of PEG/Gela/_hydrogels; The gelation time was determined by a stirring magnet bar method. (C) Storage modulus (*G'*) of PEG/Gela(A)_hydrogels (left) and PEG/Gela(B)_hydrogels (right) with various concentrations of Hepa-SH. Black circle is PEG_hydrogel. Empty circle, square, triangle, and diamond are the PEG/Gela/Hepa_hydrogel with 0%, 0.01%, 0.05%, and 0.1% Hepa-SH, respectively. Error bars denote standard deviation (N = 3) (**p < 0.01, and ***p < 0.001). Reproduce with permission from ref[32]. Copyright 2019 American Chemical Society.

In fact, increased turbidity and precipitation were observed in the PEG/Gela(A)/Hepa precursor mixture (Fig. 2.7 [b, b1]), whereas little change was observed in the precursor solution with Gela(B)-SH even at the highest concentration of Hepa-SH (0.1%) (Fig. 2.7 [c, c1, c2]). These results suggest incompatibility of Gela(A)-SH with Hepa-SH in the preparation of a dual functionalized hydrogel, as reflected by the marked increase in gelation time.

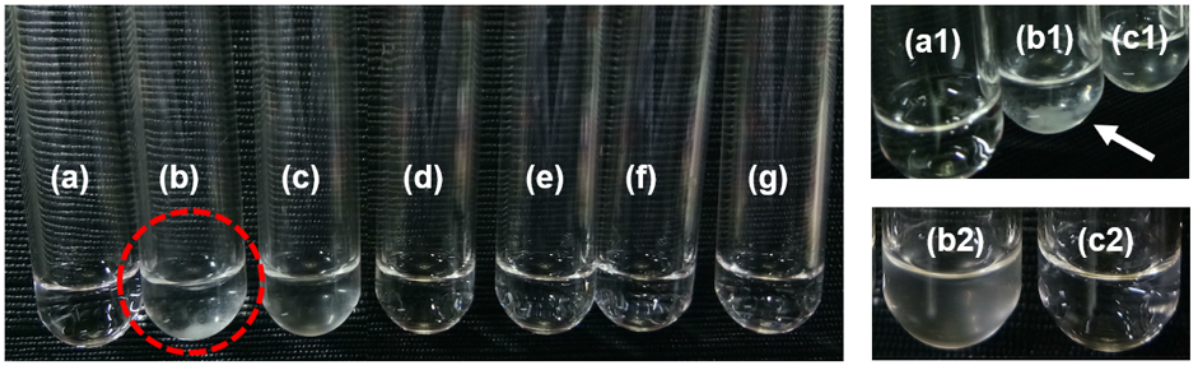

Fig. 2.7. Compatibility charge of Hepa-SH (0.1%) and Gela-SH (0.1%) in the PEG-SH hydrogel system. (a; a1) PEG_hydrogel, (b; b1) PEG/Gela(A)/Hepa_hydrogel, (c; c1) PEG/Gela(B)/Hepa_hydrogel, (d) PEG/Gela(A)_hydrogel, (e) PEG/Gela(B)_hydrogel, (f) PEG/Hepa_hydrogel, and (g) PBS. Experiments were also conducted with Hepa-SH (0.1%) and a lower Gela-SH concentration (0.01%): (b2) PEG/Gela(A)/ Hepa_hydrogel and (c2) PEG/Gela(B)/Hepa_hydrogel. Reproduce with permission from ref[32]. Copyright 2019 American Chemical Society.

The storage modulus (*G'*) of PEG/Gela(A)_hydrogels containing 0.1% Hepa-SH showed a drastic change from 2580 Pa to the lowest *G'* value (350 Pa). The same trend was observed for PEG/Gela(B)_hydrogels; however, the storage modulus was decreased steadily from ~2700 to 2291, 1703, and 1303 Pa with increasing Hepa-SH concentrations (Fig. 2.6-C).

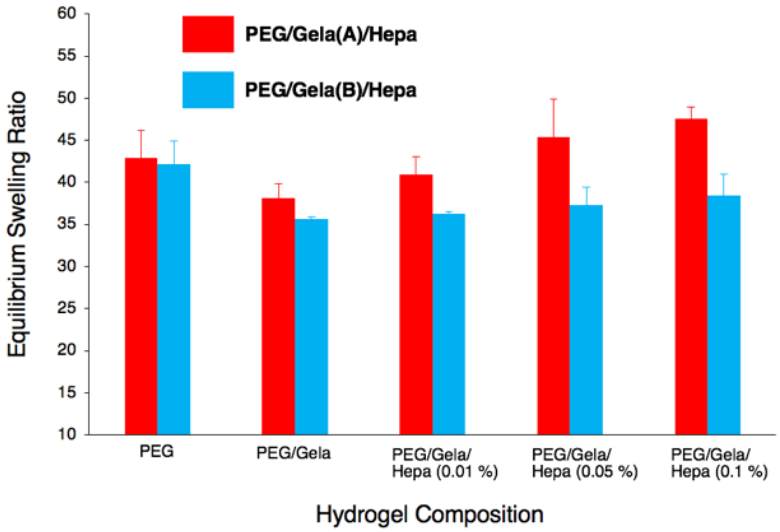

Fig 2.8. Swelling evaluation of PEG/Gela/Hepa_hydrogels with different Gel-SH types and Hepa-SH concentrations. Reproduce with permission from ref[32]. Copyright 2019 American Chemical Society.

We also evaluated equilibrium swelling ratios (Q_M) (Fig. 2.8), which related to the crosslink density of a hydrogel. The swelling ratio of the PEG/Gela_hydrogel was increased as the crosslink density was decreased, especially for PEG/Gela(A)_hydrogels. The incompatibility of Gela(A)-SH and Hepa-SH in the precursor solution may have resulted in heterogeneous crosslinking with PEG-SH, thus increasing in the sol fraction of hydrogels and affecting the physical properties[42].

Additionally, it was reported that natural type-B gelatin (Gela(B)) contained the slightly higher amount of Pro and Hyp compared with that of porcine (Gela(A)), resulting in structural differences and leading to higher sol-gel temperature. Furthermore, higher content of arginine (Fig. 2.4) and other amino acids with free hydroxyl groups (serine, threonine and tyrosine) of Gela(B) may contribute to form more hydrogen bonding than Gela(A) that will affect the physical properties of a resultant hydrogel[19,43–45].

2.3.2 Cell proliferation assay on dual functionalized hydrogels

The abilities of cells to attach, spread, and proliferate on a hydrogel are important for a cell culture scaffold. First, the adhesiveness of NIH3T3 cells on PEG/Gela_hydrogels was evaluated. NIH3T3 cells ($5 \times 10^4/cm^2$) were seeded on the hydrogels. After 6 h of incubation, almost no adherent cells were observed on the PEG_hydrogel as a negative control. In contrast, most cells had adhered on PEG/Gela_hydrogels (Fig. 2.9), indicating that incorporation of thiolated gelatin was effective to promote the adhesion of fibroblasts[15].

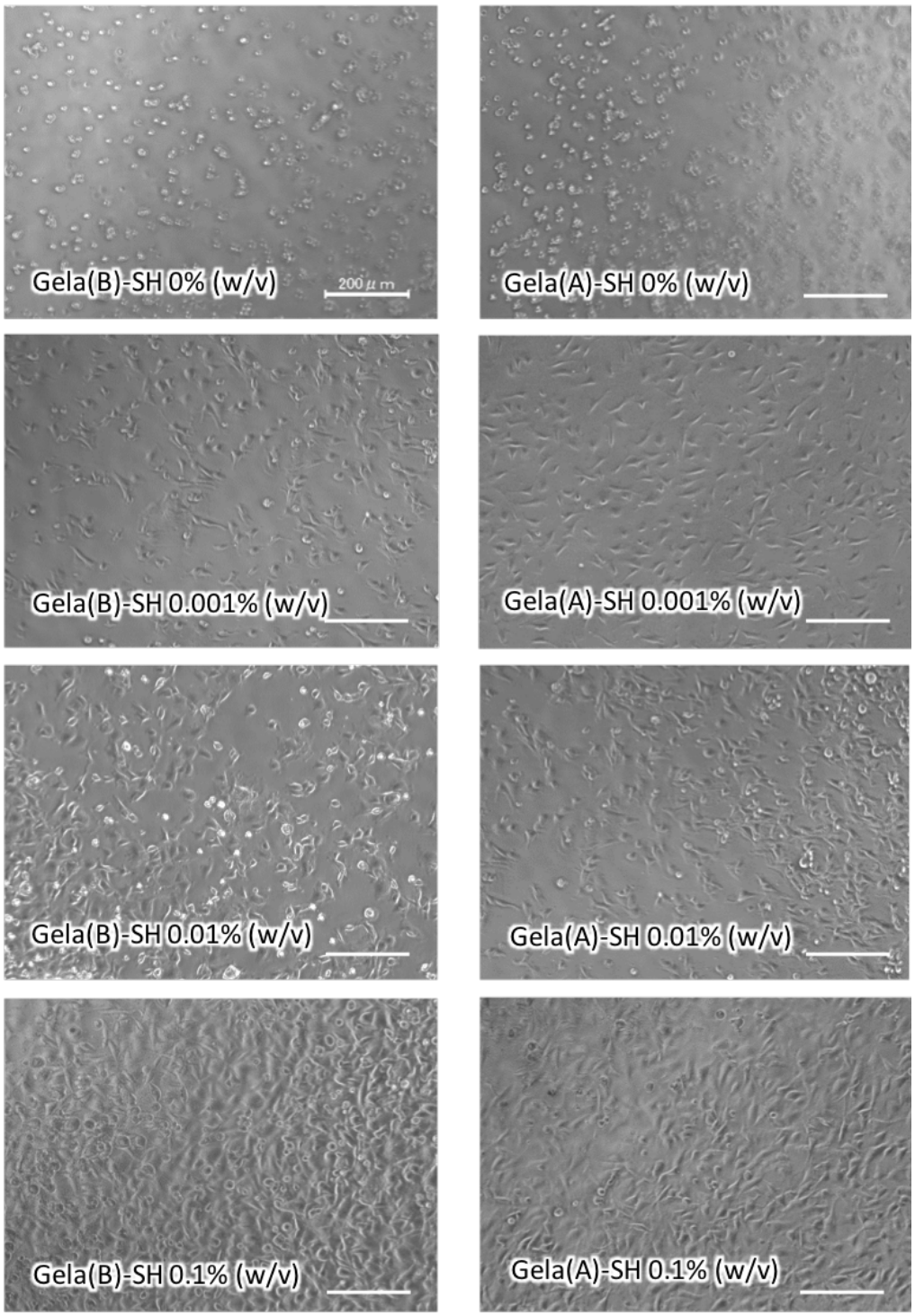

Fig. 2.9. NIH3T3 cells adhesion evaluation after 6 h of culture on PEG/Gela_ hydrogels. Reproduce with permission from ref[32]. Copyright 2019 American Chemical Society.

At the highest Gela-SH concentration (0.1%), the cell adhesion percentages were 93.2 ± 1.7% and 98.1 ± 0.7 % for PEG/Gela(A) and PEG/Gela(B)_hydrogels, respectively. Better adhesion of NIH3T3 cells on hydrogels containing Gela(B)-SH is

possibly because of the slightly higher storage modulus (G′) of Gela(B)-SH than that of Gela(A)-SH. In terms of Hepa-SH concentration, the cellular adhesiveness was more than 80% for all hydrogel prepared in the presence of 0.01 and 0.05% (w/v) Hepa-SH. However, 0.1% of Hepa-SH exhibited lower adhesiveness than other hydrogels, especially in the PEG/Gela(A)/Hepa_hydrogel (Fig. 2.10-A).

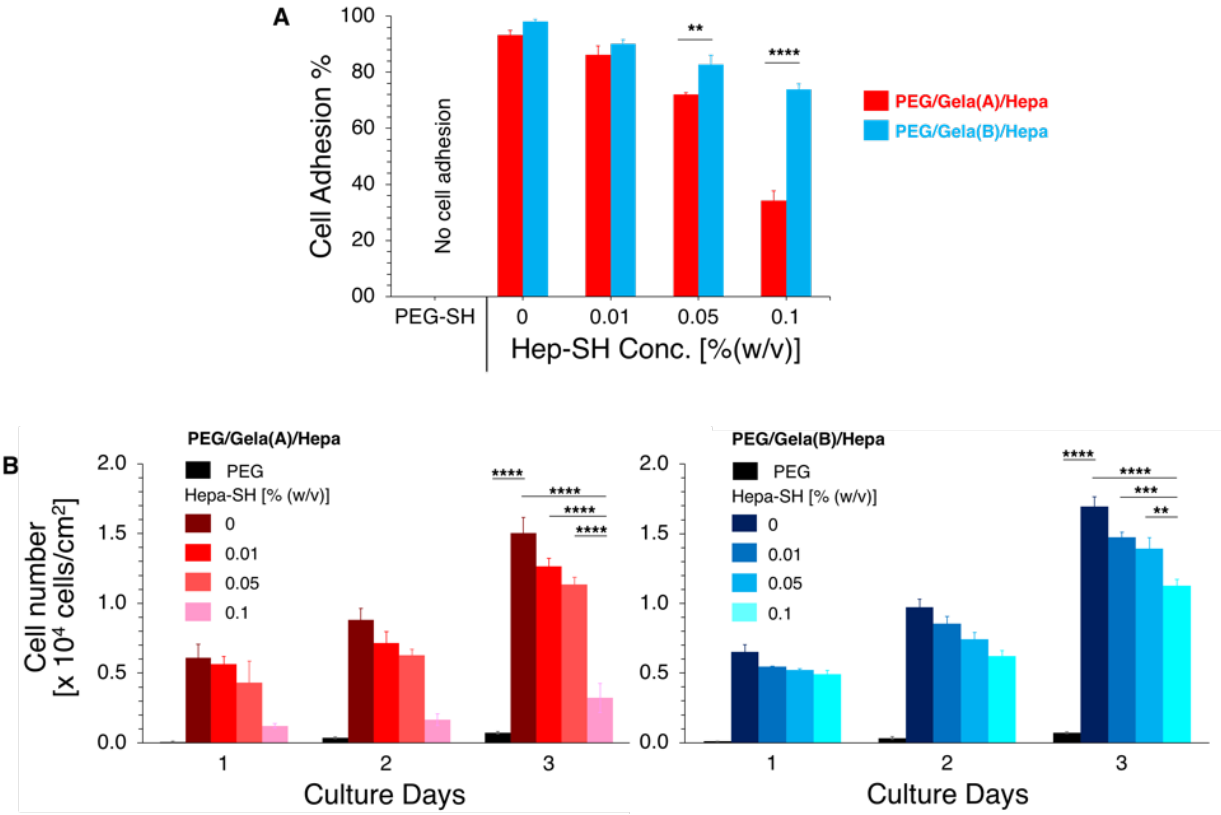

Fig. 2.10. (A) Cellular adhesiveness (cell adhesion ratio) after 6 h incubation of NIH3T3 cells and (B) Proliferation profile of NIH3T3 cells on PEG/Gela/Hepa_hydrogels. Error bars denote standard deviation (N = 3) (**p < 0.01, ***p < 0.001, **** p < 0.0001). Reproduce with permission from ref[32]. Copyright 2019 American Chemical Society.

To determine the number of cells that proliferated on PEG/Gela/Hepa_hydrogels, the cell proliferation assay was conducted. NIH3T3 cells (5×10^3/cm^2) were incubated for 3 days. Fig. 2.10-B shows that the number of proliferated cells on the hydrogels was affected by addition of Hepa-SH. PEG/Gela(B)/Hepa_hydrogels had higher cell numbers than PEG/Gela(A)/Hepa_hydrogels. Regardless of the presence of Hepa-

SH, hydrogels containing Gela(B)-SH had better affinity for cells. The trend of the decrease in cell number was more pronounced when the Hepa-SH concentration was increased in PEG/Gela_hydrogels. It has been reported that heparin has antiproliferative effects[46,47]. In fact, addition of both heparin and Hepa-SH resulted in growth inhibition (Fig. 2.11).

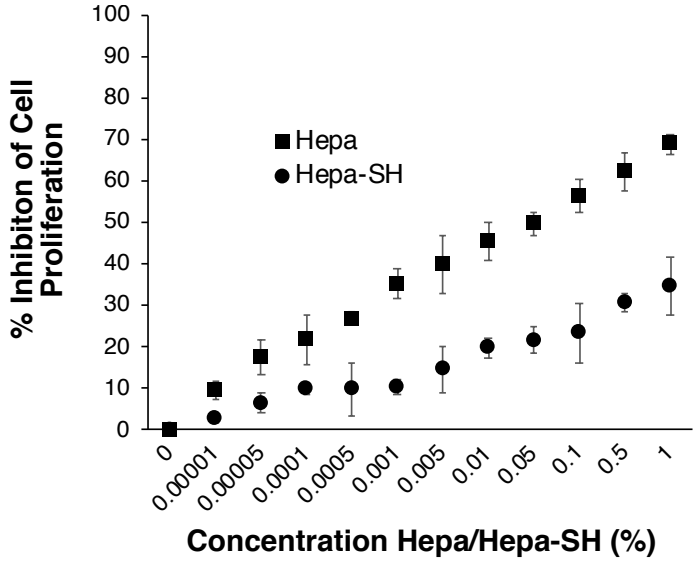

Fig. 2.11. Anti-proliferative effect of native heparin (Hepa) vs Hepa-SH in a PEG/Gela(B)/Hepa_hydrogel. Reproduce with permission from ref[32]. Copyright 2019 American Chemical Society.

A lower inhibition rate of Hepa-SH compared with that of native heparin suggested immobilization of Hepa-SH through disulfide bonds in the hydrogel, which reduced the antiproliferative effect caused by free heparin. Considering that 0.1% Hepa-SH caused about a 20% reduction in proliferation (Fig. 2.11), the marked decrease of cell number from 0.05% to 0.1% caused by Hepa-SH in PEG/Gela(A)/Hepa_hydrogel could be mainly attributed to the incompatibility between Gela(A)-SH and Hepa-SH (Fig. 2.7). Hence, Gela(B)-SH was chosen for further experiments based on the physical and biological characteristics of the resultant hydrogels.

2.3.3 In situ immobilization of bFGF in dual functionalized hydrogels

To better understand the effect of Hepa-SH on the PEG/Gela(B)/Hepa_hydrogel, the hydrogel was prepared in the presence of bFGF (10 ng/mL) and changing the Hepa-SH concentration. By following strategy I, bFGF was immobilized in situ in the PEG/Gela(B)/Hepa_hydrogel with various Hepa-SH concentrations to evaluate the proliferation of NIH3T3 cells (Fig. 2.12). A gradual increase in the cell number was observed at the lower range of Hepa-SH concentrations (up to 0.05%), implying that the binding affinity between Hepa-SH and bFGF may contribute to stabilize bFGF[48], thus increasing the cell number.

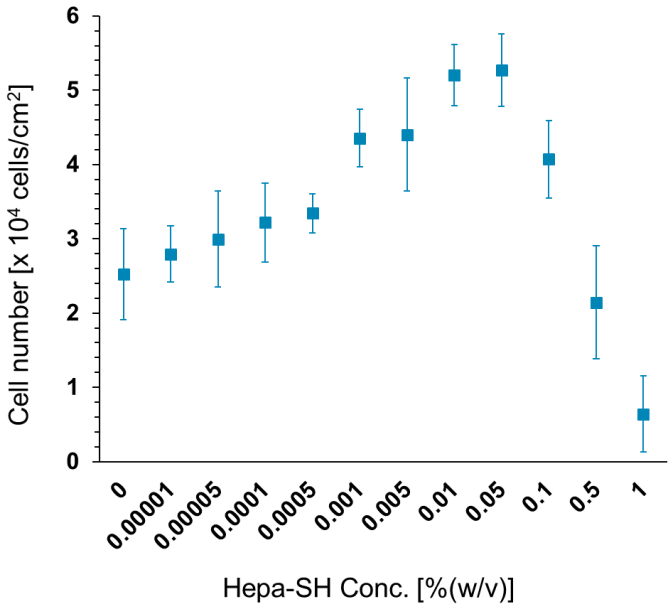

Fig. 2.12. Effect of various Hepa-SH concentrations on the numbers of NIH3T3 cells treated with exogenous bFGF (10 ng/mL). Cells were seeded on a PEG/Gela(B)/Hepa_hydrogel containing 5% PEG-SH, 0.1% Gel(B)-SH, and various concentrations of Hepa-SH. Error bars denote standard deviation (*N* = 3). Reproduce with permission from ref[32]. Copyright 2019 American Chemical Society.

Further increases in the Hepa-SH concentration (0.1%–1%) significantly decreased the cell number because of the increase in the antiproliferative effect of Hepa-SH on NIH3T3 cells[49]. Thus, 0.01% Hepa-SH was selected for the subsequent experiments.

To assess the effect of the bFGF concentration on the proliferation rate, further proliferation assays with a range of bFGF concentrations were conducted. The number of cells was increased by increasing the amount of bFGF (Fig. 2.13). Significant differences in the proliferation rate were observed among 1, 10, and 100 ng/mL bFGF after 3 day of culture with 100 ng/mL inducing the highest proliferation rate. However, no significant difference was observed in cell proliferation between 10 and 100 ng/mL bFGF after 5 days of culture.

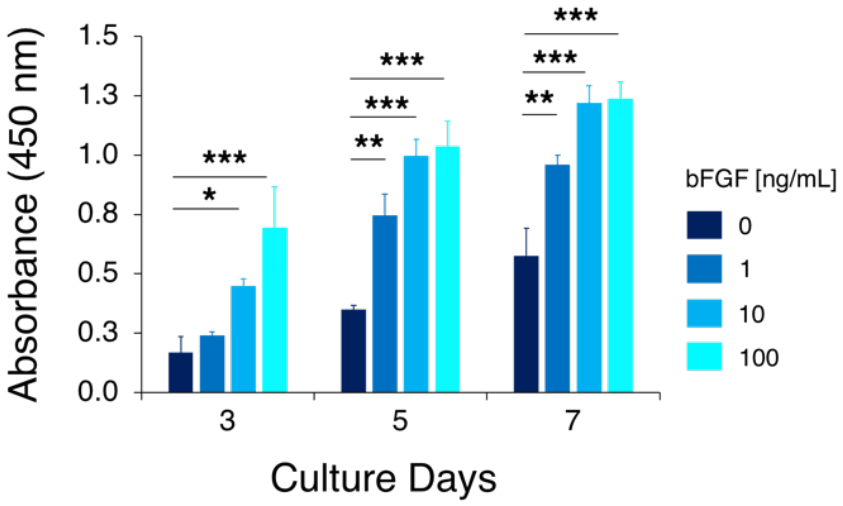

Fig. 2.13. Effect of bFGF immobilization (0, 1, 10, and 100 ng/mL) on NIH3T3 cell proliferation by WST-8 assay (based on the absorbance at 450 nm) for 7 days of culture in the PEG/Gela(B)/Hepa_hydrogel. The hydrogel contained 5% of PEG-SH, 0.1% Gela(B)-SH, 0.01% Hepa-SH, and various bFGF concentrations. Error bars denote standard deviation (N = 3) (*p < 0.05 **p < 0.01 and ***p < 0.001). Reproduce with permission from ref[32]. Copyright 2019 American Chemical Society.

To evade the inhibitory effect of Hepa-SH and bFGF at a high concentration[50], 10 ng/mL bFGF was selected as the optimal concentration for further experiments. It has been reported that, in one cell cycle, bFGF exerts a mitogenic effect on NIH3T3 cells and stimulates maximal DNA synthesis at 0.5 ng/mL[51]. By immobilization of 10 ng/mL bFGF in the dual functionalized hydrogel system, the NIH3T3 cell proliferation rate was increased by ~38% after 3 days of culture (Fig. 2.13). The rate of increase in

proliferation was comparable with that in a previous report with a bFGF-conjugated acryloyl-PEG-RGDS hydrogel prepared by photopolymerization[52].

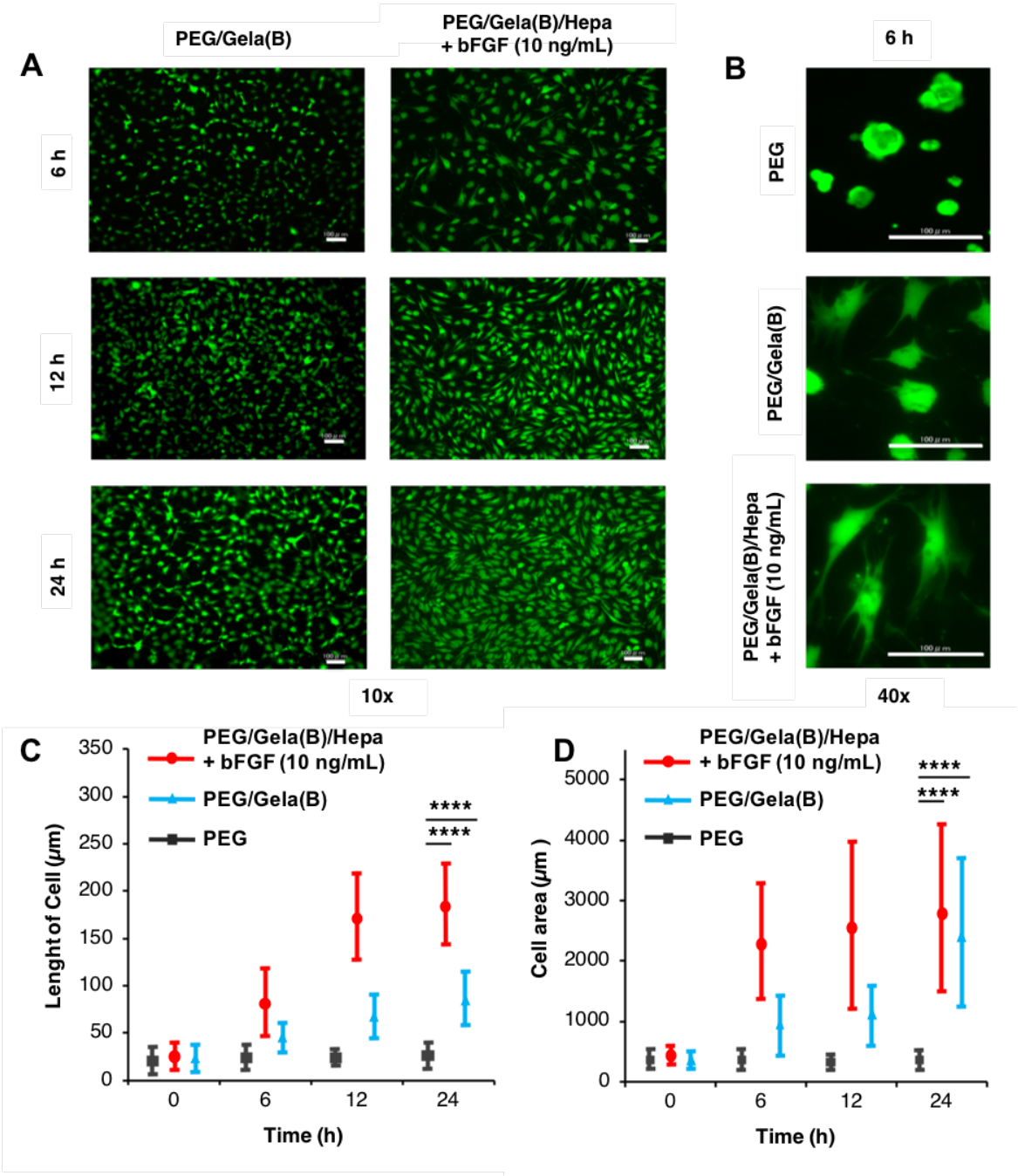

Fig. 2.14. Photographs of NIH3T3 cells cultured on hydrogels after culture for 24 h (A) and 6 h (B). Cells were stained with calcein-AM (live cells: green) and propidium iodide (dead cells: red). (C) Evaluation of the morphological change of NIH3T3 cells by average cell length (left) and (D) cell area (μm^2) (right). Cell lengths were quantified by measuring the longest end-to-end distance on a cell using ImageJ software. (N = 100, ****p < 0.0001). Scale bars in (A) and (B) are 100 μm. Reproduce with permission from ref[32]. Copyright 2019 American Chemical Society.

To gain further insights into the effects of Gela-SH and bFGF on cell proliferation, time course observations of morphological changes of the cells were performed. Fig. 2.14-A shows the dynamics of morphometric parameters of NIH3T3 cells on different hydrogels during spreading for 24 h. Because an antiproliferative activity of PEG/Gela(B)/Hepa_hydrogel without exogenous bFGF was observed (Fig. 2.11), the cellular morphology on PEG/Gela(B)_hydrogel as the standard and compared it with that on PEG/Gela(B)/Hepa_hydrogel in the presence of bFGF was used. Interestingly, significant differences in the orientation and morphology of cells were observed with co-immobilization of Hepa-SH and bFGF by strategy I (Fig. 2.14-B). It has been reported that bFGF induces a phenotype transformation of NIH3T3 cells to a thin and dendritic shape[53]. The transformation of the cell phenotype was indeed observed in the case of cells spread on PEG/Gela(B)/Hepa_hydrogels containing bFGF.

To quantitatively analyze cell spreading over time, average cell length and area were measured by NIH ImageJ software (Fig. 2.14-C). The average length of cells treated with bFGF for 6 h (84.8 μm) was longer than that of control cells (20.8 μm), suggesting that bFGF entrapped in the hydrogel exhibited biological activity. In contrast, the cell areas of the PEG/Gela(B)/Hepa_hydrogel and PEG/Gela(B)_hydrogel were similar after 24 h, possibly because NIH3T3 cells were transformed into a refractile shape. The quantitative analysis of cell viability was also conducted by the trypan blue counting method. After 24 h, the viability of NIH3T3 cells on PEG/Gela(B) and PEG/Gela(B)/Hepa_hydrogel are 99.3±1.2 % and 99.7±0.6 %, respectively.

2.3.4 Administration of GFs in different hydrogel systems for adherent cell culture

To validate the effective immobilization pathway of GFs to sustain the cell culture on the functionalized hydrogels, different techniques of GF administration were tested (Fig. 2.15).

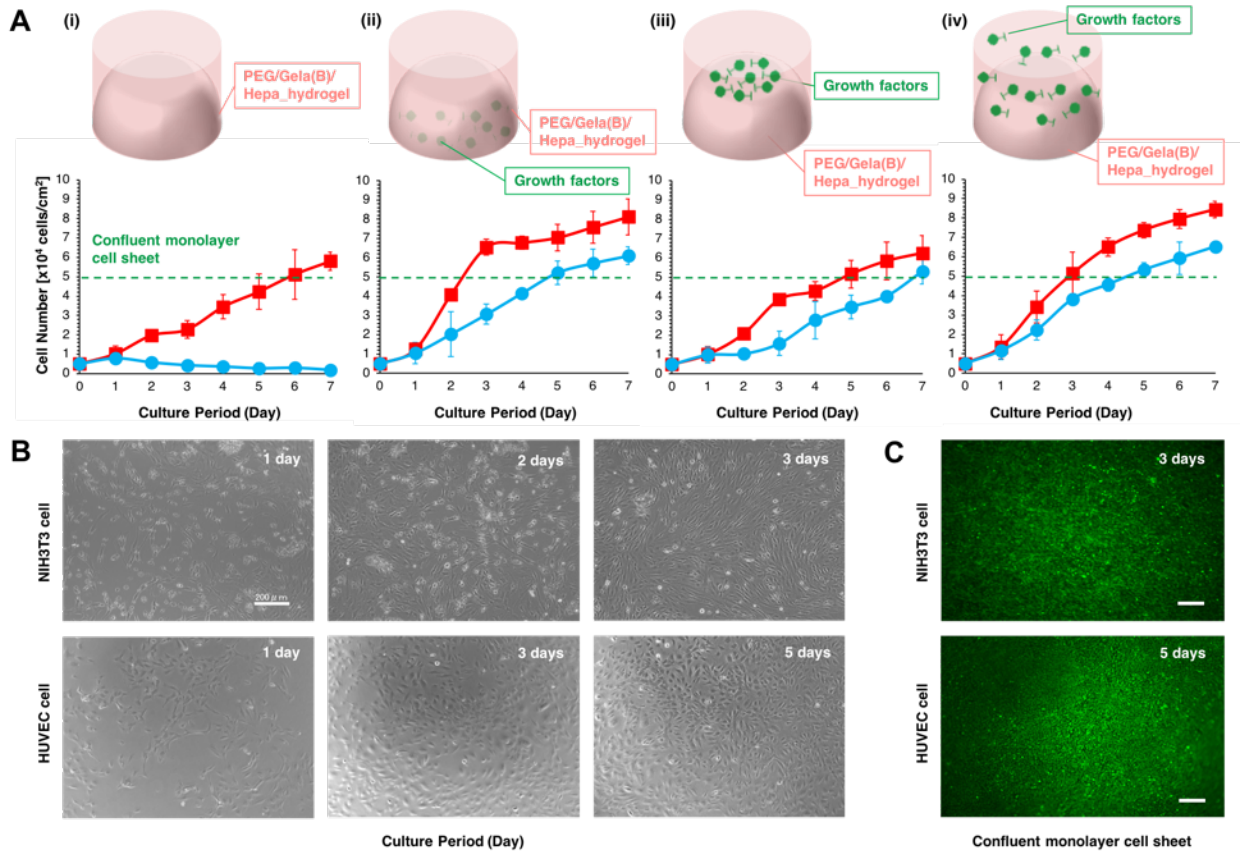

Fig. 2.15. (A) Effect of GF administration on cell growth. Negative control treatment (i), strategy I (ii), strategy II (iii), and positive control (iv) (right). Red square/line marker is NIH3T3 cells treated with a single GF (bFGF), blue circle/line marker is HUVECs treated with multiple GFs (bFGF, VEGF, R3-IGF-1, and hEGF). (B) Bright field images of NIH3T3 cells at 1, 2 and 3 days of culture and HUVECs at 1, 3 and 5 days of culture (magnification, ×10). (C) Live NIH3T3 cell and HUVEC sheets after reaching confluency using strategy I (ii). Cell sheets were stained using a Live/Dead staining kit (calcein-AM and propidium iodide) (magnification, ×4). Scale bars are 200 μm. Reproduce with permission from ref[32]. Copyright 2019 American Chemical Society.

Two types of GF localization strategies were explored, namely in situ immobilization of GFs by Hepa-SH-mediated binding in the PEG/Gela/Hepa_hydrogel (strategy I) and surface immobilization by physical adsorption of GFs on the

PEG/Gela/Hepa_hydrogel (strategy II). A conventional method to culture cells in GF-containing medium was used as a positive control. In the negative control, cells were seeded on hydrogel without GFs (Fig. 2.2). Two types of adherent cells were employed: fibroblasts (NIH3T3) and endothelial cells (HUVECs).

Strategy I provided faster cell growth, resulting in a higher number of NIH3T3 cells than both the positive control and strategy II (surface immobilization) (Fig. 2.15--A). Strategy I thus allowed NIH3T3 cells to reach confluency after 2.5 days. However, in the positive control, strategy II and negative control, cells reached confluency after 3, 5, and 6 days, respectively. These results indicated the sustained release of biologically active bFGF from inside to the outside of the PEG/Gela(B)/Hepa_hydrogel induced faster cell proliferation compared with other systems. It was likely that the binding of Hepa-SH to bFGF leaded to stable and long-term stimulation of NIH3T3 cells[54].

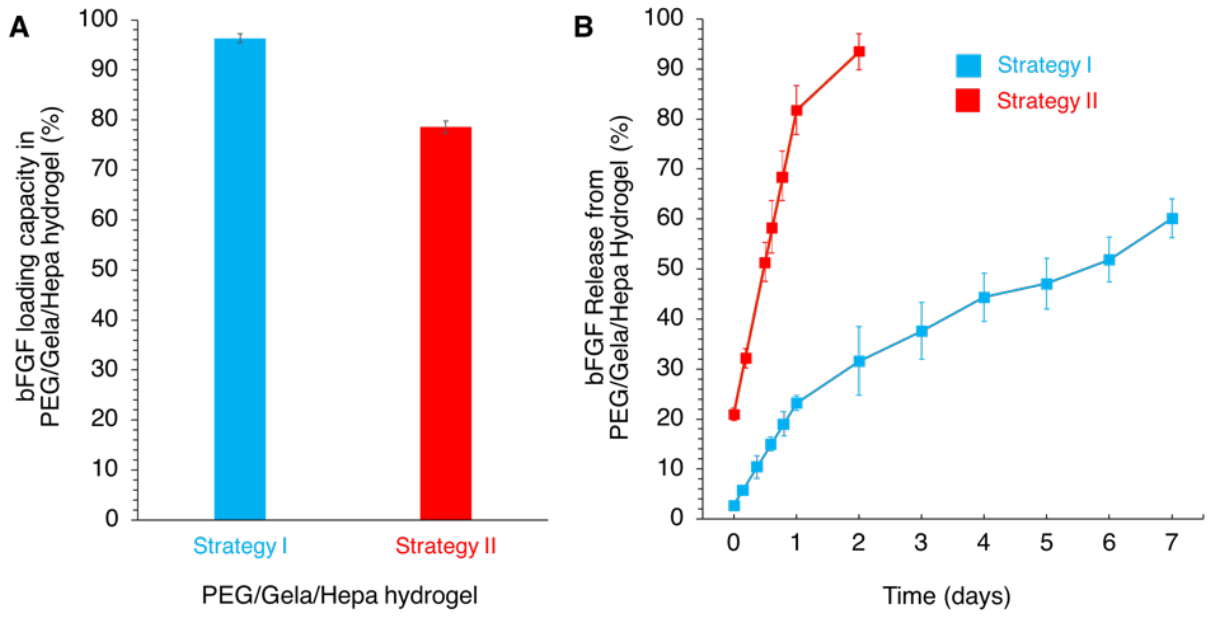

Fig. 2.16. (A) Loading capacity of bFGF on PEG/Gela/Hepa_hydrogels prepared by strategy I and II; (B) Release profile of bFGF from PEG/Gela/Hepa_hydrogels prepared by strategy I and II. Reproduce with permission from ref[32]. Copyright 2019 American Chemical Society.

The amount of bFGF loaded in PEG/Gela/Hepa_hydrogel (strategy I) was about 96.3% whereas that of strategy II had lower loading capacity (78.6%) (Fig. 2.16-A). The release profile of bFGF from the hydrogel showed that strategy I exhibited the sustained release over 7 days while strategy II showed the burst release in 2 days (Fig. 2.16-B). These results implied that strategy I is effective to load bFGF quantitatively in the hydrogel and to retain biological activity of bFGF much longer than that of strategy II.

In addition to NIH3T3, HUVEC cells were cultured on the hydrogels to assess the biological characterization of the hydrogels. It is known that HUVECs require multiple growth factors and supplements for sufficient growth.[55] HUVECs had an extremely low cell proliferation rate without the multiple GFs because of increased susceptibility to apoptosis. Although strategy I did not reach the same level of effectiveness as the positive control culture of HUVECs, it allowed HUVECs to reach confluency at the same time (5 days) as the positive control (Fig. 2.15-B). Moreover, the PEG/Gela/Hepa_hydrogel immobilized other heparin-binding GFs, such as bFGF, VEGF, R3-IGF-1, and hEGF, to further enhance the adhesion, growth, and differentiation of HUVECs.

Our results showed enhanced cell proliferation and differentiation by simple modulation of the scaffold design consisting of thiol-modified PEG, gelatin, and heparin (strategy I). The resultant hydrogels had mitogenic and chemotactic activities regulated by the gradual release of GFs entrapped in hydrogel matrices. Because of the ability to shorten the cell culture period and enhance cell confluency, NIH3T3 cells and HUVECs were cultured using strategy I to fabricate the live cell sheets (Fig. 2.13-C). The trypan blue counting method also revealed that the number of viable NIH3T3 and HUVEC cells in 2D sheets are 94.7±4.9% and 89.3±1.5%, respectively. Because

few dead cells were observed in both cases, our strategy would allow efficient and effective use of GFs, which in turn could reduce the cost of a cell culture system.

2.4. Conclusion

A multifunctional PEG-based hydrogel prepared feasibly by HRP-mediated hydrogelation was developed. Chemically modified gelatin and heparin with thiol groups, Gela-SH and Hepa-SH, can be incorporated within the PEG-SH hydrogel through disulfide linkage. Interestingly, the type of gelatin had a significant effect on the physical and biological aspects of hydrogels. The concentration of Hepa-SH should be optimized because of its conflicting properties observed in the incorporation of Gela-SH hydrogels and its intrinsic anti-proliferative effect were also described. Taken together, our results suggest that 0.1% Gela(B)-SH and 0.01% Hepa-SH were the most suitable condition to immobilize GFs and sustain cell proliferation. This hydrogel system also facilitated faster fibroblast and endothelial cell confluency, which makes it possible to fabricate cellular sheets efficiently.

2.5 References

1. Patterson, J., Martino, M. M. & Hubbell, J. A. Biomimetic materials in tissue engineering. *Mater. Today* **13**, 14–22 (2010).
2. Green, J. J. & Elisseeff, J. H. Mimicking biological functionality with polymers for biomedical applications. *Nature* **540**, 386–394 (2016).
3. Buwalda, S. J. *et al.* Hydrogels in a historical perspective: From simple networks to smart materials. *J. Control. Release* **190**, 254–273 (2014).
4. Steward, A. J., Liu, Y. & Wagner, D. R. Engineering cell attachments to scaffolds in cartilage tissue engineering. *JOM* **63**, 74–82 (2011).
5. Edwards, S. *et al.* Injectable Macroporous Hydrogel Formed by Enzymatic Cross-Linking of Gelatin Microgels. *ACS Appl. Bio Mater.* **1**, 1430–1439 (2018).
6. Moreira Teixeira, L. S., Feijen, J., van Blitterswijk, C. A., Dijkstra, P. J. & Karperien, M. Enzyme-catalyzed crosslinkable hydrogels: Emerging strategies for tissue

engineering. *Biomaterials* **33**, 1281–1290 (2012).

7. Sakai, S. & Nakahata, M. Horseradish Peroxidase Catalyzed Hydrogelation for Biomedical, Biopharmaceutical, and Biofabrication Applications. *Chem. - An Asian J.* **12**, 3098–3109 (2017).
8. Khanmohammadi, M. *et al.* Horseradish peroxidase-catalyzed hydrogelation for biomedical applications. *Biomater. Sci.* **6**, 1286–1298 (2018).
9. Lee, F., Bae, K. H. & Kurisawa, M. Injectable hydrogel systems crosslinked by horseradish peroxidase. *Biomed. Mater.* **11**, 14101 (2015).
10. Macdougall, L. J., Pérez-Madrigal, M. M., Arno, M. C. & Dove, A. P. Nonswelling Thiol-Yne Cross-Linked Hydrogel Materials as Cytocompatible Soft Tissue Scaffolds. *Biomacromolecules* **19**, 1378–1388 (2018).
11. Zhu, J. Bioactive modification of poly(ethylene glycol) hydrogels for tissue engineering. *Biomaterials* **31**, 4639–4656 (2010).
12. Moriyama, K., Minamihata, K., Wakabayashi, R., Goto, M. & Kamiya, N. Enzymatic preparation of a redox-responsive hydrogel for encapsulating and releasing living cells. *Chem. Commun.* **50**, 5895–5898 (2014).
13. Moriyama, K., Naito, S., Wakabayashi, R., Goto, M. & Kamiya, N. Enzymatically prepared redox-responsive hydrogels as potent matrices for hepatocellular carcinoma cell spheroid formation. *Biotechnol. J.* **11**, 1452–1460 (2016).
14. Owaki, T., Shimizu, T., Yamato, M. & Okano, T. Cell sheet engineering for regenerative medicine: Current challenges and strategies. *Biotechnol. J.* **9**, 904–914 (2014).
15. Moriyama, K., Wakabayashi, R., Goto, M. & Kamiya, N. Enzyme-mediated preparation of hydrogels composed of poly(ethylene glycol) and gelatin as cell culture platforms. *RSC Adv.* **5**, 3070–3073 (2015).
16. Davidenko, N. *et al.* Evaluation of cell binding to collagen and gelatin: a study of the effect of 2D and 3D architecture and surface chemistry. *J. Mater. Sci. Mater. Med.* **29**, 39 (2018).
17. Ruoslahti, E. RGD and Other Recognition Sequences for Integrins. *Annu. Rev. Cell Dev. Biol.* **12**, 697–715 (1996).
18. Park, K. M., Ko, K. S., Joung, Y. K., Shin, H. & Park, K. D. In situ cross-linkable gelatin-poly(ethylene glycol)-tyramine hydrogel via enzyme-mediated reaction for tissue regenerative medicine. *J. Mater. Chem.* **21**, 13180–13187 (2011).
19. Jaipan, P., Nguyen, A. & Narayan, R. J. Gelatin-based hydrogels for biomedical

applications. *MRS Commun.* **7**, 416–426 (2017).

20. Kleinman, H. K., Philp, D. & Hoffman, M. P. Role of the extracellular matrix in morphogenesis. *Curr. Opin. Biotechnol.* **14**, 526–532 (2003).
21. Kuhl, P. R. & Griffith-Cima, L. G. Tethered epidermal growth factor as a paradigm for growth factor–induced stimulation from the solid phase. *Nat. Med.* **2**, 1022–1027 (1996).
22. Hodneland, C. D., Lee, Y.-S., Min, D.-H. & Mrksich, M. Selective immobilization of proteins to self-assembled monolayers presenting active site-directed capture ligands. *Proc. Natl. Acad. Sci.* **99**, 5048–5052 (2002).
23. Jones, C. J., Beni, S., Limtiaco, J. F. K., Langeslay, D. J. & Larive, C. K. Heparin Characterization: Challenges and Solutions. *Annu. Rev. Anal. Chem.* **4**, 439–465 (2011).
24. Makino, T. *et al.* Basic fibroblast growth factor stimulates the proliferation of human dermal fibroblasts via the ERK1/2 and JNK pathways. *Br. J. Dermatol.* **162**, 717–723 (2009).
25. Tae, G. *et al.* Formation of a Novel Heparin-Based Hydrogel in the Presence of Heparin-Binding Biomolecules. *Biomacromolecules* **8**, 1979–1986 (2007).
26. Kim, M., Youn, J., Jones, C. N., Revzin, A. & Tae, G. Biomaterials Heparin-based hydrogel as a matrix for encapsulation and cultivation of primary hepatocytes. *Biomaterials* **31**, 3596–3603 (2010).
27. Sakiyama-Elbert, S. E. Incorporation of heparin into biomaterials. *Acta Biomater.* **10**, 1581–1587 (2014).
28. Liang, Y. & Kiick, K. L. Heparin-functionalized polymeric biomaterials in tissue engineering and drug delivery applications. *Acta Biomater.* **10**, 1588–1600 (2014).
29. Claaßen, C., Sewald, L., Tovar, G. & Borchers, K. Controlled Release of Vascular Endothelial Growth Factor from Heparin-Functionalized Gelatin Type A and Albumin Hydrogels. *Gels* **3**, 35 (2017).
30. Li, Z. *et al.* Injectable gelatin derivative hydrogels with sustained vascular endothelial growth factor release for induced angiogenesis. *Acta Biomater.* **13**, 88–100 (2015).
31. Fu, A., Gwon, K., Kim, M., Tae, G. & Kornfield, J. A. Visible-light-initiated thiol-acrylate photopolymerization of heparin-based hydrogels. *Biomacromolecules* **16**, 497–506 (2015).
32. Ramadhan, W. *et al.* Enzymatically Prepared Dual Functionalized Hydrogels with

Gelatin and Heparin To Facilitate Cellular Attachment and Proliferation. *ACS Appl. Bio Mater.* **2**, 2600–2609 (2019).

33. Li, X. *et al.* 3D culture of chondrocytes in gelatin hydrogels with different stiffness. *Polymers (Basel).* **8**, (2016).
34. Smith, R. E. & MacQuarrie, R. A sensitive fluorometric method for the determination of arginine using 9,10-phenanthrenequinone. *Anal. Biochem.* **90**, 246–255 (1978).
35. Liu, T. *et al.* Immobilization of heparin/poly- L -lysine nanoparticles on dopamine-coated surface to create a heparin density gradient for selective direction of platelet and vascular cells behavior. *Acta Biomater.* **10**, 1940–1954 (2014).
36. Moriyama, K., Wakabayashi, R., Goto, M. & Kamiya, N. Characterization of enzymatically gellable, phenolated linear poly(ethylene glycol) with different molecular weights for encapsulating living cells. *Biochem. Eng. J.* **93**, 25–30 (2014).
37. Lee, K. Y. & Mooney, D. J. Hydrogels for Tissue Engineering. *Chem. Rev.* **101**, 1869–1880 (2001).
38. Morin, K. T., Carlson, P. D. & Tranquillo, R. T. Automated image analysis programs for the quantification of microvascular network characteristics. *Methods* **84**, 76–83 (2015).
39. Masters, J. R. & Stacey, G. N. Changing medium and passaging cell lines. *Nat. Protoc.* **2**, 2276–2284 (2007).
40. Seliktar, D. Designing Cell-Compatible Hydrogels for Biomedical Applications. *Science (80-.).* **336**, 1124–1128 (2012).
41. Xu, Y. *et al.* Effect of heparin on protein aggregation: Inhibition versus promotion. *Biomacromolecules* **13**, 1642–1651 (2012).
42. Berger, J. *et al.* Structure and interactions in covalently and ionically crosslinked chitosan hydrogels for biomedical applications. *Eur. J. Pharm. Biopharm.* **57**, 19–34 (2004).
43. Djabourov, M., Lechaire, J.-P. & Gaill, F. Structure and rheology of gelatin and collagen gels. *Biorheology* **30**, 191–205 (1993).
44. Ahsan, S. M. & Rao, C. M. The role of surface charge in the desolvation process of gelatin: Implications in nanoparticle synthesis and modulation of drug release. *Int. J. Nanomedicine* **12**, 795–808 (2017).
45. Ross-Murphy, S. B. Structure and rheology of gelatin gels: recent progress. *Polymer (Guildf).* **33**, 2622–2627 (1992).

46. Cavari, S. Antiproliferative effects of heparin on normal and transformed NIH/3T3 fibroblasts. *Cell Biol. Int.* **17**, 781–786 (1993).
47. Garg, H. G., Joseph, P. A. M., Yoshida, K., Thompson, B. T. & Hales, C. A. Antiproliferative role of 3-O-sulfate glucosamine in heparin on cultured pulmonary artery smooth muscle cells. *Biochem. Biophys. Res. Commun.* **224**, 468–473 (1996).
48. Matějka, R. *et al.* Cellular Responses Modulated by FGF-2 Adsorbed on Albumin/Heparin Layer-by-Layer Assemblies. *PLoS One* **10**, e0125484 (2015).
49. Yun, Y. R. *et al.* Fibroblast growth factors: Biology, function, and application for tissue regeneration. *J. Tissue Eng.* **1**, 1–18 (2010).
50. Quang, T., Marquez, M., Blanco, G. & Zhao, Y. Dosage and Cell Line Dependent Inhibitory Effect of bFGF Supplement in Human Pluripotent Stem Cell Culture on Inactivated Human Mesenchymal Stem Cells. *PLoS One* **9**, e86031 (2014).
51. Florkiewicz, R. Z., Majack, R. A., Buechler, R. D. & Florkiewicz, E. Quantitative export of FGF-2 occurs through an alternative, energy-dependent, non-ER/Golgi pathway. *J. Cell. Physiol.* **162**, 388–399 (1995).
52. DeLong, S. A., Moon, J. J. & West, J. L. Covalently immobilized gradients of bFGF on hydrogel scaffolds for directed cell migration. *Biomaterials* **26**, 3227–3234 (2005).
53. Moscatelli, D. & Quarto, N. Transformation of NIH 3T3 Cells with Basic Fibroblast Growth Factor or the hst/K-fgfOncogene Causes Downregulation of the Fibroblast Growth Factor Receptor: Reversal of Morphological Transformation and Restoration of Receptor Number by Suramin. *J. Cell Biol.* **109**, 2519–2527 (1989).
54. Arisaka, Y., Kobayashi, J., Yamato, M., Akiyama, Y. & Okano, T. Biomaterials Switching of cell growth / detachment on heparin-functionalized thermoresponsive surface for rapid cell sheet fabrication and manipulation. *Biomaterials* **34**, 4214–4222 (2013).
55. Huttala, O. Human vascular model with defined stimulation medium – a characterization study. *ALTEX* **32**, 125–136 (2015).

CHAPTER 3 CONSTRUCTION OF HIGHER-ORDER CELLULAR MICRO-STRUCTURES BY A SELF-WRAPPING CO-CULTURE STRATEGY USING A REDOX-RESPONSIVE HYDROGEL

3.1 Introduction

Recreation of the three-dimensional (3D) architecture of viable cells is an emerging technology[1,2] for developing tissue-like structures with functions in the field of tissue engineering and as a new cell-based tool in the early phase of drug discovery[3,4]. These bottom-up approaches[5–7] have attracted significant attention for use in the fabrication of 3D cellular microstructures, including the cell sheet[8], and multi-cellular aggregate technologies such as microstructure blocks[6], fibers[7], spheroids[9] and organoids[10]. However, the construction of a fully viable, heterogeneous tissue-like structure using 3D cell culture techniques has yet been challenging[11–13]. Thus, it remains a major challenge to establish efficient and effective ways to upgrade recent technologies for 3D cell culture techniques[14–16], where co-culturing of different types of cells is a promising approach to formulate and to better mimic a natural tissue with a complex heterogeneous 3D cellular microstructures. Additionally, development of a 3D co-culture approach holds great potential for fundamental research efforts and its application toward monoculture systems[2]. Current combinatorial methods for the development of 3D co-culture systems are mainly classified by scaffold-free or scaffold-based techniques[2,17]. Form the viewpoint of cell-to-cell interaction, the co-culture techniques can be categorized by cell contact orders[2] such as simple and randomly mixed co-culture, segregated co-culture (culturing cells in different plates), sandwich or layered co-culture, cell patterning approach using a designed platform, and cell encapsulation techniques[18].

Although scaffold-free co-culture techniques have shown a great progress in terms of viability and functionality of various cell sources, from the engineering perspective it is hard to attain the spatial distribution and organization of cells in a 3D cellular microstructure. Conversely, scaffold-based techniques such as transwell plate, bioreactor, microfluid technology, micropatterning and other methods[20–23]. require a specialized method, require more resources, is labour-intensive, and require costly medical procedures[24–26]. In particular, it requires specialized equipment that may not be readily accessible to a standard laboratory. From this context, a cost-effective alternative approach for the construction of 3D cellular microstructures with standard equipment should be of great interest from basic studies to practical applications in biomedical fields[2].

To date, the configuration of encapsulation-based co-culture system that enables covering cells with another cell previsaged a promising technique to increase the cell-to-cell contact during culturing of multiple cells. These systems have been used to evaluate the cellular movement on continual regulation and the response to the physiologic stimuli, e.g., cell invasion, migration, angiogenesis and metastasis in complex tissues. Since the pioneering work of cell encapsulation with another cell coating[19], cells are often encapsulated within biomaterial-based scaffolds. However, the incomplete adherence of cells on the culture substrate and the difficulties to control the cell density and cellular movement on the outer membrane layer of encapsulated cell have been reported in this system[20,21]. One simple solution to overcome this limitation is to encapsulate target cells directly with an established cell layer from other origins without the aid of scaffold materials.

Cell sheet engineering itself is another powerful approach to co-culture cells[22–24]. Cell sheets are thin confluent monolayers of cells connected to each other in a flat,

sheet-like manner[25], and overlaying the cell sheets enables the construction of heterogeneous 3D cellular structures[26]. In the field of tissue engineering, this system also has been used to graft a cell sheet onto an organ surface, which attenuates deleterious host immune responses toward encapsulated cells used in autologous cell therapy applications[27–29].

The advance of current manipulation methods of living cells motivated us to propose a new way to encapsulate living cells within a confluent monolayer of cells (i.e., cell sheet). To the best of our knowledge, there has been no report on the utilization of a live cell sheet as a foldable cell layer to initiate the co-culture process. Herein, a facile method using a two-dimensional (2D) cell sheet to wrap 3D cellular aggregates and other biological entities was demonstrated. As a proof-of-concept study, a redox-degradable PEG-based hydrogel linked by disulfide bonds[30–33] that degrades under mild, cell-friendly reductive conditions was used. I found that by simply altering the concentration of cysteine (Cys) the degradation of the redox-responsive hydrogel can be controlled, indicating that detachment of the cell sheet can be regulated. In the present study, the self-folding process of a 2D fibroblast (NIH3T3) cell sheet to wrap 3D HepG2 spheroids and other cells (human umbilical vein endothelial cells (HUVECs)) and/or collagen beads into higher-order cellular microstructures are optimized (Fig. 3.1). The aggregated human hepatocellular carcinoma (HepG2) spheroids were employed as a model of small tissue. Increase in the hepatic function of co-cultured HepG2 cells affords opportunities to create a unique microenvironment for multicellular aggregates to promote direct cell-cell contacts, which will benefit further development of a simple, microplate-based co-culture technology. I called the new self-wrapping co-culture strategy ‘cellular Furoshiki’, in

which, a cell sheet is used to wrap other cellular aggregates, like the traditional Japanese fabric Furoshiki.

3.2 Experimental

3.2.1 Materials.

PTE-200 SH (Sunbright) (4arm PEG-$((CH_2)_2$-$SH)_4$, Mw 20 kDa) was supplied by the NOF Corporation (Tokyo, Japan). Glycyl-L tyrosine hydrate and 1-ethyl-3-(3 dimethyl aminopropyl) carbodiimide (EDC) were purchased from Tokyo Chemical Industry (Tokyo, Japan). Horseradish peroxidase (HRP; activity 100 unit/mg) was purchased from Wako Pure Chemical Industries (Osaka, Japan). Gelatine type A was purchased from Sigma-Aldrich (St Louis, MO, USA). 5,5'-Dithiobis (2-nitrobenzoic acid) (DTNB) and the Cell Stain-Double Staining kit were purchased from Dojindo (Kumamoto, Japan). L-Cysteine (Cys) was supplied from TCI Chemicals (Tokyo, Japan). Trypan blue (0.4%), Minimum Essential Medium (MEM) (1×) + GlutaMAX-I, 10% fetal bovine serum (FBS) and MEM Non-Essential Amino Acids solution were purchased from Thermo Fisher Scientific (Waltham, MA, USA). Cystamine, 1% antibiotic-antimycotic, trypsin 0.25%/1 mM EDTA and Dulbecco's phosphate buffer saline (D-PBS) were purchased from Nacalai Tesque (Kyoto, Japan). Endothelial growth medium (EGM-2) in the presence of FBS, hydrocortisone, growth factors (including hFGF, VEGF, R3-IGF-1 and hEGF), ascorbic acid and GA-1000 was supplied by Lonza (Walkersville, MD, USA). Collagen type I (bovine skin), the urea quantification assay kit (DIUR-100, BAS) and the human albumin ELISA quantitation set were purchased from Funakoshi (Tokyo, Japan). The Vybrant DiD Cell-Labeling solution kit was acquired from Biotium (Fremont, CA, USA). Elplasia micro space cell culture plates (MPC 3506) were purchased from Kuraray (Okayama, Japan) and

Prime Surface non-adherent 96-well plates MS-9096 U were from Sumitomo Bakelite (Tokyo, Japan). Ultra-high pure water was used during experiments (Milli-Q Integral MT3S.kit, Tokyo, Japan).

3.2.2 Fabrication of the redox responsive hydrogel.

The hydrogel was prepared by HRP-mediated crosslinking of thiolated polymers with a slight modification[31], and Gela-SH was prepared by following the protocol in our previous study[32]. In brief, a specific amount of 4-arm PEG-SH (5%, w/v), Gela-SH (0.01%, w/v) and Gly-Tyr (5 mM) were dissolved in D-PBS (pH 7.4). Subsequently, an aqueous solution of HRP (5 U/mL) was added to the mixture and mixed immediately by gentle pipetting. The reaction and hydrogelation proceeded by incubation at 37 °C for 4 h.

3.2.3 Cell lines and cell-culture conditions.

The NIH3T3 (RBRC-RCB1862) and HepG2 (RBRC-RCB1648) cell line were obtained from the Riken Cell Bank (Tsukuba, Japan), and HUVECs (KE-4109P10) was purchased from KURABO (Osaka, Japan). All cells were maintained as recommended. Briefly, NIH3T3 were maintained in MEM (1×) + GlutaMAX-I and 10% FBS. HepG2 cells were cultured in MEM supplemented with non-essential amino acids (NEAA) and 10% FBS. All media were further supplemented with 1% antibiotic-antimycotic. HUVECs were maintained in EGM-2. For long-term co-culturing of the cell sheet, HepG2 and HUVECS, the heterogeneous cell mixture was prepared in Dulbecco's minimum essential media (DMEM, Gibco) and EGM-2 (HUVEC basal medium) at a ratio of 1:1, supplemented with the F-12 nutrient mixture (Gibco) and recommended growth factors. Cells were maintained in a humid atmosphere at 37 °C with 5% CO_2.

3.2.4 Preparation of the NIH3T3 cell sheet, HepG2 spheroids, HUVECs and collagen beads.

The NIH3T3 cell sheet was prepared by seeding the cells on the redox responsive hydrogel. The redox responsive hydrogel was fabricated in 96-well non-adherent plates (MS-9690U). The total volume of the hydrogel was 20 μL per well. After hydrogelation, 100 μL of MEM was added, which contained NIH3T3 cells (3.4×10^4 cells/mL) and incubated for 3 d. HepG2 spheroid cells were fabricated by using the 6-well plate Elplasia system that has 648 microholes. The HepG2 cells density was 2.4×10^4 cells/mL or 150 cells/microhole. The cells were cultured with MEM-NEAA and the medium was changed on the second day. The addition of HepG2 spheroids to the cell sheet was calculated by diluting the 648 spheroids stock to the targeted spheroid number (0–100 spheroids per well). HUVECs were cultured and maintained in EGM-2 medium for 5 d, followed by subculturing to obtain 4.0×10^3 cells/well. Collagen beads or collagen microparticles were prepared by the membrane emulsification method[34,35], and the number of beads was counted by using a haemocytometer.

3.2.5 Observation of the wrapping process and cell viability characterization.

The required Cys concentration (1–50 mM) as a reductant was examined by measuring the duration time of hydrogel degradation, the initial time of cell sheet detachment and the folding behaviour of the cell sheet. The required time for complete degradation of the hydrogel was determined by measuring the duration time during transformation from the gel state to the solution state. The start time and lapping images were recorded using a Keyence Microscope BZ-9000 from BIOREVO (Tokyo, Japan).

The behaviour of cell sheet detachment in the presence of other cells was evaluated by integrating HepG2 spheroids on the cell sheet. The co-cultured cells were incubated for 4 h at 37 °C with 5% CO_2 to ensure the spheroids adhered to the cell sheet. After 4 h incubation, the medium was removed and 100 μL Cys solution (20 mM) was added to each well. Observation of the initial wrapping process was conduct just after Cys addition. The initial wrapping process was recorded every 15 min and after 1 h the wrapping process was recorded at 3, 6, 12 and 24 h incubation time points by using the Keyence Microscope. Optimization of the wrapping process was performed in the absence and presence of 5, 15, 25, 50 and 100 spheroids per cell sheet, and observations were conducted using a confocal laser scanning microscope (CLSM) LSM-700 from ZEISS (Tokyo, Japan) after 1 d of culturing.

The imaging of cell viability was performed by double stain Calcein-AM for live cell and propidium iodide red staining for recognition of dead cells. Fifteen HepG2 spheroids, 4.0×10^3 cells/well HUVECs and 50 collagen beads were added onto the cell sheet. The wrapped cellular structure was fabricated by adding 20 mM Cys. Only HepG2 spheroids and only NIH3T3 samples in the wrapped and unwrapped conditions were prepared in wells as controls. The medium was changed every day, and observations were conducted using the CLSM at 1, 3 and 5 d of co-culturing. The collagen bead number was increased to 50, 150 and 250 beads per well, and the cell viability ratio was quantified using a Cell Counting Kit-8 (WST-8; Dojindo Laboratories) according to the manufacturer's protocol. After incubation for 5 d, the absorbance of WST-8 at 450 nm was measured using a microplate reader. The cell viability ratio was defined as:

$$\text{Cell viability ratio} = \{Abs_{450}\ (5^{th}\ \text{day living cell}) - Abs_{450}\ (\text{blank})\}/\{Abs_{450}\ (1^{st}\ \text{day cell number}) - Abs_{450}\ (\text{blank})\}$$

To validate the function of the wrapped cellular structure as a co-culture system, comparison of a wrapped co-culture and unwrapped co-culture were defined by measuring particular metabolic markers for 7 d culturing. The amount of albumin and urea was measured using the Human Albumin ELISA Quantitation Set and QuantiChrom Urea Assay Kit, respectively, and according to the manufacturer's instructions. To evaluate the DNA content, the collected co-culture cells were suspended in 0.5 mL 0.2% Triton X-100 solution, sonicated in an ice bath and centrifuged at 5000 × *g* for 5 min (4° C). Then, 20 µL of the cell lysate was diluted with 80 µL Tris-EDTA buffer (pH 9) and incubated with 100 µL of the working solution of dsDNA reagent in 96-well plates for 2–5 min at room temperature. The DNA concentration in the cell lysate was determined using a Quant-iT Picogreen dsDNA assay kit (Invitrogen, Thermo Fisher Scientific). The DNA content of each sample was determined by measuring the florescence intensity of the mixed well with a SpectraMax i3x Multi-Mode microplate reader (Molecular Devices, Osaka, Japan), with excitation at 480 nm and emission at 520 nm. Data were analysed by plotting fluorescence intensity versus DNA concentration.

3.2.6 Immunofluorescence staining of HUVECs

Direct immunofluorescence staining was conducted to visualize the distribution of HUVECs in the wrapped cellular structure. Briefly, after 7 d co-culture of cell, the wrapped cells were washed three times with PBS, and fixed with 4% paraformaldehyde for 30 min at 4 °C. The samples were then incubated in 0.1% Triton X-100 in PBS for 20 min at room temperature. Wrapped cells then incubated for 1 hour with the mouse anti-human platelet endothelial cell adhesion molecule (PECAM-1) or cluster of differentiation 31 (CD31) antibody conjugate with FITC (eBioscience, clone 390, USA), at a dilution of 1:20 in PBS. After washing with distilled water, the samples

of the wrapped cells were then ready for observing using CLSM-700 as above under excitation and emission wavelengths of 490 nm and 530 nm for FITC. The fluorescence signal was merged with the phase contrast image to confirm the position of HUVECs in the wrapped structure.

3.2.7 Statistical tests.

Significant differences of monocultures compared with that of dual and triple co-cultured cells were determined using a Tukey's multiple comparison test following a one-way analysis of variance. The secretion of albumin and urea, and DNA concentration data from wrapped cells and unwrapped cells were compared by t-test analyses. Data analysis was conducted with Graph Pad Prism 6 and the level of significance was set at $*p < 0.05$, $**p < 0.01$, $***p < 0.001$ and $****p < 0.0001$.

3.3 Results and discussion

Most studies have explored how to harvest intact cell sheets from scaffolds[28,36]. In contrast, there are only a few studies that have attempted to fold a cell sheet by cells detaching from the substrate, especially to manipulate the wrapping-process to form 3D or higher-order cellular microstructures by co-culturing with other cells. In the previous reports showing the immune response of transplanted tissues layered with a cell sheet[19,37,38], a cell scraper had been used to harvest the cell sheet, which may weaken the cell junctions and ECM condition. It is well reported that in the harvesting step, cell sheet needs a supporting material and manipulation technique to prevent the shrinking and folding of cytoskeleton during the detachment processes[36]. Eventually, the harvesting process of cell sheets is hard to control in general, thus it was not feasible to stratify the cell sheet to the other cells, spheroids, or small tissue.

Inspired by previous encapsulation technologies of cells, herein a self-wrapping technique with a cell sheet was proposed (Fig. 3.1). Fibroblast cell sheet was utilized

as a model of confluent monolayer cells to wrap the immortal liver cells (HepG2 spheroids). The underlying idea behind this work is the cell-cell interaction theory where encapsulation of living cells with other cells should extend cellular functions[39]. When the cell sheet detaches from the basement of the culture substrate, a contractile force produced by actin filaments pulls the neighbouring cells and 3D spheroids on the cell sheet, which leads to the wrapping process, that is, a core-shell type higher-order cellular aggregate is obtained. This design and construction of a co-culture system by the wrapping cell sheet process should provide an alternative cell culture system was postulated. A stimuli-responsive cell culture substrate based on polymeric materials to achieve this goal was utilized[40–42].

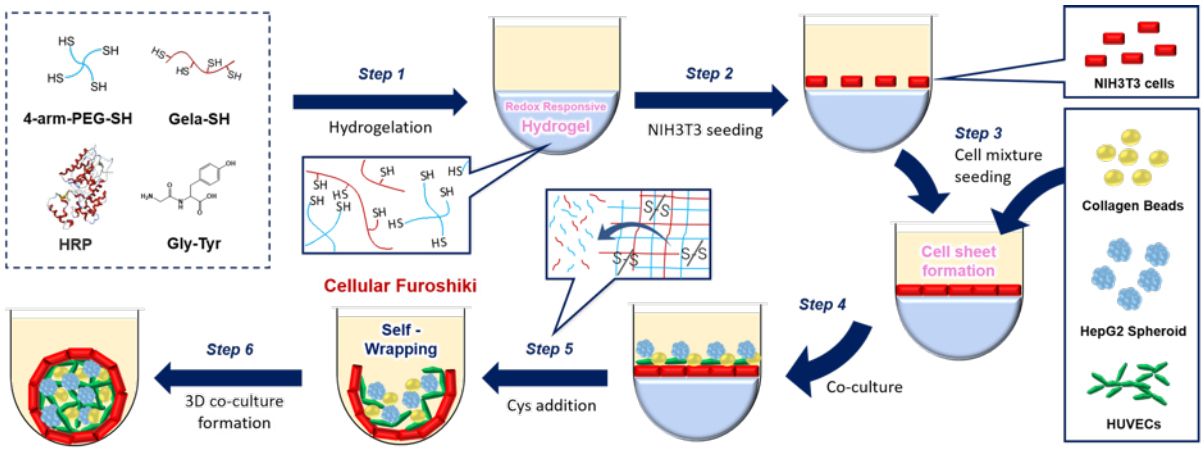

Fig. 3.1. Overall schematic illustration for the fabrication of the 'cellular Furoshiki' using redox responsive hydrogels. Step 1: Enzymatic preparation of a redox responsive hydrogel. Step 2: Seeding of NIH3T3 cells on the hydrogel. Step 3: Seeding of collagen beads, HepG2 and HUVECs. Step 4: The cells adhere to the cell sheet surface. Step 5: Hydrogel degradation. Step 6: Self-wrapping of the co-cultured cells. Reproduce with permission from ref[43]. Copyright 2020 Springer Nature.

3.3.1 Kinetic analysis of the detachment of a cell sheet from the redox-responsive hydrogel.

The redox-responsive hydrogel system is a promising stimuli-responsive matrix that has been used to fabricate live fibroblast cell sheets[31,44,45]. Biological entities cultured on the disulfide-linked PEG-based hydrogel were harvested by cleaving the

S–S bonds in the polymeric network. Cysteine was selected because it is a mild reductant under physiological conditions when compared with that of glutathione, β-mercaptoethanol, dithiothreitol and other reducing agents[31,46,47]. Previously the redox-responsive hydrogel degradation rate and complete detachment of the cell sheet typically occur ~30 min after incubation with 5 mM Cys were showed[31].

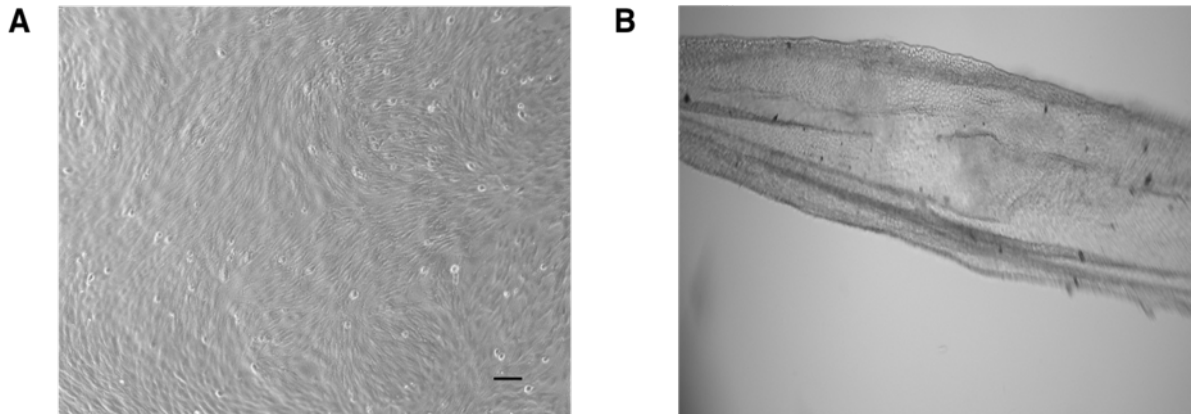

Fig. 3.2. A. NIH3T3 Cell sheet formation on the redox responsive hydrogel after 3 d incubation. B. Hydrogel was degraded after the addition of 5 mM Cys. Cell sheet shrunk and folded after the detachment from the redox responsive hydrogel (Scale bar is 200 μm). Reproduce with permission from ref[43]. Copyright 2020 Springer Nature.

However, the effect of the Cys concentration on harvesting, specifically the folding process of the fibroblast cell sheet, has not been examined. Therefore, the kinetic behaviour of cell sheet detachment from the hydrogel by varying the Cys concentration was examined. The shrinking ability of the cell sheet is mediated by the interplay between the wrapping behaviour of the cell sheet by redox responsive degradation and the state of other entities including cells on the cell sheet. Initially, NIH3T3 cells were cultured on the redox-responsive hydrogel for 3 d to fabricate the cell sheet (Fig. 3.2).

Because the rate of degradation of the redox-responsive hydrogel is affected by the reductant concentration, the folding behaviour of the cell sheet detachment from

the hydrogel was evaluated by varying the Cys concentration (1–50 mM). In addition, the time required for the complete degradation of hydrogels was assessed.

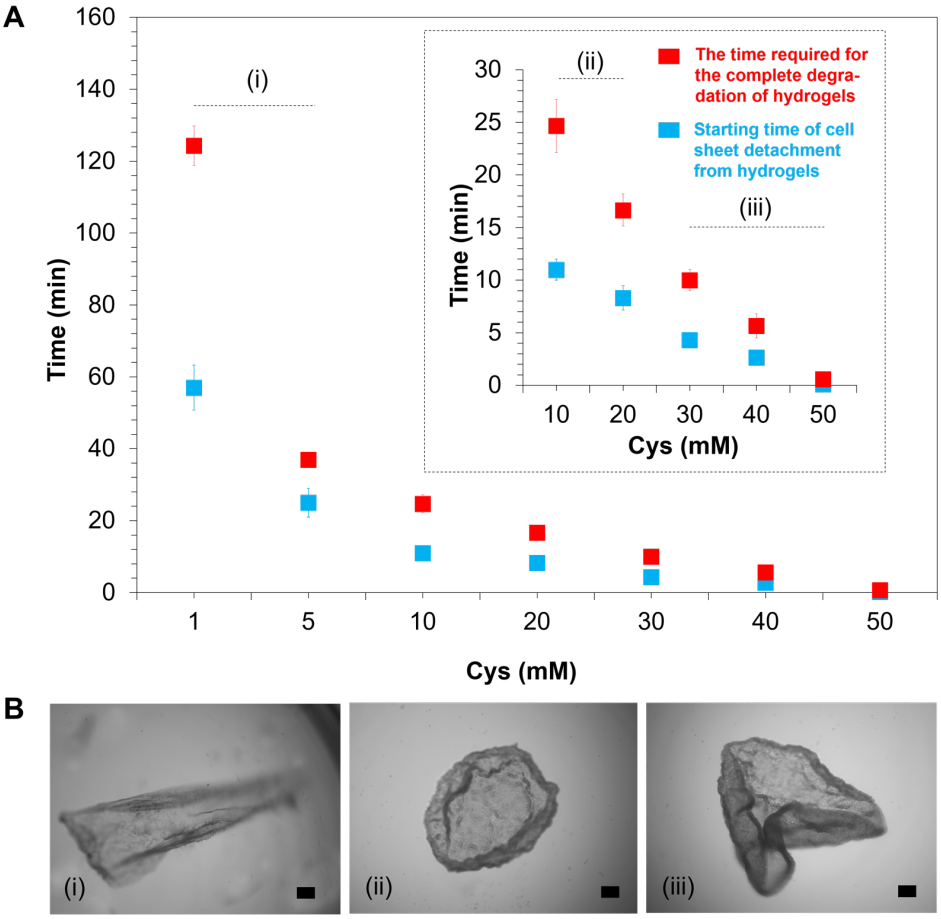

Fig. 3.3. Kinetic behaviour of the detachment of a cell sheet from the redox-responsive hydrogel. (A) Effect of cysteine (Cys) concentration on the duration time of cell sheet detachment from the redox responsive hydrogel (*n* = 3). Inset: enlarged figure after 30 min in the presence of 10–50 mM Cys. (B) Observation of cell sheet detachment behaviour. Hydrogels were degraded using 1–50 mM Cys. Photo (i), (ii) and (iii) present images of the cell sheet wrapping behaviour after adding 1–5, 10–20 and 30–50 mM Cys, respectively. All photos were captured by Keyence BZ-9000 microscope. Scale bar is 200 μm. Reproduce with permission from ref[43]. Copyright 2020 Springer Nature.

The results showed that the initial time point for detachment of the cell sheet decreased as the concentration of Cys increased (Fig. 3.3-A), whereas the required time for the complete degradation of the hydrogel increased as the Cys concentration decreased. At the highest Cys concentration (50 mM), the cell sheet detached immediately from the hydrogel upon transition to the sol state (within 1 min). In contrast,

at the lowest Cys concentration (1 mM), the cell sheet started to fold at 57 ± 6 min, and had completely degraded after incubation for 124 ± 6 min.

The folding behaviour of the cell sheet was observed to gain further insights into the effects of the Cys concentration on cell sheet detachment. Using 1 and 5 mM Cys, cells detached from the hydrogel under mild conditions; however, the detachment only occurred from one side of the cell edge (Fig. 3.3-Bi, Fig. 3.2-B). Interestingly, in the presence of 10 and 20 mM Cys, detachment occurred from the outer edge of the cell sheet, as expected (Fig. 3.3-Bii). Further increases in the Cys concentration to 30, 40 and 50 mM dramatically reduced the starting time of cell sheet detachment (less than 1 min); however, the folding process was difficult to control (Fig. 3.3-Biii). These results demonstrated that solely adjusting the Cys concentration without disrupting the cell-to-cell connection could control the detachment and shrinkage behaviour of the NIH3T3 cell sheet layer. Twenty millimolar Cys was selected for subsequent experiments because gentle cell sheet detachment behaviour was observed at this Cys concentration.

3.3.2 Self-wrapping behaviour of the cell sheet upon detachment from the redox-responsive hydrogel.

Hepatocellular carcinoma spheroids (HepG2) were immobilize on the cell sheet surface to test the possibility of wrapping other cells on the cell sheet layer during the folding process. Initially, HepG2 spheroids were fabricated by using Elplasia at a specific density (Fig. 3.4). The harvested spheroids (119±21μm in diameter) were then co-cultured on the cell sheet (6.5±0.1 mm in diameter) for 4 h. Twenty millimolar Cys was added to the hydrogel and time-lapse observations of wrapping cells was conducted (Fig. 3.5). As expected, the spontaneous shrinking of the cell sheet began within 10 min after exposure to the aqueous Cys solution (Fig. 3.5-A).

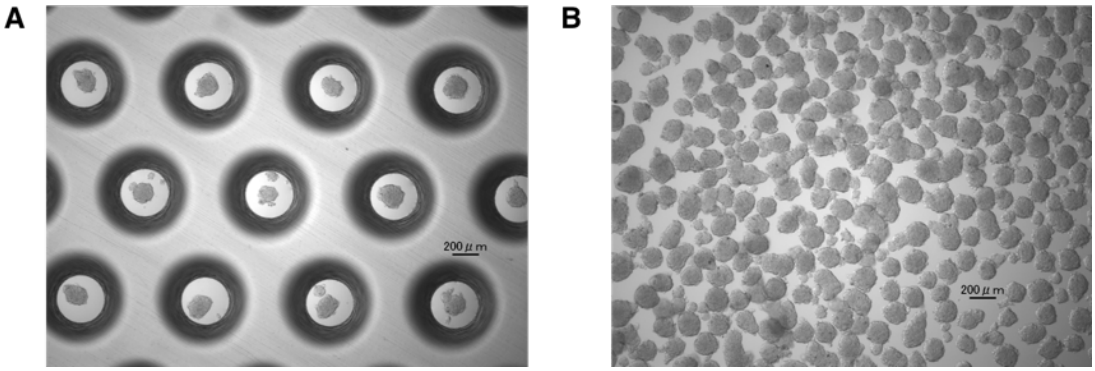

Fig. 3.4. Fabrication of HepG2 spheroid using Elplasia system. A. Seeding the HepG2 cells in the Elplasia™ microhole, B. Uniform HepG2 Spheroid formation after harvesting from Elplasia plate (Spheroid size is 119±21μm in diameter). Reproduce with permission from ref[43]. Copyright 2020 Springer Nature.

The folding process of the cell sheet was systematically controlled, and the hydrogel was readily degraded with 20 mM Cys under cyto-compatible conditions. During shrinkage, HepG2 spheroids remained attached to the cell sheet. The edge of cell sheets started to fold around 9 min after exposure to Cys, and all HepG2 spheroids were dispatched successfully to the centre of the well. No fragmentation of the cell layer was observed, indicating that the NIH3T3 cell sheet could shrink and hold the spheroids while maintaining the wrapped structure.

The visible space between spheroids on the cell sheet decreased with the self-folding process of the NIH3T3 cell layer. After wrapping the spheroids within ~9 min, the top part of wrapped cell aggregates showed an opened structure. Despite no significant change in the whole wrapped structure was observed, the top part of wrapped structure tended to fold gradually in 24 h culture (Fig. 3.5-B). Importantly, the coexistence of the spheroids in the inner part of wrapped structure was attained after 1 d of culturing (Fig. 3.5-C) and closed completely at 7 d of co-culture (Fig. 3.5-D).

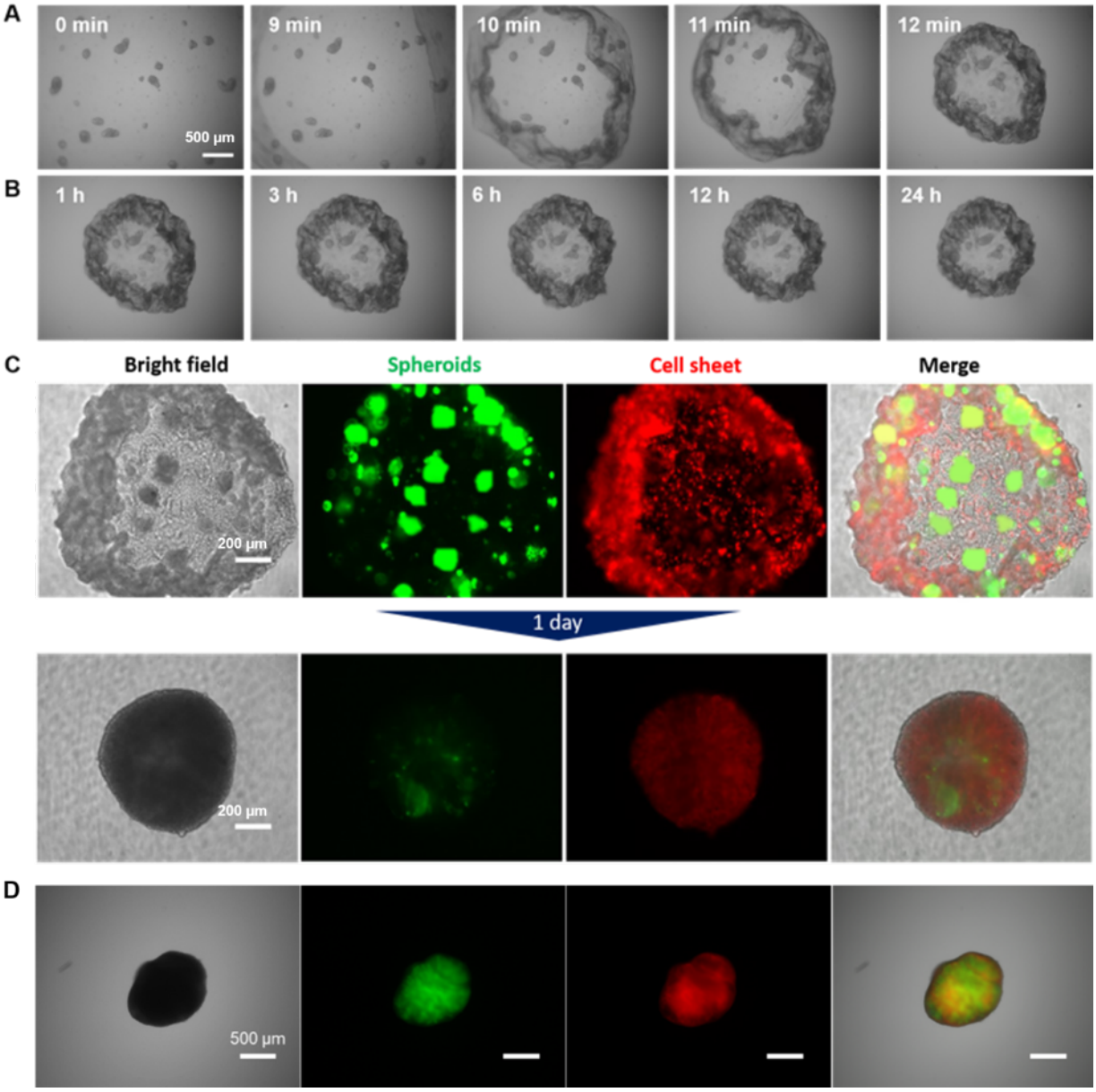

Fig. 3.5. Wrapping spheroids with a cell sheet by the 'cellular Furoshiki' technique. (A) Phase contrast time lapse imaging of HepG2 cells wrapped by a NIH3T3 cell sheet during the initial folding process. (B) Representative images of the wrapped cellular structure at and after 1 h incubation. (C) Co-existence of HepG2 spheroids in the NIH3T3 cell sheet. Images present the double staining wrapping process between 30 min and 1 d incubation. (D) The closed position of wrapped structure after 7 d culturing. Images in the right column are merged using the image analysis software BZ Analyzer from the Keyence BZ-9000 microscope. Adapted with permission from ref[43]. Copyright 2020 Springer Nature.

Various numbers of spheroids (0, 25, 50 and 100 per well) were seeded on the cell sheet to quantitatively analyse the number of spheroids that can be wrapped by the cell sheet (Fig. 3.6). A large number of spheroids significantly affected the size of

the wrapped structure and interfered with the process of cell layering. This condition also affected the closed or opened structure on the top of the wrapped structure during the incubation period. Incorporation of approximately 100 spheroids increased the size of the wrapped structure to more than ~1500 μm. Hence, the spheroid number to less than 25 per well to maintain the size of the wrapped structure and increase the possibility of incorporating another cell type into the remaining space in the wrapped structure was reduced (Fig. 3.6-A).

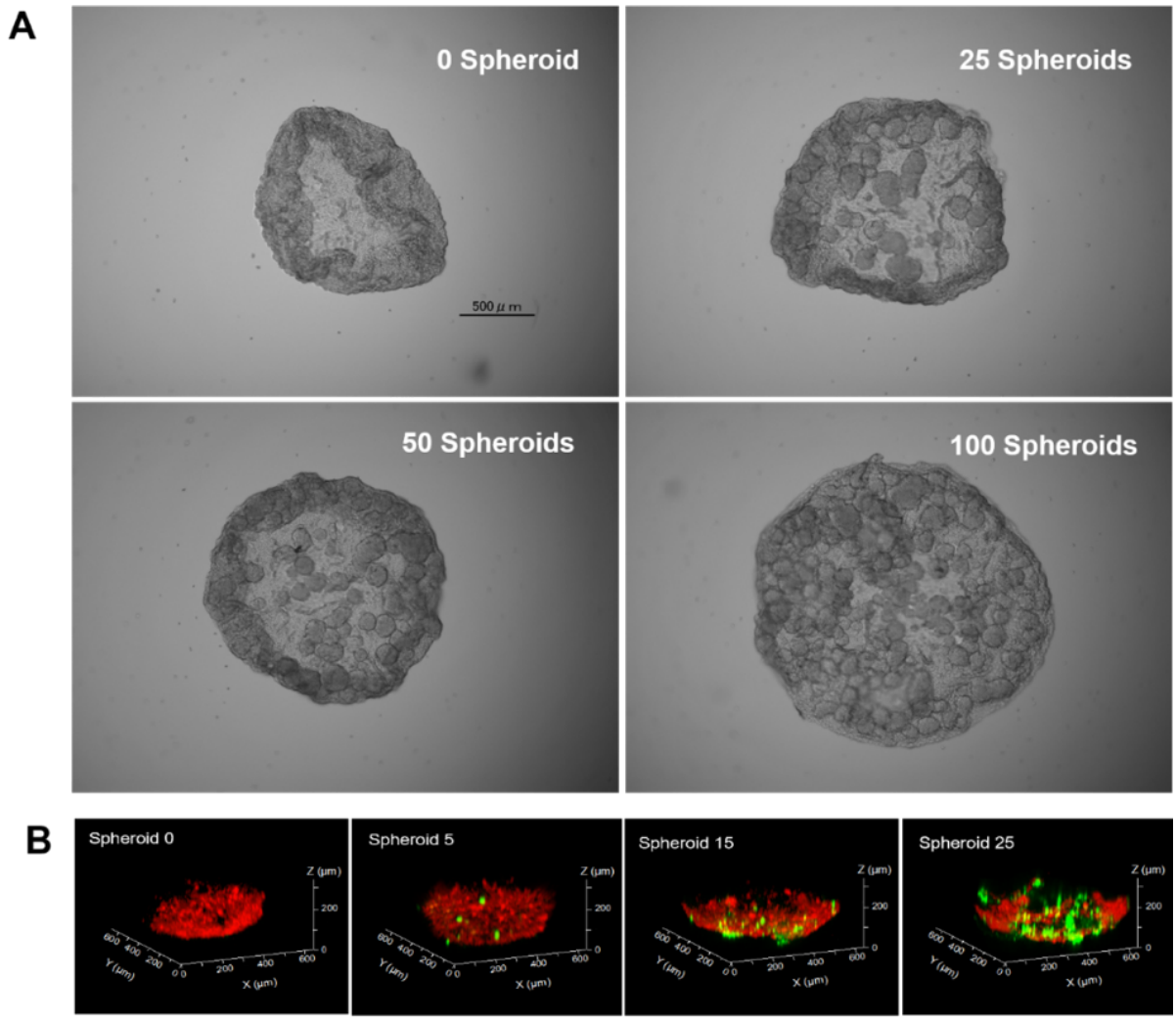

Fig. 3.6. Different numbers of HepG2 spheroids in the NIH3T3 cell sheet after 1 d co-culturing; (A) 0, 25, 50 and 100 spheroids per well and (B) 0, 5, 15 and 25 spheroids per well. 3D co-culture images were captured by the CLSM-700. The NIH3T3 cell sheet is stained with DiD red fluorescence and HepG2 spheroids are stained with Calcein-AM green fluorescence. Adapted with permission from ref[43]. Copyright 2020 Springer Nature.

As shown in Fig. 3.6-B, after 1 d incubation without HepG2 spheroids, the cell sheet formed a cellular aggregate with the size ca. ~500 μm. Similar results were observed when five spheroids were loaded into the cell sheet. Further increases in the spheroid number, that is, 15–25 spheroids per well, showed a small increase in the size (i.e., ca. ~ 600 μm) of the wrapped structure.

The presence of HepG2 spheroids on the cell sheet did not affect the cell detachment behaviour but affected the size and structure (opened or closed on the top) of the resultant wrapped structure and the viability of the co-cultured cells significantly. Thus, controlling the spheroid number was critical for effective cellular wrapping, and the HepG2 cell function in the spheroid form was expected to increase heterogeneous cell-cell interactions. Here, ~15 spheroids to ensure that the size of the wrapped structure did not increase dramatically and that bare areas were available for the incorporation of another cell type was selected.

3.3.3 Viability of co-cultured cells in the wrapped cellular structure.

The evaluation of the viability of encapsulated cells in the wrapping network was conducted because a co-culture system exhibits increasing complexity. In this part, HUVECs (4000 cells/well) and collagen microparticles (50 beads) into the wrapped structure were introduced. The results of the live/dead assay showed that after 5 d culturing only a few dead cells were observed in the HepG2 spheroid (Fig. 3.7-A) and NIH3T3 cell sheet (Fig. 3.7-B). However, incubation for an additional day gave a larger number of dead cells in the monoculture (Fig. 3.7-C) and dual co-culture (Fig. 3.7-Di) in the centre of the wrapped structure. Comparable results were found with HepG2 spheroids and collagen beads inside the network (Fig. 3.7-Dii).

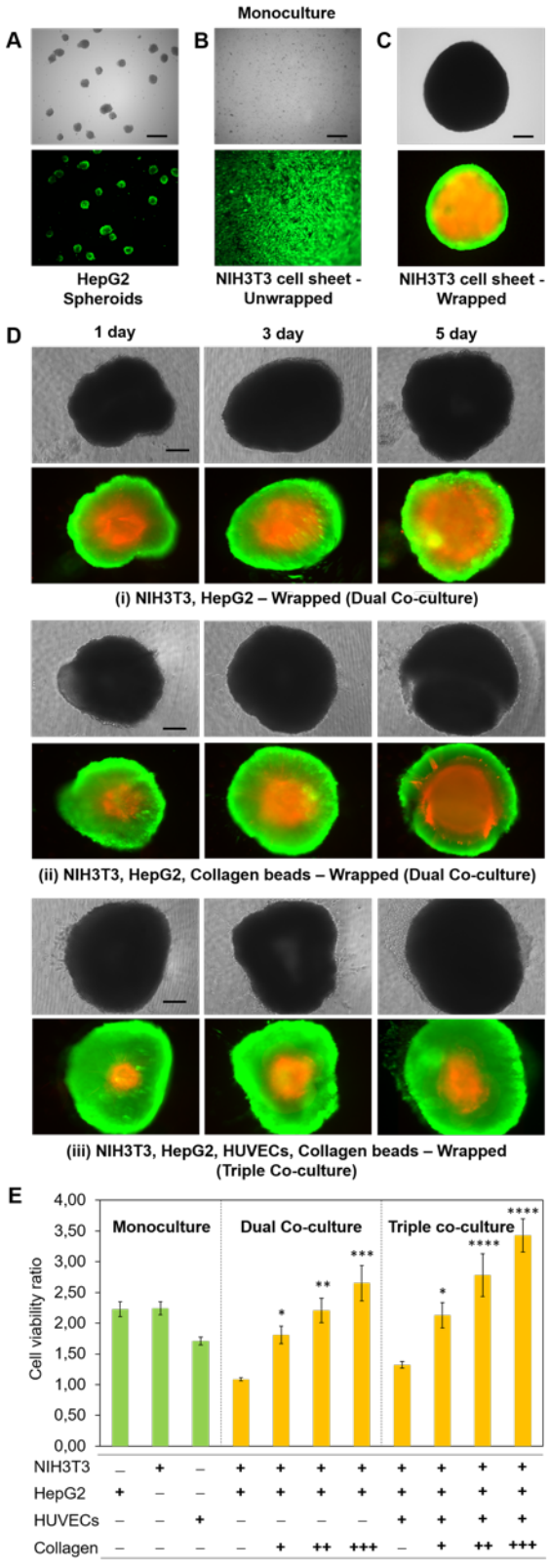

Fig. 3.7. Viability of co-cultured cells in the wrapped cellular structure. (A) Cell viability of HepG2 spheroids, (B) the NIH3T3 cell sheet and (C) the NIH3T3 cell sheet in the wrapped structure state after 5 d culturing. (D) NIH3T3-HepG2 co-culturing in the wrapped structure after 1, 3 and 5 d culturing. The initial cell numbers are 15 HepG2 spheroids, 100,000 NIH3T3 cells forming a monolayer and 50 collagen beads. Viable cells are stained green with calcein-

AM and dead cells are stained red by propidium iodide. Images were merged directly using the image analysis software BZ Analyzer from the Keyence BZ-9000 microscope. Scale bar is 100 μm. (E) Evaluation of the cell viability ratio for different wrapped structures after 5 d culturing. Data of viable cells at day 5 were normalized to cell viability at day 1. The initial cell numbers are 15 HepG2 spheroids, 100,000 NIH3T3 cells forming a monolayer and 4000 cells/well HUVECs. Collagen microparticle numbers are approximately 50 (+), 150 (++) and 250 (+++) in the wrapped cellular structures. Error bars denote standard deviation (N = 3). *p < 0.05, **p < 0.01, ***p < 0.001 and **** p < 0.0001 when compared with that of the wrapped structure without collagen beads. Reproduce with permission from ref[43]. Copyright 2020 Springer Nature.

The viability ratio of the HepG2 spheroids in the wrapped structure was significantly lower when compared with that of HepG2 cells in monoculture (Fig. 3.7-A). The hypoxic areas found in the central part of the wrapped structure are caused by insufficient permeation of oxygen because of the thickness of the cell sheet structure. Although the top of wrapped cell aggregates opened to bulk culture medium, the necrotic area in the multicellular spheroid was a predictable condition and is a general problem in the construction of 3D cell cultures[48]. According to previous report, the size limit of normal engineered tissue is around 100-200 μm[49,50] because of the inadequate gas exchange, nutrients, and elimination of cellular waste product[51].

Collagen is a major component of the extracellular matrix (ECM) and plays an important role in artificial scaffold developments for the alignment and organization of cells[52]. Various types of collagen microparticles have been used for *in vitro* 3D cell culture engineering[16,34,53,54]. I thus produced collagen (type I) beads[34] and placed them on the cell sheet before the cell sheet detachment. Inclusion of collagen beads into the NIH3T3 cell sheet and HepG2 spheroids increased the viability of the co-cultured cells. The necrotic area was reduced from 87% (without collagen beads) to 59% (with collagen beads) of the total area of the wrapped structure (Fig. 3.7-Di, 3.7-Dii).

A significant increase of the necrotic zone and decrease of the quiescent zone were observed after incubating the wrapped structure for 3 and 5 d. During the dual co-

culture, the necrotic zone (the red fluorescent region) increased from 48% (1 d) to 87% (5 d) in the total area of the wrapped structure (Fig. 3.7-Di), while with the inclusion of collagen beads inside the wrapped structure, the necrotic zones were reduced from 34% to 59% for 1 and 5 d culturing, respectively (Fig. 3.7-Dii).

However, designing large 3D cellular microstructures while maintaining cell viability still remains a challenge. Based on the ability to distribute oxygen, metabolites and nutrient, presenting endothelial cells are favorable in tissue engineering fileld[51], especially for promoting vascularization in the 3D cell culture[55–57]. The incorporation of endothelial cells (e.g., HUVECs) was thus used in an attempt to improve the cellular function of the wrapped structure (triple co-culture, Fig. 3.7-Diii)[55,58].

Incorporating HUVECs on the cell sheet persevered cell viability. Despite the region of the necrotic zone slightly increased from 24% (1 d) to 41% (5 d), the relative portion of dead cells of the wrapped structure clearly reduced when compared with those of the wrapped structures without HUVECs (Fig. 3.7-Diii). Accordingly, after 5 d culturing, the results of cell viability with the wrapped co-culture system increased significantly, especially when raising the number of collagen beads in dual and triple co-culture conditions (Figs. 3.7-E and 3.8). The gradual increase in the size of wrapped structure (initially ~ 500 μm) by 7% (Fig. 3.7-Di), 13% (Fig. 3.7-Dii) and 16% (Fig. 3.7-Diii) after 5 d culturing by introducing collagen beads and HUVECs were also found.

Interestingly, incorporating HUVECs improved the viability of co-culture cells when compared with the other wrapped structures without HUVECs (Fig. 3.7-D). This is possibly because HUVECs provide a crucial role in regulating interactions between cells by forming microvascular structures[55,59]. In the presence of HUVECs, the cell viability rate also increased when collagen beads were included (Fig. 3.7-E); however,

this increase differed from the co-cultured group without HUVECs. These results indicate that cellular interactions between HepG2 and HUVECs achieved a superior performance when compared with just HepG2 and NIH3T3 cells[60,61]. Although NIH3T3 cells have been shown to support hepatocytes in maintaining their differential function for long periods, NIH3T3 cells or fibroblasts are not in physical contact with hepatocytes in native liver tissue[61,62]. Naturally, hepatocytes and HUVECs together account for more than 80% of the liver of mass[63].

Since the increasing number of collagen beads either in dual or triple co-culture conditions gave significant effect to the cell viability of the wrapped structure (Fig. 3.7-E), collagen beads might work as a spacer and concurrently as a scaffold in the wrapped structure. Yamada and coworker[34,35] reported that collagen beads have function to create an internal conduit space for the effective diffusion of nutrients and oxygen to the center of the cellular aggregates. The increase in the cell viability is strongly related to the opened structure of wrapped cell, where the increase in the number of collagen beads result in the larger opened structure of that system (Fig. 3.8).

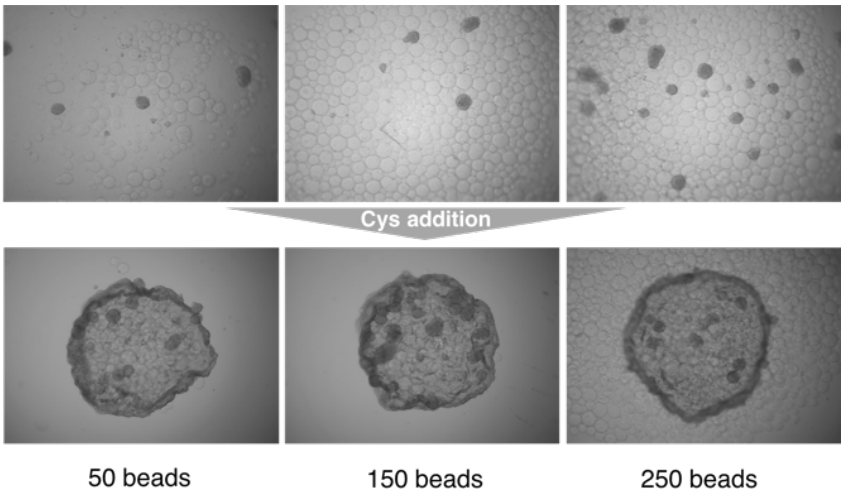

Fig. 3.8. Various number of collagen beads inside the wrapped structure. Reproduce with permission from ref[43]. Copyright 2020 Springer Nature.

Organization of collagen beads might facilitates the diffusion of the culture medium to the centre of the wrapped structure[51]. Owing to the adhesive property of collagen type I to enhance cell adhesion on the surface, collagen beads have also played a role as a scaffold to promote the growth of HUVECs. Accordingly, the inclusion of HUVECs could enhanced cell-ECM interactions to increase the cell viability. Importantly, the wrapped cellular structure of HepG2, HUVECs, and collagen beads inside the NIH3T3 cell sheet (triple co-culture with collagen beads) gave significantly higher cell viability than HepG2 spheroids alone, indicating that this self-wrapping technique is capable of maintaining healthy conditions for co-culturing cells by appropriate combinations of different cell types.

3.3.4 Metabolism of co-cultured cells inside the wrapped cellular structure.

To assess the function of HepG2 spheroids under triple co-culture conditions inside the wrapped structure, the metabolism from the co-culture cells in unwrapped and wrapped groups was evaluated. The triple co-culture cells consisted of 15 spheroids of HepG2, 4000 cells of HUVECs and 50 collagen beads on the confluent of NIH3T3 cell sheet. Comparison of the wrapped structure (triple co-culture with collagen beads) with the unwrapped structure was performed for 7 d of culturing. The results showed not only clear differences in morphology, but also significantly improved urea and albumin secretion as the HepG2 specific functions for the wrapped co-culture system (Fig 3.9-A; B).

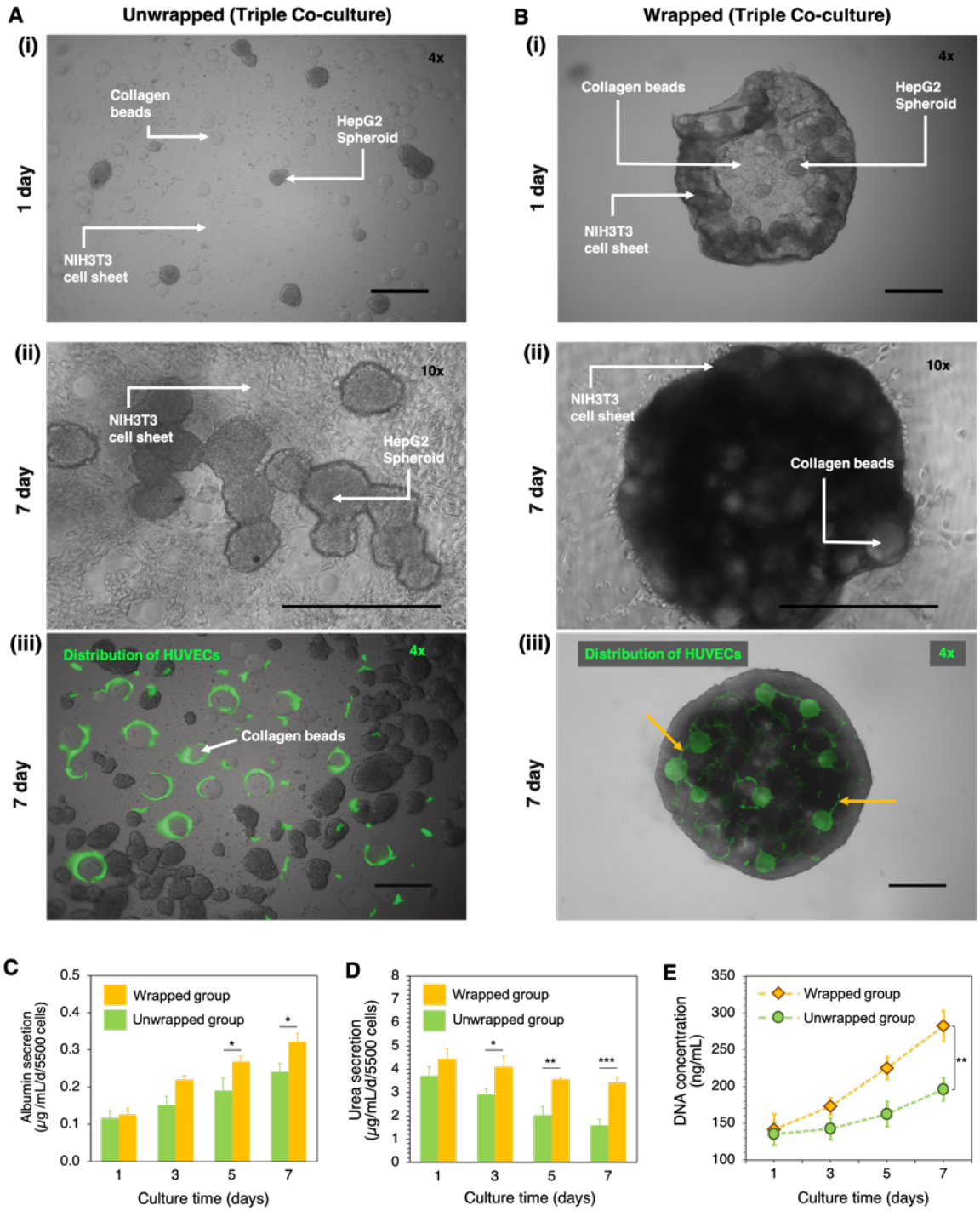

Fig. 3.9. Comparison of metabolism of co-cultured cells between the unwrapped and wrapped cellular structures**.** Unwrapped (A) and wrapped (B) groups of triple co-cultured HepG2, HUVECs and collagen beads on the NIH3T3 cell sheet. Representative phase contrast images of unwrapped group (A-i) and wrapped group (B-i) after 1 d of co-culture (images were taken at 4X magnification). Representative phase contrast images of unwrapped group (A-ii) and wrapped group (B-ii) after 7 d of co-culture (images were taken at 10X magnification). The existence of NIH3T3, HepG2 spheroid, and collagen beads are indicated by white arrows and labelling. Representative images of CD31 staining (green fluorescence) of HUVECs on the unwrapped structure (A-iii) and within the wrapped structure (B-iii) (images were taken at 4X magnification). A connected part of HUVECs is indicated by an orange arrow. The co-culture

images were captured by CLSM-700. Scale bar is 500 μm. Albumin (C) and urea (D) secretion from wrapped and unwrapped triple co-cultured cells for 7 d. (E) Quantitative data for proliferation of the triple co-cultured cells as determined by DNA content. Error bars denote standard deviation (N = 3) and *p < 0.05, **p < 0.01, ***p < 0.001. Reproduce with permission from ref[43]. Copyright 2020 Springer Nature.

In the unwrapped group, cells were cultured on the hydrogel without the degradation process (2D culture) (Fig. 3.9-Ai, 3.9-Aii), whereas in the wrapped group cells were adhered onto the NIH3T3 cell sheet and were wrapped and packed after the addition of 20 mM Cys (Fig. 3.9-Bi, 3.9-Bii)). In the wrapped structure, the HepG2, HUVECs and collagen beads were surrounded by the cell sheet and were packed into a higher-order microstructure. The large contact area among cells provided an increase in cell-to-cell interactions to enhance the higher cellular functions of HepG2. In contrast, in the unwrapped group, HepG2 cells adhered to form spheroidal structures on the surface of HUVECs and NIH3TH cells after 7 d of culturing.

HUVECs were randomly attached to the surface of collagen beads in the unwrapped structure (Fig. 3.9-Aiii), in contrast in the wrapped structure the beads were fully covered with adhered HUVECs, which results in the formation of a capillary-like structure under the culture period (Fig. 3.9-Biii). The distribution of HUVECs was clearly visualized by the CD31, a marker protein highly expressed on the endothelial cell membrane[64]. Fig. 3.9-B-iii shows that HUVECs proliferated around the collagen beads and well-dispersed in the wrapped structure. The adherence behavior and distribution of cells on the collagen beads surface was similar to that found in previous report[16]. Since the positive stain of CD31 relates to the initial step of angiogenesis and migration[65], HUVECs located in the interspace of collagen beads could form a capillary-like structures[61,66,67].

In general, hepatocyte (either normal cell or immortal cell) is a cell of the main parenchymal tissue of the liver[60,68]. One of the detoxifying functions is to modify

ammonia into urea for excretion. While albumin is often employed as an important secreted protein in the liver metabolism[60]. Both of urea and albumin is generally employed as a marker of hepatocyte metabolic activity *in vitro* and to evaluate the liver-specific function.

The effect of the two different culturing conditions by measuring the secretion of albumin, urea and DNA contents for 7 d of culturing were examined (Fig. 3.9-C; D; E). The secretion of albumin in both unwrapped and wrapped groups increased as the culturing period increased with the secretion level in the wrapped group significantly higher (*$p < 0.05$) than that in the unwrapped group after 5 and 7 d of culturing (Fig. 3.9-C) were observed. Urea secretion decreased during the culturing period for both groups with a significant difference (***$p < 0.001$) in urea secretion between the unwrapped and wrapped groups observed after 7 d incubation with values of 1.6 and 3.4 μg/mL/d/5500 cells, respectively (Fig. 3.9-D). The quantitative data of cellular proliferation within co-cultured HepG2 spheroids and HUVECs on the NIH3T3 cell sheet were examined by measuring DNA content. DNA synthesis was observed to increase for both groups over the 7 d culturing period with the wrapped group showing higher levels of cell proliferation (Fig. 3.9-E). At 7 d, the wrapped group had a 38.4% greater level of DNA synthesis when compared with the unwrapped group (**$p < 0.01$).

The wrapped structure showed marked increases in the secretion of albumin (1.3-fold), urea (2.1-fold) and DNA content (1.4-fold) when compared with that of the unwrapped structure. A similar trend were reported in previous works where the presence of hepatocyte in connected culture with endothelial cell gave a positive effect on the urea and albumin synthesis compared with a monoculture system[68–71]. Since DNA content is a measure of cell proliferation[72], dsDNA was selected as the representative of the proliferation rate of wrapped structures. The increase in

metabolism and DNA content indicated a better interplay among the wrapped cells, HepG2, HUVECs and collagen during the co-culturing. It is notable that the number of HepG2 spheroid, the amount of collagen beads, and the presence of HUVECs that affects cellular morphology and physiological responsiveness of the resultant wrapped structure.

Finally, 'Furoshiki' is recognized as a perfect fabric design for wrapping valuable items. Inspired by the traditional engineered Japanese item, a self-folding NIH3T3 cell sheet that wrapped biological entities and termed this the 'cellular Furoshiki' technique was presented. As demonstrated, the cell sheet was capable of wrapping other cells, and thus the cellular Furoshiki should provide an alternative approach for constructing complex, higher-order cellular microstructures.

3.4 Conclusions

The cellular Furoshiki technique as a new construction technique for the design of a higher-order cellular microstructure composed of a NIH3T3 cell sheet, HepG2 spheroids, HUVECs and collagen beads were demonstrated. Compared with the conventional co-culture system (i.e., unwrapped system), the cellular Furoshiki provided an increase in cell viability and metabolism of cellular components. The present concept is based on a simple microplate-based cell culture technique, which is accessible to standard laboratories.

3.5 References

1. Shamir, E. R. & Ewald, A. J. Three-dimensional organotypic culture: Experimental models of mammalian biology and disease. *Nat. Rev. Mol. Cell Biol.* **15**, 647–664 (2014).
2. Goers, L., Freemont, P. & Polizzi, K. M. Co-culture systems and technologies: taking synthetic biology to the next level. *J. R. Soc. Interface* **11**, 20140065–

20140065 (2014).
3. Langhans, S. A. Three-dimensional in vitro cell culture models in drug discovery and drug repositioning. *Front. Pharmacol.* **9**, 1–14 (2018).
4. Alhaque, S., Themis, M. & Rashidi, H. Three-dimensional cell culture: from evolution to revolution. *Philos. Trans. R. Soc. B Biol. Sci.* **373**, 20170216 (2018).
5. Langer, R. & Vacanti, J. P. Tissue Engineering. *Science (80-.).* **260**, 920–926 (1993).
6. Gurkan, U. A., Tasoglu, S., Kavaz, D., Demirel, M. C. & Demirci, U. Emerging technologies for assembly of microscale hydrogels. *Adv. Healthc. Mater.* **1**, 149–158 (2012).
7. Onoe, H. *et al.* Metre-long cell-laden microfibres exhibit tissue morphologies and functions. *Nat. Mater.* **12**, 584–590 (2013).
8. Tsuda, Y. *et al.* Tissue Engineering Using Laminar Cellular Assemblies. *Adv. Mater.* **21**, 3404–3409 (2009).
9. Knight, E. & Przyborski, S. Advances in 3D cell culture technologies enabling tissue-like structures to be created in vitro. *J. Anat.* **227**, 746–756 (2015).
10. Cruz-Acuña, R. *et al.* Synthetic hydrogels for human intestinal organoid generation and colonic wound repair. *Nat. Cell Biol.* **19**, 1326–1335 (2017).
11. Yuan, H., Xing, K. & Hsu, H. Y. Trinity of three-dimensional (3D) scaffold, vibration, and 3D printing on cell culture application: A systematic review and indicating future direction. *Bioengineering* **5**, 1–21 (2018).
12. Castiaux, A. D., Spence, D. M. & Martin, R. S. Review of 3D cell culture with analysis in microfluidic systems. *Anal. Methods* **11**, 4220–4232 (2019).
13. Mirbagheri, M. *et al.* Advanced cell culture platforms: a growing quest for emulating natural tissues. *Mater. Horizons* **6**, 45–71 (2019).
14. Rodrigues, T. *et al.* Emerging tumor spheroids technologies for 3D in vitro cancer modeling. *Pharmacol. Ther.* **184**, 201–211 (2018).
15. Sakai, S., Inagaki, H., Inamoto, K. & Taya, M. Wrapping tissues with a pre-established cage-like layer composed of living cells. *Biomaterials* **33**, 6721–6727 (2012).
16. Matsunaga, Y. T., Morimoto, Y. & Takeuchi, S. Molding cell beads for rapid construction of macroscopic 3D tissue architecture. *Adv. Mater.* **23**, 90–94 (2011).
17. Lazzari, G. *et al.* Multicellular spheroid based on a triple co-culture: A novel 3D model to mimic pancreatic tumor complexity. *Acta Biomater.* **78**, 296–307 (2018).

18. Orive, G. & Pedraz, J. L. Highlights and trends in cell encapsulation. *Adv. Exp. Med. Biol.* **670**, 1–4 (2010).
19. Pollok, J. M. *et al.* Long-term insulin-secretory function of islets of Langerhans encapsulated with a layer of confluent chondrocytes for immunoisolation. *Pediatr. Surg. Int.* **15**, 164–167 (1999).
20. Teramura, Y. & Iwata, H. Islet encapsulation with living cells for improvement of biocompatibility. *Biomaterials* **30**, 2270–2275 (2009).
21. Teramura, Y. & Iwata, H. Cell surface modification with polymers for biomedical studies. *Soft Matter* **6**, 1081–1091 (2010).
22. Tang, Z., Akiyama, Y. & Okano, T. Recent development of temperature-responsive cell culture surface using poly(N-isopropylacrylamide). *J. Polym. Sci. Part B Polym. Phys.* **52**, 917–926 (2014).
23. Yamato, M. & Okano, T. Cell sheet engineering. *Mater. Today* **7**, 42–47 (2004).
24. Owaki, T., Shimizu, T., Yamato, M. & Okano, T. Cell sheet engineering for regenerative medicine: Current challenges and strategies. *Biotechnol. J.* **9**, 904–914 (2014).
25. Edmondson, R., Broglie, J. J., Adcock, A. F. & Yang, L. Three-dimensional cell culture systems and their applications in drug discovery and cell-based biosensors. *Assay Drug Dev. Technol.* **12**, 207–218 (2014).
26. Harimoto, M. *et al.* Novel approach for achieving double-layered cell sheets co-culture: Overlaying endothelial cell sheets onto monolayer hepatocytes utilizing temperature-responsive culture dishes. *J. Biomed. Mater. Res.* **62**, 464–470 (2002).
27. Iwata, T. *et al.* Periodontal regeneration with autologous periodontal ligament-derived cell sheets – A safety and efficacy study in ten patients. *Regen. Ther.* **9**, 38–44 (2018).
28. Li, M., Ma, J., Gao, Y. & Yang, L. Cell sheet technology: a promising strategy in regenerative medicine. *Cytotherapy* **21**, 3–16 (2019).
29. Miyagawa, S. *et al.* Phase I Clinical Trial of Autologous Stem Cell-Sheet Transplantation Therapy for Treating Cardiomyopathy. *J. Am. Heart Assoc.* **6**, 1–12 (2017).
30. Moriyama, K., Wakabayashi, R., Goto, M. & Kamiya, N. Characterization of enzymatically gellable, phenolated linear poly(ethylene glycol) with different molecular weights for encapsulating living cells. *Biochem. Eng. J.* **93**, 25–30 (2014).

31. Moriyama, K., Wakabayashi, R., Goto, M. & Kamiya, N. Enzyme-mediated preparation of hydrogels composed of poly(ethylene glycol) and gelatin as cell culture platforms. *RSC Adv.* **5**, 3070–3073 (2015).
32. Ramadhan, W. *et al.* Enzymatically Prepared Dual Functionalized Hydrogels with Gelatin and Heparin To Facilitate Cellular Attachment and Proliferation. *ACS Appl. Bio Mater.* **2**, 2600–2609 (2019).
33. Moriyama, K., Minamihata, K., Wakabayashi, R., Goto, M. & Kamiya, N. Enzymatic preparation of streptavidin-immobilized hydrogel using a phenolated linear poly(ethylene glycol). *Biochem. Eng. J.* **76**, 37–42 (2013).
34. Yajima, Y., Yamada, M., Utoh, R. & Seki, M. Collagen Microparticle-Mediated 3D Cell Organization: A Facile Route to Bottom-up Engineering of Thick and Porous Tissues. *ACS Biomater. Sci. Eng.* **3**, 2144–2154 (2017).
35. Yamada, M. *et al.* Cell-sized condensed collagen microparticles for preparing microengineered composite spheroids of primary hepatocytes. *Lab Chip* **15**, 3941–3951 (2015).
36. Wongin, S., Viravaidya-Pasuwat, K., Chotiyarnwong, P., Waikakul, S. & Siriwatwechakul, W. Effect of Cell Sheet Manipulation Techniques on the Expression of Collagen Type II and Stress Fiber Formation in Human Chondrocyte Sheets. *Tissue Eng. Part A* **24**, 469–478 (2017).
37. Pollok, J. M., Ibarra, C. & Vacanti, J. P. A new method of xenotransplantation using autologous cartilage as an immunoisolation barrier for the transplantation of xenogeneic islets of Langerhans. *Transplant. Proc.* **29**, 909–911 (1997).
38. Jeong, I. L., Nishimura, R., Sakai, H., Sasaki, N. & Kenmochi, T. A newly developed immunoisolated bioartificial pancreas with cell sheet engineering. *Cell Transplant.* **17**, 51–59 (2008).
39. Liu, T. *et al.* Biomedical Applications of Layer-by-Layer Self-Assembly for Cell Encapsulation: Current Status and Future Perspectives. *Adv. Healthc. Mater.* **8**, 1–16 (2019).
40. Echeverria, C., Fernandes, S., Godinho, M., Borges, J. & Soares, P. Functional Stimuli-Responsive Gels: Hydrogels and Microgels. *Gels* **4**, 54 (2018).
41. Fu, X., Hosta-Rigau, L., Chandrawati, R. & Cui, J. Multi-Stimuli-Responsive Polymer Particles, Films, and Hydrogels for Drug Delivery. *Chem* **4**, 2084–2107 (2018).
42. Cao, Z. Q. & Wang, G. J. Multi-Stimuli-Responsive Polymer Materials: Particles,

Films, and Bulk Gels. *Chem. Rec.* **16**, 1398–1435 (2016).

43. Ramadhan, W., Kagawa, G., Moriyama, K. & Wakabayashi, R. Construction of higher-order cellular microstructures by a self- wrapping co-culture strategy using a redox-responsive hydrogel. *Sci. Rep.* 1–13 (2020) doi:10.1038/s41598-020-63362-4.
44. Moriyama, K., Minamihata, K., Wakabayashi, R., Goto, M. & Kamiya, N. Enzymatic preparation of a redox-responsive hydrogel for encapsulating and releasing living cells. *Chem. Commun.* **50**, 5895–5898 (2014).
45. Moriyama, K., Naito, S., Wakabayashi, R., Goto, M. & Kamiya, N. Enzymatically prepared redox-responsive hydrogels as potent matrices for hepatocellular carcinoma cell spheroid formation. *Biotechnol. J.* **11**, 1452–1460 (2016).
46. Matsusaki, M., Yoshida, H. & Akashi, M. The construction of 3D-engineered tissues composed of cells and extracellular matrices by hydrogel template approach. *Biomaterials* **28**, 2729–2737 (2007).
47. Åslund, F., Berndt, K. D. & Holmgren, A. Oxidoreductases of the thioredoxin superfamily determined by direct protein-protein redox equilibria. *J. Biol. Chem.* **272**, 30780–30786 (1997).
48. Sant, S. & Johnston, P. A. The production of 3D tumor spheroids for cancer drug discovery. *Drug Discov. Today Technol.* **23**, 27–36 (2017).
49. Folkman, J. & Hochberg, M. Self-regulation of growth in three dimensions. *J. Exp. Med.* **138**, 745–753 (1973).
50. Jain, R. K., Au, P., Tam, J., Duda, D. G. & Fukumura, D. Engineering vascularized tissue. *Nat. Biotechnol.* **23**, 821–823 (2005).
51. Baiguera, S. & Ribatti, D. Endothelialization approaches for viable engineered tissues. *Angiogenesis* **16**, 1–14 (2013).
52. Rosso, F., Giordano, A., Barbarisi, M. & Barbarisi, A. From Cell-ECM Interactions to Tissue Engineering. *J. Cell. Physiol.* **199**, 174–180 (2004).
53. Cui, X., Hartanto, Y. & Zhang, H. Advances in multicellular spheroids formation. *J. R. Soc. Interface* **14**, 20160877 (2017).
54. Roether, J., Bertels, S., Oelschlaeger, C., Bastmeyer, M. & Willenbacher, N. Microstructure, local viscoelasticity and cell culture suitability of 3D hybrid HA/collagen scaffolds. *PLoS One* **13**, 10–12 (2018).
55. Andrée, B. *et al.* Formation of three-dimensional tubular endothelial cell networks under defined serum-free cell culture conditions in human collagen hydrogels. *Sci.*

Rep. **9**, 1–11 (2019).

56. Anada, T. *et al.* Vascularized bone-mimetic hydrogel constructs by 3D bioprinting to promote osteogenesis and angiogenesis. *Int. J. Mol. Sci.* **20**, (2019).
57. Bezenah, J. R., Kong, Y. P. & Putnam, A. J. Evaluating the potential of endothelial cells derived from human induced pluripotent stem cells to form microvascular networks in 3D cultures. *Sci. Rep.* **8**, 1–14 (2018).
58. Pauty, J. *et al.* A Vascular Endothelial Growth Factor-Dependent Sprouting Angiogenesis Assay Based on an In Vitro Human Blood Vessel Model for the Study of Anti-Angiogenic Drugs. *EBioMedicine* **27**, 225–236 (2018).
59. Nishiguchi, A., Matsusaki, M., Asano, Y., Shimoda, H. & Akashi, M. Effects of angiogenic factors and 3D-microenvironments on vascularization within sandwich cultures. *Biomaterials* **35**, 4739–4748 (2014).
60. Ogoke, O., Oluwole, J. & Parashurama, N. Bioengineering considerations in liver regenerative medicine. *J. Biol. Eng.* **11**, 1–16 (2017).
61. Liu, Y., Li, H., Yan, S., Wei, J. & Li, X. Hepatocyte cocultures with endothelial cells and fibroblasts on micropatterned fibrous mats to promote liver-specific functions and capillary formation capabilities. *Biomacromolecules* **15**, 1044–1054 (2014).
62. Hui, E. E. & Bhatia, S. N. Micromechanical control of cell-cell interactions. *Proc. Natl. Acad. Sci.* **104**, 5722–5726 (2007).
63. Braet, F. & Wisse, E. Structural and functional aspects of liver sinusoidal endothelial cell fenestrae: a review. *Comp. Hepatol.* **1**, 1 (2002).
64. Strijbos, M. H. *et al.* Cells meeting our immunophenotypic criteria of endothelial cells are large platelets. *Cytom. Part B Clin. Cytom.* **72B**, 86–93 (2007).
65. Gomez-Lazaro, M. *et al.* Fibroblast-Endothelial Partners for Vascularization Strategies in Tissue Engineering. *Tissue Eng. Part A* **21**, 1055–1065 (2014).
66. Inamori, M., Mizumoto, H. & Kajiwara, T. An Approach for Formation of Vascularized Liver Tissue by Endothelial Cell–Covered Hepatocyte Spheroid Integration. *Tissue Eng. Part A* **15**, 2029–2037 (2009).
67. Patra, B. *et al.* Migration and vascular lumen formation of endothelial cells in cancer cell spheroids of various sizes. *Biomicrofluidics* **8**, 052109 (2014).
68. Vozzi, F., Heinrich, J.-M., Bader, A. & Ahluwalia, A. D. Connected Culture of Murine Hepatocytes and Human Umbilical Vein Endothelial Cells in a Multicompartmental Bioreactor. *Tissue Eng. Part A* **15**, 1291–1299 (2008).
69. Guzzardi, M. A., Vozzi, F. & Ahluwalia, A. D. Study of the Crosstalk Between

Hepatocytes and Endothelial Cells Using a Novel Multicompartmental Bioreactor: A Comparison Between Connected Cultures and Cocultures. *Tissue Eng. Part A* **15**, 3635–3644 (2009).

70. Moran, M. T., Carroll, W. M., Gorelov, A. & Rochev, Y. Intact endothelial cell sheet harvesting from thermoresponsive surfaces coated with cell adhesion promoters. *J. R. Soc. Interface* **4**, 1151–1157 (2007).
71. Sorrell, J. M., Baber, M. A. & Caplan, A. I. A self-assembled fibroblast-endothelial cell co-culture system that supports in vitro vasculogenesis by both human umbilical vein endothelial cells and human dermal microvascular endothelial cells. *Cells Tissues Organs* **186**, 157–168 (2007).
72. Madhavan, H. Simple Laboratory methods to measure cell proliferation using DNA synthesis property. *J. Stem Cells Regen. Med.* **3**, 12–4 (2007).
73. Wartenberg, M., Finkensieper, A., Hescheler, J. & Sauer, H. Confrontation Cultures of Embryonic Stem Cells With Multicellular Tumor Spheroids to Study Tumor-Induced Angiogenesis. in *Human Embryonic Stem Cell Protocols* vol. 35 313–328 (Humana Press, 2012).
74. De Ridder, L., Cornelissen, M. & De Ridder, D. Autologous spheroid culture: A screening tool for human brain tumour invasion. *Crit. Rev. Oncol. Hematol.* **36**, 107–122 (2000).
75. Choe, G., Park, J., Park, H. & Lee, J. Y. Hydrogel biomaterials for stem cell microencapsulation. *Polymers (Basel).* **10**, 1–17 (2018).
76. Skrzypek, K. *et al.* An important step towards a prevascularized islet macroencapsulation device—effect of micropatterned membranes on development of endothelial cell network. *J. Mater. Sci. Mater. Med.* **29**, (2018).
77. Wilson, J. L. & McDevitt, T. C. Stem cell microencapsulation for phenotypic control, bioprocessing, and transplantation. *Biotechnol. Bioeng.* **110**, 667–682 (2013).

CHAPTER 4 REDOX-RESPONSIVE FUNCTIONALIZED HYDROGEL MARBLE FOR THE GENERATION OF CELLULAR SPHEROIDS

4.1 Introduction

Liquid marbles (LMs) are tiny liquid droplets wrapped in and stabilized by hydrophobic microparticles with low surface tension that form a liquid–air interface[1,2]. LMs are a bioinspired concept that mimic the water droplets on a lotus leaf or the powdery wax marbles produced by aphids[3]. The valorization of LMs in biological applications is attracting more and more attention, especially for realizing miniaturized artificial milieus that are both complex and controllable[4–9]. LMs can be made with small volumes (e.g., microliter scale) and have key properties that enable the flexible adjustment of volume to achieve a desired density, allow them to easy to be formed, controlled, and moved, and prevent independent LMs from mixing with each other[10,11].

Since the pioneering work on developing LM compartments more than two decades ago[1], few studies have been done to optimize this system as a microbioreactor for three-dimensional (3D) cell culture. An important study by Arbatan and Shen[12], demonstrated the fabrication of cancer cell spheroids in LMs using a pearl drops system. Although the microenvironment of LMs allows gas exchange and cell growth, it is not clear that formation of spheroid has been achieved because of the free of cell–cell interactions or because of the gravitational sedimentation of cells in culture. Further, as they are in a liquid state, LMs may lose their spherical shape, dry out, or shrink[2,7,13,14] because of mass evaporation and changes in the humidity conditions, which is predicted to be unfavorable for long-term cell culture. Moreover, in this culture format, it is difficult to exchange the culture medium and more laborious to evaluate cell growth without breaking the hydrophobic shell[12]. One interesting approach to overcome these limitations of the LM culture system is to integrate a gel

constituent in the marble form, replacing the liquid state with a hydrogel sphere and removing the hydrophobic shell layer. These modifications are expected to improve the applicability of LM as a cell-culture platform.

Hydrogels[15] have been described in many different ways over the years, but they can be simply defined as a swollen network of polymer gels in which the solvent is water. They have attracted considerable attention from researchers due to their potential as dynamic materials that can support and embed cells[16] and even bioactive molecules[17,18]. Although hydrogels have proven to be practical in a range of cell culture platforms, our collective understanding of such applications is limited to two dimensional (2D) films, 3D free-swelling bulk gels comprising hydrogel and nanofibers, hydrogels in microplates, and injectable materials[19]. Yet, continuously adapting hydrogels into new platforms, such as LMs, may bridge the gap between the simplicity of conventional cell culture systems and the complexity of the biological extracellular matrix (ECM). Moreover, miniaturizing the cell culture system from bulk hydrogel to LMs also offers better compartmentalization, which may improve our understanding of how cells respond to modulating scaffold properties.

Herein, the potential to stabilize LMs by making them with a hydrogel i.e., creating a hydrogel marble (HM) are explored. The potential of HMs as a compartment for cancer cell spheroid formation is further exploited. An established redox-responsive hydrogelation system[20–23] as the base scaffold of the HM is employed (Fig. 4.1). Enzyme-mediated hydrogelation was used to promote disulfide crosslinking of tetra-thiol-modified polyethylene glycol (PEG-SH) with thiolated gelatin (Gela-SH) to facilitate spheroid formation in the HMs. The cell-laden scaffolds can then be degraded under reducing conditions to recover the spheroids. The cellular functions of the spheroids recovered from the HMs were compared with those of cells cultured in a

conventional hydrogel, LM, and 2D cell culture system. Herein, the compatibility of enzymatic hydrogelation to convert LMs to HMs with viable cells and characterize the flexible physical properties and redox-responsive chemical characteristics of the HMs, which is expected to lead to new avenues in the field of cellular spheroid research are experimentally evaluated.

4.2 Experimental

4.2.1 Materials

PTE-200 SH (Sunbright®) (4-arm PEG-$((CH_2)_2$-$SH)_4$, Mw 20 kDa) was purchased by the NOF Corporation (Tokyo, Japan). Gelatin type A and poly(tetrafluoroethylene) (PTFE; particle size: 1 μm) were supplied by Sigma-Aldrich (St Louis, MO, USA). Horseradish peroxidase (HRP; activity: 100 unit/mg) was supplied by Wako Pure Chemical Industries (Osaka, Japan). Glycyll-tyrosine hydrate (Gly-Tyr), L-cysteine (Cys), 1-ethyl-3-(3 dimethyl aminopropyl) carbodiimide (EDC), and squalene oil were acquired by Tokyo Chemical Industry (Tokyo, Japan). Cell Stain-Double Staining kit and 5,5′-dithiobis (2-nitrobenzoic acid) (DTNB) were supplied by Dojindo Laboratories (Kumamoto, Japan). Minimum Essential Medium (MEM) (1´) + GlutaMAX™-I, 10% fetal bovine serum (FBS), MEM Non-Essential Amino Acids (MEM-NEAA) solution, and nuclei stain (Hoechst 33342 and trypan blue, 0.4%) were supplied by Thermo Fisher Scientific (Waltham, MA, USA). Dulbecco's phosphate buffer saline (PBS), trypsin 0.25% with 1 mM EDTA, 1% antibiotic-antimycotic solution, and cystamine were purchased from Nacalai Tesque (Kyoto, Japan). The human albumin enzyme-linked immunosorbent assay (ELISA) quantitation kit and the urea quantification assay kit (DIUR-100, BAS) were supplied by Funakoshi (Tokyo, Japan). A commercial oil-blotting sheet was purchased from Mandom Corp. (Tokyo, Japan). Ultra-high-purity

water was used during the experiments (Milli-Q Integral MT3S.kit, Merck Milipore, Tokyo, Japan).

4.2.2 Fabrication and Hydrogelation of HM.

Gela-SH was prepared as described in the protocol outlined in our previous study[21,24]. A solution of 5% w/v 4-arm PEG-SH, 0-1% w/v Gela-SH, and 5 mM Gly-Tyr was prepared in PBS (1X, pH 7.4), and HRP was added at a concentration of 5 U/mL. Then, cells were added at the desired cell density to 20 µL of the mixed solution. The cell-laden solution was then dropped onto a PTFE powder bed in a 6-well plate (35-mm well diameter, Thermo Fisher Scientific K. K., Tokyo, Japan). The droplet was spread and rolled several times until the entire surface was covered with PTFE. The coated droplet was then transferred to a 96-well plate (Thermo Fisher Scientific K. K., Tokyo, Japan) containing 100 µL of MEM-NEAA and incubated for 6 h at 37 °C. After gelation, the resulting HMs were washed with squalene oil and PBS several times, then subsequently scrubbed with an oil-absorbing sheet to remove all hydrophobic components from the surfaces of the HMs. The HMs were then moved to a new 96-well plate and immersed in 150 µL of the MEM-NEAA medium for cell culture (Fig. 4.1).

4.2.3 Equilibrium swelling ratio (Q_M) and gel content.

The equilibrium swelling ratio (Q_M) and gel content were measured as described previously[22]. HMs (20 µL) were immersed in 10 mL of PBS and incubated at 37°C for two days to all them to reach equilibrium, and their mass was measured (M_s). The HMs were then dried, and the mass was measured again (M_D). Thus, Q_M was calculated as the ratio M_s/M_D. The gel content was evaluated by measuring the mass of the HMs after hydrogelation (W_P). The obtained HMs were subsequently immersed in MilliQ water (10 mL) for three days to remove the salts and uncrosslinked polymer.

The HMs were then dried, and their mass was measured (W_D). The gel content was calculated as $W_D / W_P \times 100\%$.

4.2.4 Gelation time.

The gelation time of the HMs was determined by the stirring magnet bar method[21]. The HM polymer solution (200 µL) was transferred to each well of a 48-well plate (Iwaki, Tokyo, Japan) and stirred at 200 rpm using magnetic stirrer bars (length: 7 mm; width: 3 mm). Solutions with different Gela-SH concentrations and constant concentrations of PEG-SH (5% w/v), Gly-Tyr (5 mM), and HRP (5 U/mL) were tested. The sol-gel transition time was determined as the time at which when the motion of the stirrer bar in the gel was hindered, and the sample appeared swollen; this time was recorded as the gelation time.

4.2.5 Rheological evaluation.

The rheological properties of the HMs, i.e., elastic modulus (G') and viscous modulus (G'') were assessed using a rheometer MCR302 (Anton Paar, Graz, Austria). A parallel plate (diameter: 25 mm; 2.003°) in oscillatory mode (EMS/TEK 500 disposable dishes) was set up, and the gel precursor solution was applied to it. Hydrogelation was induced by incubation at 37°C for 6 h before the measurement. The strain and frequency were set at 1% and 0.1Hz, respectively.

4.2.6 Cell lines and cell culture conditions.

The human hepatocellular carcinoma cell line (HepG2 cells, RCB1648) was obtained from the RIKEN Cell Bank (Tsukuba, Japan) and maintained as recommended. Briefly, HepG2 cells were cultured in MEM-NEAA supplemented with 10% FBS and 1% antibiotic-antimycotic. HepG2 cells were maintained in a humid atmosphere at 37 °C with 5% CO_2. The number of cells was counted with an automated cell counter (BioRad Laboratories, Inc., Hercules, CA, USA).

For HM encapsulation, 3000 or 6000 cells were added to 20 μL of the gel precursor solution. Then, cell-laden HMs were seeded in MEM-NEAA (200 μL) in a 96-well plate, with a single HM placed in each well. In case of the cell encapsulation using LMs, we followed a protocol described in a previous study [5]. Briefly, to culture cells in LMs, the cells were diluted at 6000 cells in MEM-NEAA, and the cell-containing MEM-NEAA (20 μL) was then dropped onto a PTFE powder bed in a 6-well plate. The droplet was rolled several times until the entire surface was covered with PTFE particles. The LMs were then transferred to a 96-well plate and submerged in 150 μL of MEM-NEAA medium in a humid atmosphere at 37 °C with 5% CO2. The medium was changed every 2–3 days over long-term culture. For the evaluation of cellular functions cultured in LMs, the hydrophobic PTFE layer was broken with a needle to release the spheroids.

4.2.7 Evaluation of cultured cells and spheroids.

To degrade the HMs, 100 μL of Cys solution (5 mM) was added to each HM well. The HepG2 spheroids were then harvested after incubation for 20 min and observed using a confocal laser scanning microscope (LSM700, Zeiss, Oberkochen, Germany). The spheroid size was evaluated by measuring more than 100 spheroids under the microscope and quantified by NIH ImageJ Software (Free software for Mac OS X, National Institutes of Health, Bethesda, MD, USA).

Live/dead staining was performed using a Cellstain Double Staining Kit (Dojindo Laboratories) to evaluate cell viability in the HMs. After 1 or 7 days of culture, the HMs containing HepG2 spheroids were washed with PBS and incubated in serum-free medium containing calcein-AM (2 μM) and propidium iodide (4 μM) for 15 min. Then, the live and dead cells within each spheroid were observed under a fluorescence microscope (BZ-9000, Keyence, Osaka, Japan). To visualize the spheroid distribution

in the HMs, HMs containing spheroids were stained with Hoechst 33342 from Thermo Fisher Scientific.

To evaluate the cell functions in the harvested spheroids, two metabolic markers (urea and albumin secretion) and the total dsDNA content were measured after 3, 12 and 30 days in culture. Supernatants of culture media at the predetermined days were collected, centrifuged at 1500 rpm for 10 minutes at 4 °C to remove cell debris and stored at −80 °C. The amount of urea and albumin secreted were determined by using the QuantiChrom™ Urea Assay Kit and Human Albumin ELISA Quantitation Kit, respectively. In parallel, harvested spheroids were treated with trypsin to disperse them into single cells and the number of cells was counted with an automated cell counter (BioRad Laboratories, Inc., Hercules, CA, USA). Amount of urea and albumin were normalized by 6000 of viable cells per day of cultivation (µg or ng/mL/day/6000 cells). The total DNA concentration of spheroids were determined using a Quant-iT™ Picogreen™ dsDNA assay kit (Invitrogen, Thermo Fisher Scientific). All quantification procedures were carried out according to the manufacturer's instructions.

4.2.8 Morphology analysis of hydrogel marbles.

Scanning electron microscopy (SEM) SU3500 (Hitachi High-Tech Coporation, Tokyo, Japan) was used to observe the morphology of freeze-dried HMs. Briefly, HMs were frozen rapidly in liquid nitrogen followed by wetting-off, then freeze dried. Cross-sections of freeze-dried HMs were observed using SEM imaging.

Scanning probe microscopy (SPM) was conducted to evaluate the original structures of the HMs in the gel (semi-wet) state. A 5-µL sample of the HM solution was placed onto mica (Nilaco Corp., Tokyo, Japan) and incubated for 6 h at 37°C to induce gelation. The mica was then rinsed with ultrapure water and dried under ambient conditions. SPM images of HM surfaces were captured using a Nanocute

(Hitachi High-Tech Science Corp., Japan) with a SI-DF3P2 microcantilever (Hitachi) in dynamic force mode. The pore size of the HMs in the dried and semi-wet (gel) states were measured using NIH ImageJ software.

4.2.9 Statistical test.

Statistical significance was evaluated by one-way analysis of variance (ANOVA) followed by Tukey's post hoc test using Graph Pad Prism 6 software. The significance levels were set at $p < 0.05$ (denoted by *), $p < 0.01$ (**), and $p < 0.001$ (***).

4.3 Results and Discussion

Many approaches have been proposed for the fabrication of 3D cellular spheroids[25–29]. Among them, hydrogels have been the most widely studied as 3D cell culture in the past decade as they enable biomimetic extracellular matrix[30]. Normally, the hydrogelation process requires hydrogen peroxide (H_2O_2) for HRP-catalyzed gelation. However, too much H_2O_2 may negatively impact the biological components in the hydrogel system[21]. Therefore, in previous studies, our group developed a novel enzyme-mediated hydrogelation system based on HRP enzymatic fabrication[31–34]. The technique utilizes phenol moieties to generate disulfide bonds without exogenous H_2O_2, yielding a redox-degradable hydrogel under physiological conditions. In another study, we demonstrated the use of this new enzymatic hydrogelation to fabricate a matrix for spheroid formation[31]. However, the size of the harvested spheroids was limited to about 60 μm in diameter after seven days in culture, which suggests that there was room for further optimization. Furthermore, one of the emerging trends in cell scaffold technology is the miniaturization of cell culture systems from bulk to tiny compartment systems. For this objective, LMs have been considered a useful and unique platform as a micro-bioreactor for many applications[5,6]. However, as previously

described, this system suffers from the evaporation phenomenon[13,14], which limits its application for cell culture.

To overcome the limitations of our previous PEG-based hydrogel system and the LM system in general, Gela-SH to the previous PEG-based hydrogel as a natural moiety to facilitate cellular spheroid formation is incorporated. I then implemented this new enzymatic hydrogelation system to replace the liquid phase in LMs in order to mitigate the evaporation problem and enhance their biophysical properties. This approach gave rise to novel HMs, which can be used as a unique cell culture platform.

4.3.1 Physicochemical properties of hydrogel marbles prepared by HRP catalysis under various Gela-SH concentrations

The physicochemical properties of HMs depend on the intrinsic properties of the polymer backbone. The HMs were prepared by incorporating four components (4-arm

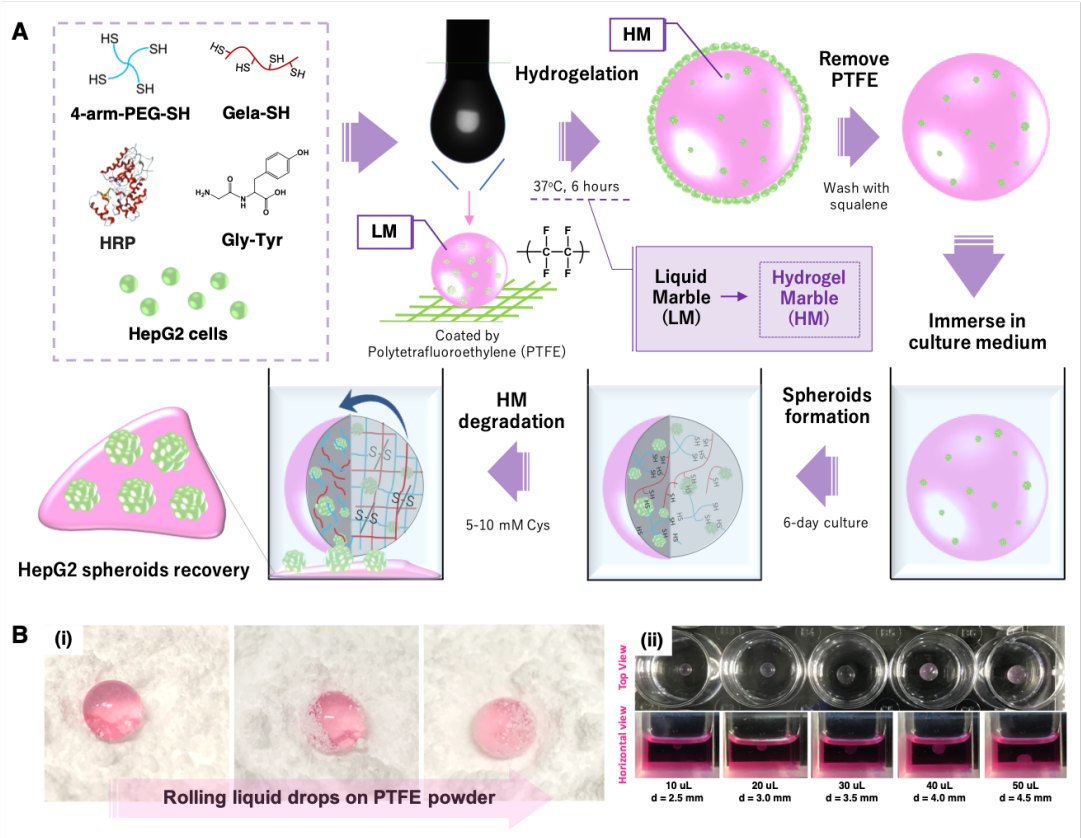

Fig. 4.1. Fabrication of three-dimensional cellular spheroids in disulfide-based redox-responsive cell-laden hydrogel marbles (HMs). (A). Schematic illustration of the preparation

of HMs by enzyme-mediated hydrogelation (B) (i) Photograph of a HM rotated in circular motions to coated it with PTFE in a powder bed, (ii) Top-view micrograph of HMs with different volume during the PTFE removal process using squalene oil and a horizontal-view micrograph of HMs with different volumes showing their floating behavior in the culture medium. Reproduce with permission from ref[35]. Copyright 2020 Elsevier.

PEG-SH, Gela-SH, HRP, and Gly-Tyr) for hydrogelation and covering a droplet of this solution in a superhydrophobic powder (Fig. 1A, Bi). The HMs can be produced with any desired volume between 10 and 50 μL (Fig. 1B-ii), which results in HMs with diameters around 2.5 to 4.5 mm, respectively. Drops with large volumes (50 μL) of aqueous polymer tended to form non-spherical HMs. Conversely, those prepared with a volume of 20 μL were easier to handle and exhibit appropriate volume to abridge the evaporation phenomena during hydrogelation process. Therefore, a 20-μL volume was determined as the optimal volume for the subsequent experiments.

The physicochemical properties of HMs were initially evaluated. The equilibrium swelling ratio and gelation time of the HM precursor solution decreased as the Gela-SH concentration increased (0–1% w/v) under the experimental conditions (Table 1).

Table 1. Equilibrium swelling ratio, gel content, gelation time, elastic and viscous moduli of hydrogel marble under various Gela-SH concentration.

Gela-SH concentration (% w/v)	Equilibrium swelling ratio (Q_M)	Gel content (%)	Gelation time (min)	Elastic modulus (G', Pa)	Viscous modulus (G'', Pa)
0	38.1 ± 2.7	84.2 ± 1.7	25.5 ± 2.1	2480	106
0.01	35.8 ± 0.8	86.1 ± 4.6	21.3 ± 1.8	2572	119
0.1	31.4 ± 1.3	89.3 ± 3.3	18.9 ± 1.5	2904	185
1	26.2 ± 0.3	94.6 ± 2.7	11.1 ± 2.3	3480	231

Data are presented as mean ± standard deviation (N = 3 for all parameters).
Reproduce with permission from ref[35]. Copyright 2020 Elsevier.

First, the influence of the Gela-SH concentration on the equilibrium swelling ratio (Q_M) of the obtained HMs was evaluated. Results showed that the Q_M decreased as the Gela-SH concentration increased from 0% to 1% w/v with a constant concentration of PEG-SH (5 % w/v) (Table 1). Theoretically, the Q_M of a polymer gel should decrease with increasing crosslinking density. The gel content was >84% for HMs prepared with 0%, 0.01%, and 0.1% w/v Gela-SH, and 94% for HMs fabricated with 1% w/v Gela-SH. This finding indicates that the PEG-SH underwent an acceptable crosslinking reaction with Gela-SH (Table 1). Results also showed that the gelation time for HMs at room temperature decreased with increasing Gela-SH concentration. The gelation time was about 14 min faster when the Gela-SH concentration was 1% w/v than in the absence of Gela-SH (Table 1). This change was attributed to the higher total polymer concentration, which decreased the water uptake. Sarker et al. reported that the gelation time of an alginate–gelatin crosslinked hydrogel decreased as the gelatin concentration increased[36]. Another report from Truong et al.[37] showed that the presence of gelatin-MA allows rapid crosslinking in hydrogels and reduces the gelation time. Our group previously reported that the rate of substitution for thiol groups in Gela-SH was approximately 0.39-0.50 mmol-SH/g-gelatin[24]. The presence of additional thiol groups contributes to the formation of a more highly crosslinked network, which improves the stability of the resulting hydrogel. Therefore, increasing the crosslinking density is expected to result in a higher gel content and shorter gelation time in HMs.

The elastic moduli (*G′)* and viscous moduli (*G″)* of the HMs were determined by rheological experiments. Results showed that *G′* and *G″* increased with increasing of Gela-SH concentration. *G′* and *G″* were 2480 and 106, respectively, when the Gela-SH concentration was 0% w/v. *G′* and *G″* increased to 3480 and 231, respectively, when the Gela-SH concentration was increased to 1% w/v. Importantly, the increase

in the Gela-SH concentration resulted in positive trends in the other physical properties, which indicates that almost all precursors were crosslinked without significant residual crosslinking.

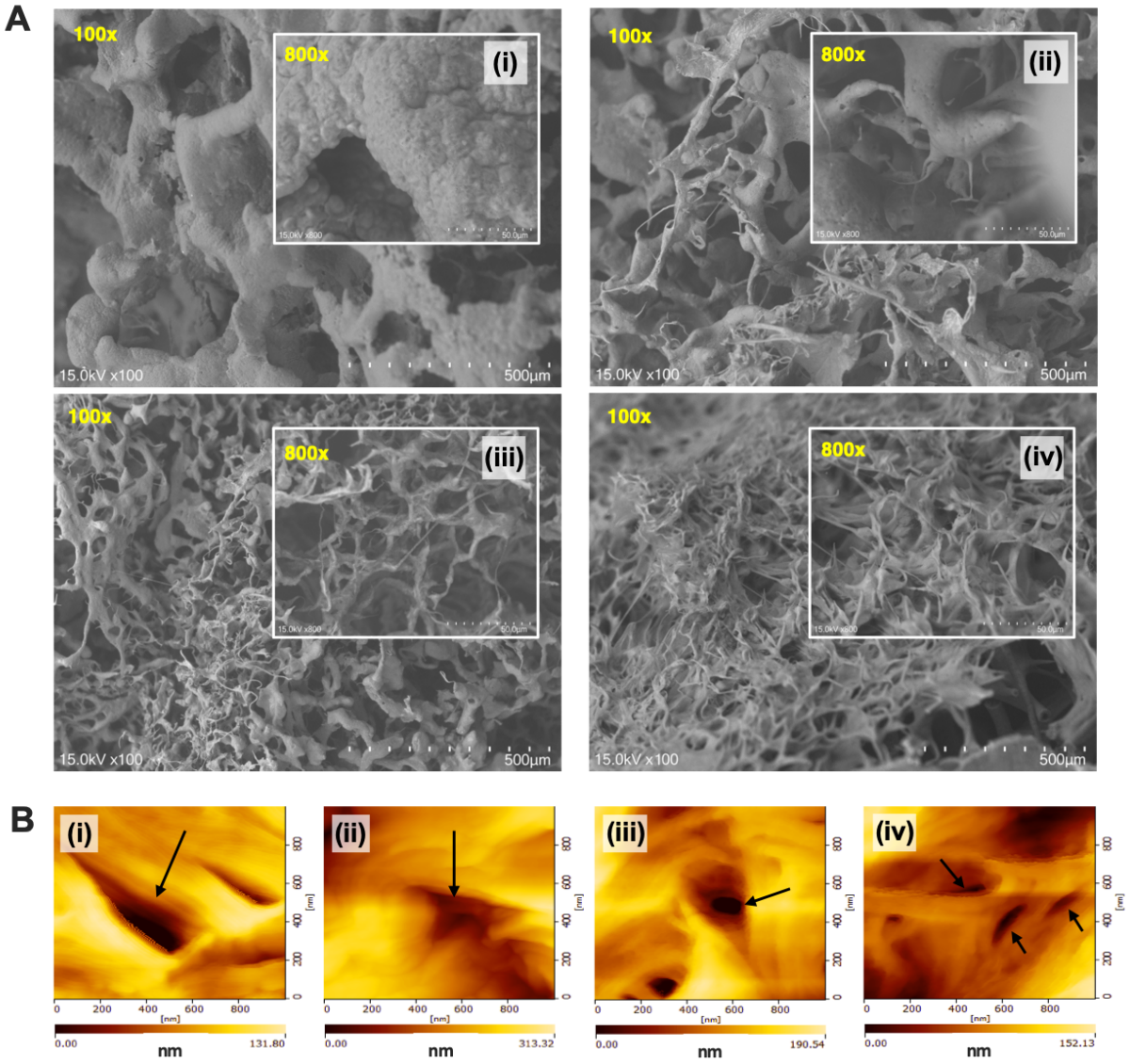

Fig. 4.2. Effects of thiolated gelatin (Gela-SH) inclusion on the microstructure of hydrogel marble (HM). (A). Scanning electron microscopy (SEM) images of the microstructures of HM sections and corresponding enlarged local images of HMs in the dried state (B). Scanning probe microscopy (SPM) images depicting phase of HM surface sections in the gel state. (i-iv) HMs prepared with 0% (i), 0.01% (ii), 0.1% (iii), and 1% Gela-SH (iv). Reproduce with permission from ref[35]. Copyright 2020 Elsevier.

The main consideration for culturing cells in HMs is the flexibility and degradability of the inside part of the hydrogel system, which promote cellular adhesion and proliferation. The main chain of the original system is polyoxyethylene,

and the PEG-SH induces little cellular adhesiveness and limited spheroid formation; the combination of these properties initially induces cell aggregation.

The microstructures of the freeze-dried HMs were observed by SEM, and the pore sizes of semi-wet HMs were observed by SPM (Fig. 4.2). The solid, thick structure of PEG-SH appears to influence the size of the cellular spheroids in culture. Interestingly, this microstructure network changed significantly with the inclusion of Gela-SH. As the Gela-SH concentration increased, the fibrous network appeared in the HM system (Fig. 4.2-A). The pore sizes of the HMs in the gel (semi-wet) state decreased by 4.8-fold (from *ca.* 330 to 70 nm) as the Gela-SH concentration was increased from 0% to 1% w/v. The difference in the HM pore sizes in the totally dried state was more significant: decreased from 180 to 28 μm or a 6.4-fold change between 0% and 1% w/v Gela-SH. It can be seen from the SEM and SPM images that more fibrous networks with smaller and thinner fibrils are formed as the Gela-SH concentration increases. This observation is consistent with the trend in the pore size of HMs in the semi-wet state with varying Gela-SH concentration (Fig. 4.2-B).

4.3.2 Formation and distribution of HepG2 cellular aggregates in hydrogel marbles

To demonstrate the feasibility of using HMs as a platform to generate cellular spheroids, HepG2 cells were encapsulated and cultured for 30 days in the HMs. HepG2 cells were mixed with the gel precursor solution, dropped onto the PTFE powder bed, and incubated to form the HMs. Immediately after encapsulation (12 h), single cells or aggregates of a few cells were observed to be distributed uniformly inside each HM. After 6 days in culture, spheroids had formed and were distributed in the HMs prepared with 5% PEG-SH and 0.1% Gela-SH (w/v), as observed using a microscope (Fig. 4.3-A).

The cellular spheroid size depends on the initial cell seeding density in the HM were further demonstrated. The 20 µL of HM containing two different initial cell seeding densities (either 3000 or 6000 cells). After 3 days of culture, the HepG2 spheroids were recovered by degrading the HM with Cys solution (5 mM) for 20 min.

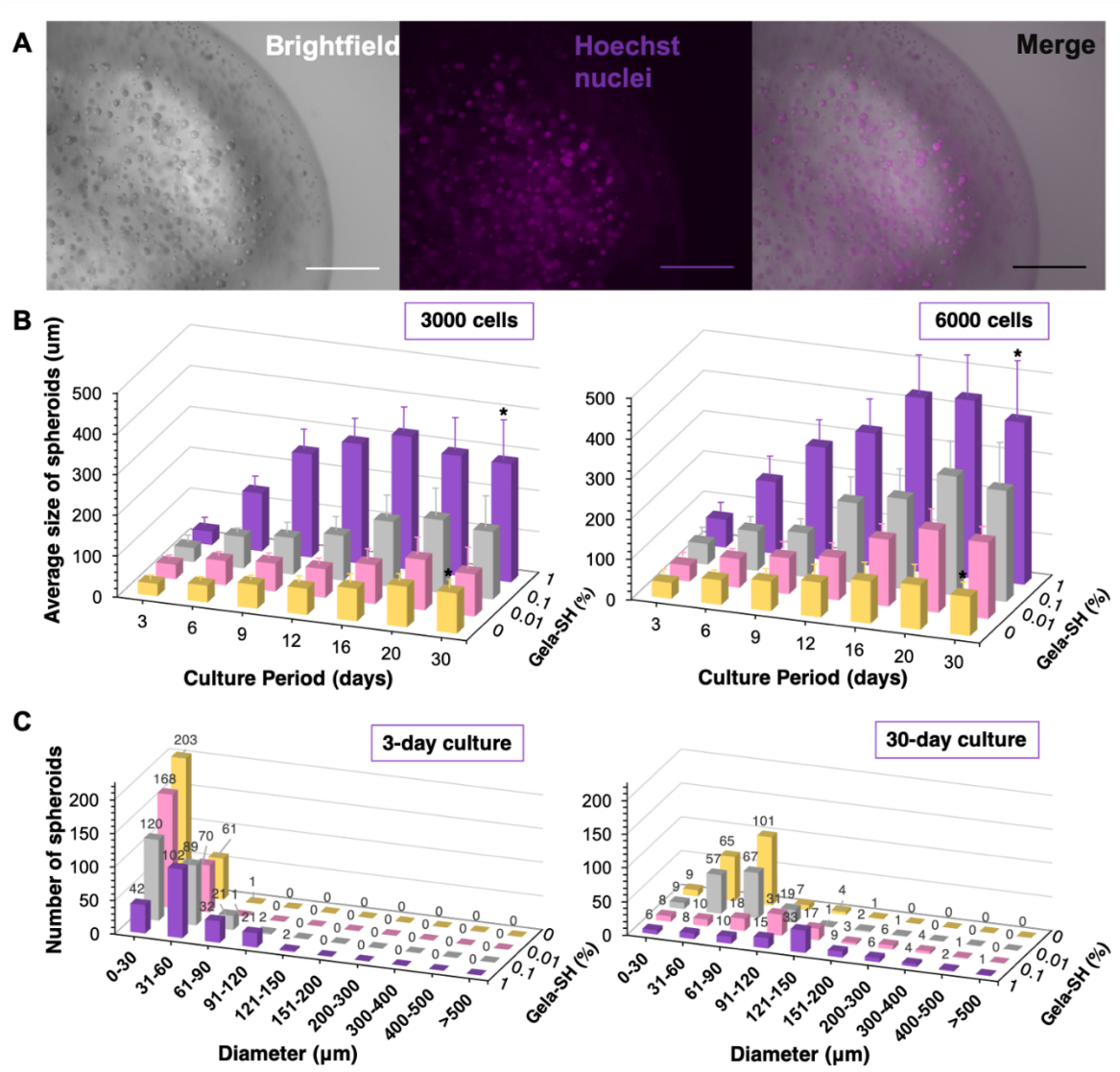

Fig. 4.3. Focal adhesions of HepG2 spheroids in a hydrogel marble (HM). (A) Representative images of spheroid formation and distribution in a HM with 0.1% w/v thiolated gelatin (Gela-SH) after 3 days in culture. The initial cell seeding density was 6000 cells per 20 µL. Images were taken at 4x magnification; scale bar: 500 µm. The nuclei of the HepG2 cells were stained with Hoechst 33342. The image in the right column were merged using the image analysis software BZ Analyzer associated with the Keyence BZ-9000 microscope. (B) Effects of cell seeding density and Gela-SH concentration on the sizes of the HepG2 spheroids in the HM. Error bars denote standard deviation (N = 100). * $p < 0.05$. (C) Effect of Gela-SH concentration on the HepG2 spheroid size distribution after 3 and 30 days in culture. Reproduce with permission from ref[35]. Copyright 2020 Elsevier.

The harvested spheroids were then transferred to another well and observed under a microscope. The spheroid size increased in the HMs containing 3000 cells as the Gela-SH concentration increased: the spheroid size was 41, 60, 76, and 141 μm in HMs with 0%, 0.01%, 0.1%, and 1% w/v Gela-SH, respectively. Conversely, the spheroids were larger in the HMs containing 6000 cells than in those containing 3000 cells: the spheroid size was 61, 71, 98, and 178 μm in HMs with 0%, 0.01%, 0.1%, to 1% w/v Gela-SH, respectively (Fig. 4.3-B). The spheroids were approximately 1.4-fold larger with an initial cell density of 6000 cells than with an initial cell density of 3000 cells after long-term culture (30 days) the HMs with 1% Gela-SH. Moreover, the spheroids were 3–4-fold larger in the presence of Gela-SH (1%) than in the absence of Gela-SH (Fig. 4.3-B) ($p < 0.05$). This result implies that the size of the resultant spheroids is significantly influenced by the Gela-SH concentration and concurrently strongly influenced by the initial cell density in the HMs. This fibrous network in HMs with Gela-SH may also have contributed to the formation of larger spheroids[38,39] which mimics the fibrous structure of the native ECM[40,41].

To evaluate the range of the obtained spheroid sizes from each HMs, the spheroid size distribution in HMs initially containing 6000 cells was evaluated between the early stage of culture (3 days) and (long-term culture) 30 days (Fig. 4.3-C). Early in the culture period (i.e., after 3 days), HMs with 1% Gela-SH formed significantly more spheroids of the size range of 31–60 μm. Conversely, HMs containing 0% of Gela-SH generated a high yield of spheroids in the size range of 0–30 μm. Furthermore, after 30 days in culture, the spheroids in HMs with 1% of Gela-SH were mostly in the range of 121–150 μm, while those in HMs without Gela-SH generated more spheroids in the range of 61–90 μm.

Seeding higher cell densities (6000 cell/20 µL) leads to more preaggregation of the cells, giving rise to larger spheroids (> 100 µm). This mechanism may be attributed to the network formation in HMs containing Gela-SH, where the disulfide chains of the fibrous network can be easily broken by HepG2 cells. Additionally, the presence of gelatin, which is a collagen derivative, may be degraded by matrix metalloproteinase (MMP), which is secreted from HepG2 cells[42]. MMP from glioblastoma cells has also been found to mediate the degradation of PEG-based hydrogel matrixes[43]. A study by Liang et al. described how the MMP enzyme regulates the softening of the matrix for hepatocarcinoma cells[44]. Results demonstrated that exposure to MMP-1 decreased the elastic modulus of a collagen hydrogel from 4.0 to 0.5 kPa.

It should be noted that the encapsulated cells in the HM proliferated to form spheroids, which require soft culture substrates. The elastic modulus of a healthy liver is about 1.5 kPa[45]. As the Gela-SH concentration increased, the elasticity and viscosity of the HMs increased. Over 30 days in culture, these rheological parameters dramatically decreased from about 2 to 0.4 kPa (Fig. 4.4).

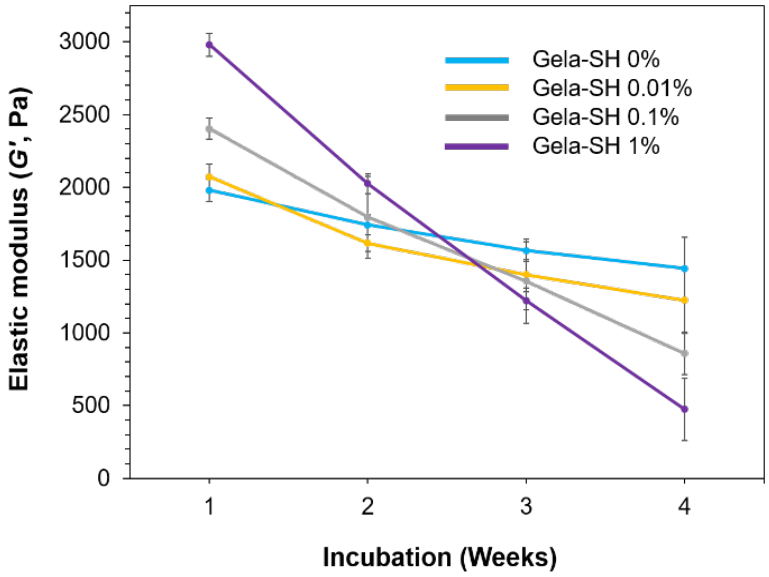

Fig. 4.4. Elastic modulus (*G'*) of hydrogel marble with various concentration of Gela-SH during the HepG2 culturing for 4 weeks of incubation. Reproduce with permission from ref[35]. Copyright 2020 Elsevier.

A similar trend was reported in previous studies, where gelatin inclusion in an injectable gelatin–hydroxyphenyl propionic acid hydrogel resulted in a decrease in the *G* value by 30% after 3 weeks[46].

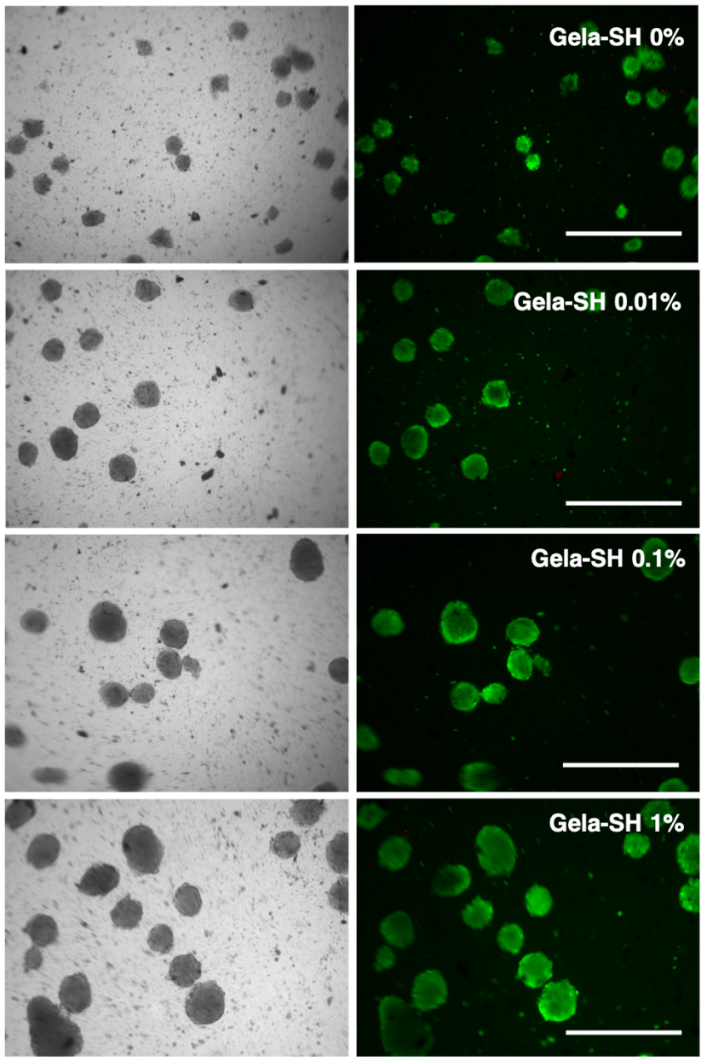

Fig. 4.5. Photomicrographs of HepG2 spheroids recovered from HMs. Evaluation of the HepG2 spheroid viability in HMs of different Gela-SH concentrations after 6 days in culture. Viable cells are stained with calcein-AM (green) and dead cells are stained red with propidium iodide (red). All images were captured using a Keyence BZ-9000 microscope. Scale bar: 500 μm. Reproduce with permission from ref[35]. Copyright 2020 Elsevier.

It is believed that spheroid formation in HMs is a response to changes in the functions of the cells themselves and the degradability of the HM during the culture period. Gelatin is similarly known as a natural component that contains RGD moieties, which facilitate cell binding[47]. Additionally, specific chemokine receptors expressed from the

surfaces of cancer cells are particularly adept at sensing protein derivatives and recognizing changes in the mechanical strain energy density[48].

Large multi-cellular aggregates are usually limited to 100–200 μm in size, and this limit was reached by the spheroids cultured in HMs with 1% Gela-SH after 6 days in culture (Fig. 4.3-B). To more clearly see the effect of Gela-SH concentration on the size of the formed spheroids, the cell viability was compared after 6 days in culture (Fig. 4.5). The HepG2 spheroids were harvested from the HMs by degrading the hydrogel using a Cys solution and stained with the Cell Stain double-staining viability kit. Most of the cells were stained with green fluorescence, indicating high viability of the HepG2 cells in the spheroids (Fig. 4.5).

4.3.3 Evaluation of cellular functions in HMs

Three important metrics of hepatic function—urea, albumin secretion, and DNA content—were measured as a general marker for the HepG2 metabolic activity *in vitro* after given culture times (3, 12 and 30 days) in different cell culture systems (the HM culture system versus the conventional hydrogel in 2D form, LM, and tissue culture plate methods to generate spheroids) (Fig. 4.6). The total amount of albumin production from HepG2 cells in HMs increased with the culture time. Additionally, the spheroids cultured in HMs exhibited increasing albumin secretion as the Gela-SH concentration increased (Fig. 6A). However, the spheroids in LMs showed much higher albumin production (0.84 ± 0.12 ng/mL/day/6000 cells) than the spheroids in other culture systems (0.1–0.6 ng/mL/day/6000 cells). Surprisingly, after 12 days in culture, the LMs shrunk, which resulted in a significant decrease in albumin secretion compared with the spheroids cultured in HMs. This finding indicates that the shrinking of LMs might have a negative effect on the spheroid culture. After 30 days in culture, all spheroids in the LMs were dead.

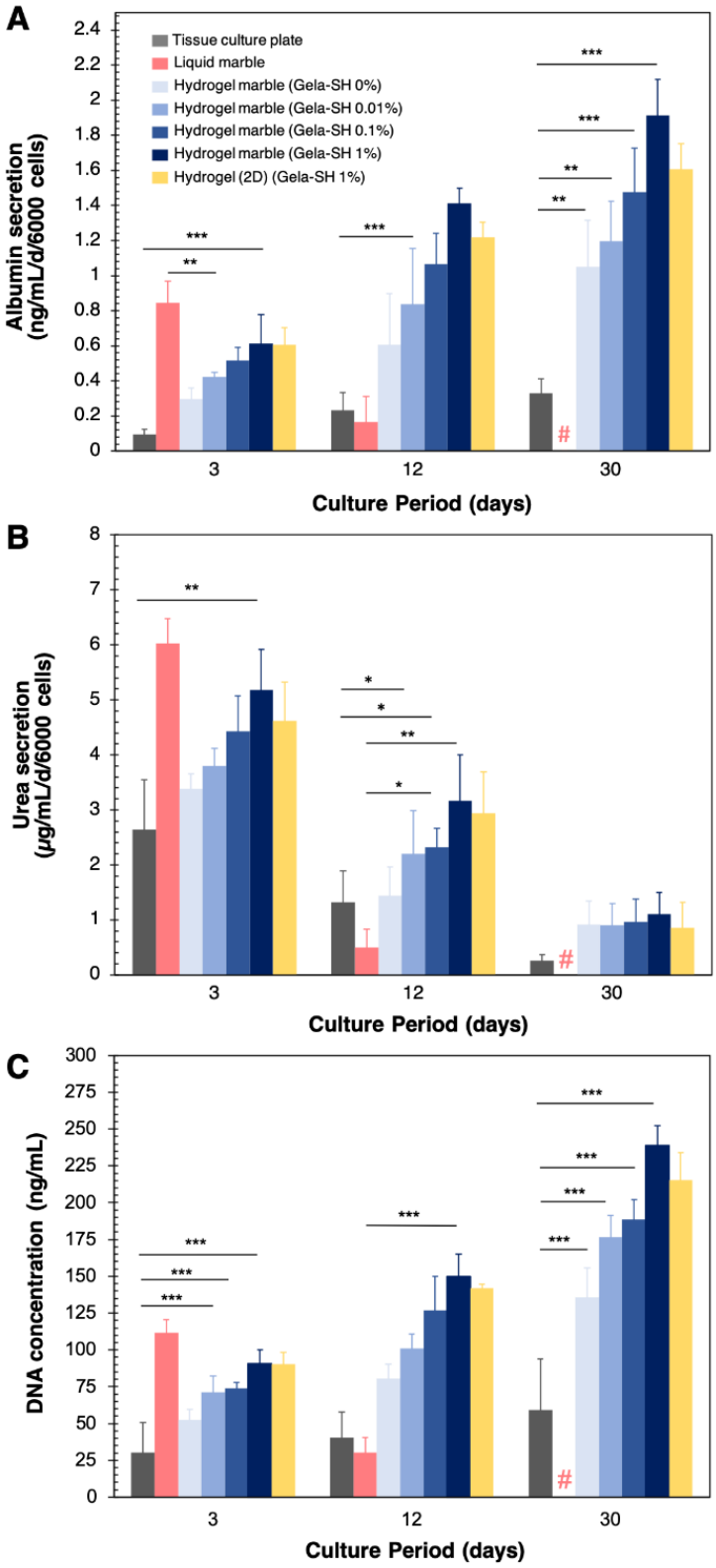

Fig. 4.6. Metabolism of harvested spheroids in different culture conditions. (A) Albumin, (B) urea and (C) total dsDNA content of harvested HepG2 spheroids after 3, 12, and 30 days in culture. The number sign (#) denotes the dead cells in the HM spheroids after 30 days in culture. The error bars denote the standard deviation (N = 3), *p < 0.05, **p < 0.01, and ***p < 0.001. Reproduce with permission from ref[35]. Copyright 2020 Elsevier.

Conversely, cells in the HMs containing Gela-SH exhibited higher albumin secretion (1.9 ± 0.2 ng/mL/day/6000 cells) than those in other cell culture formats ($p < 0.001$), including conventional hydrogels (1.6 ± 0.1 ng/mL/day/6000 cells).

The same results were observed in the urea secretion and DNA content. After 3 days in culture, the spheroids in the LM exhibited significantly increased urea (6.0 ± 0.5 μg/mL/day/6000 cells) and DNA (111.5 ± 9.2 ng/mL) levels compared with those in other cell culture formats, but the levels of cells function in LM dramatically decreased after 12 days in culture to 0.5 ± 0.3 μg/mL/d/6000 cells and 30.5 ± 10.2 ng/mL, respectively. Conversely, the spheroids in the HMs demonstrated better cellular functions over long-term culture than those the spheroids in other culture systems. Urea secretion increased as the Gela-SH concentration increased at 3 and 12 days in culture. However, after 30 days in culture, the urea secretion did not differ significantly between cell culture platforms. The total dsDNA content showed a similar increasing trend as the albumin content after 30 days in culture, where spheroids in HM exhibited highest DNA content (239 ± 13.2 ng/mL) that those DNA concentration from spheroids in other cell culture systems (59.3–215.1 ng/mL).

The spheroids obtained from the LM system showed higher levels of albumin production, urea secretion, and DNA content than spheroids cultured in other systems after 3 days in culture. However, the spheroids harvested from this system were largely non-uniform due to obvious gravitational effects leading to sedimentation of the cells. Subsequently, after 12 days in culture, the spheroids from the LMs showed significantly decreased cellular functions. These results could be attributed to the shrinking of the LM, which limited the permeation of nutrients and gases to the cells. Another possibility is that the close contact of cells with the hydrophobic shell at the air-liquid interface of LMs might cause the cell death (as observed after 30 days of cell

culture in LMs in Fig. 4.6). However, further studies are required to fully comprehend these phenomena.

Conversely, the spheroids obtained from HMs showed excellent performance in urea secretion, albumin and total DNA after 12 days in culture compared with other systems. In particular, the spheroids cultured in the HMs exhibited slightly higher cell functions than those in the traditional hydrogel system (Fig. 4.6). The spheroids cultured in the HM system also had more size uniformity compared with those cultured in conventional hydrogels (Fig. 4.7).

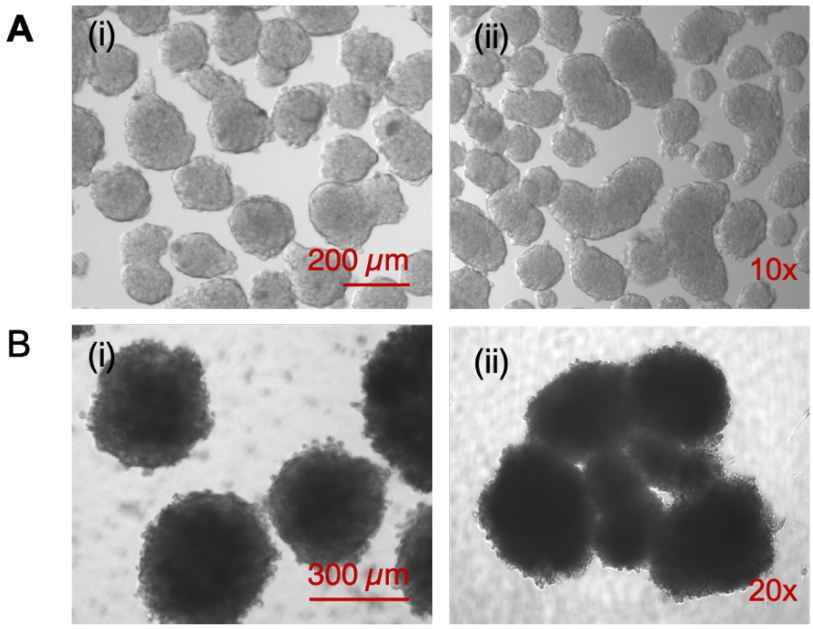

Fig. 4.7. Evaluation of the morphology of harvested HepG2 spheroids from hydrogel marble (i) and conventional hydrogel (ii) after six (A) and nine days (B) in culture. Reproduce with permission from ref[35]. Copyright 2020 Elsevier.

These results may be attributed to the gravitational effects, where the floating behavior and rotational movement of HMs readily expose them to the medium on all sides, allowing air to penetrate the spherical gel. From another viewpoint, the size of spheroids was 3–4-fold larger in the presence of Gela-SH (1%) than in the absence of Gela-SH, while the secretion of urea and albumin were also enhanced about 1.2–2.-fold and 1.8–2.3-fold during the culturing period, respectively (Fig. 4.8). The formation of larger HepG2 spheroids in HMs would also contribute to better cellular functions.

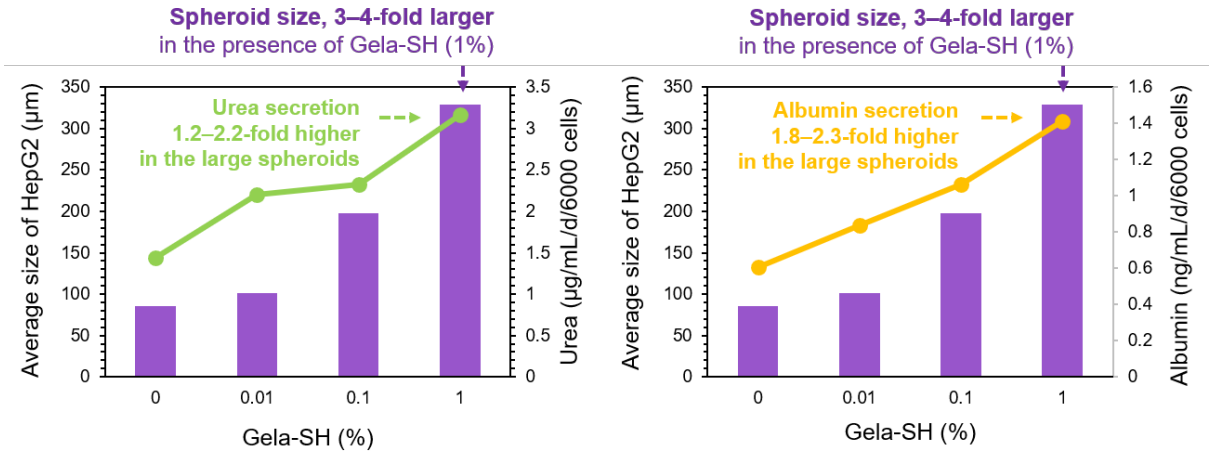

Fig. 4.8 Effect of Gela-SH concentration on the size of HepG2 spheroids and the secretion of urea (left) and albumin (right) after 12-day cell culture.

Conversely, in a conventional hydrogel culture system, as in all stationary culture systems, the flow of medium only occurs in the vertical direction. Thus, diffusion of nutrients, gasses, and waste accumulated within the hydrogel occurs more readily in the HM system than in the conventional hydrogel system. Importantly, our results imply that the physicochemical properties of HMs could affect to the spheroid metabolism during long-term cell culture. Moreover, HMs appear to provide a better microenvironment for cell culture than conventional hydrogels, LMs, and cell culture plates.

4.4 Conclusion

In summary, the enzymatic fabrication of redox-degradable HMs for the generation and culture of cellular spheroids was successfully demonstrated. Gela-SH can be introduced to impart more dynamic properties and facilitate the formation of a fibrous and viscoelastic network in the microstructure of the HMs. The Gela-SH inclusion influenced the size of the spheroids that were formed and did not affect the viability of the encapsulated cells. The results obtained here suggest that the redox-degradable HMs prepared by an HRP-catalyzed approach have potential use for more accurately

recreating the biochemical and biophysical signals of the complex biological milieu, especially as a new cell culture platform for the preparation of cellular spheroids.

4.5 References

1. Aussillous, P. & Quéré, D. Liquid marbles. *Nature* **411**, 924–927 (2001).
2. McHale, G. & Newton, M. I. Liquid marbles: Principles and applications. *Soft Matter* **7**, 5473–5481 (2011).
3. Kasahara, M. *et al.* Liquid Marbles in Nature: Craft of Aphids for Survival. *Langmuir* **35**, 6169–6178 (2019).
4. Vadivelu, R. K. *et al.* Generation of three-dimensional multiple spheroid model of olfactory ensheathing cells using floating liquid marbles. *Sci. Rep.* **5**, 1–12 (2015).
5. Vadivelu, R. K., Kamble, H., Munaz, A. & Nguyen, N. T. Liquid marbles as bioreactors for the study of three-dimensional cell interactions. *Biomed. Microdevices* **19**, 1–9 (2017).
6. Chen, M. *et al.* Naked Liquid Marbles: A Robust Three-Dimensional Low-Volume Cell-Culturing System. *ACS Appl. Mater. Interfaces* **11**, 9814–9823 (2019).
7. McHale, G. & Newton, M. I. Liquid marbles: Topical context within soft matter and recent progress. *Soft Matter* **11**, 2530–2546 (2015).
8. Kamiya, N., Ohama, Y., Minamihata, K., Wakabayashi, R. & Goto, M. Liquid Marbles as an Easy-to-Handle Compartment for Cell-Free Synthesis and In Situ Immobilization of Recombinant Proteins. *Biotechnol. J.* **13**, 1–5 (2018).
9. Sarvi, F. *et al.* Cardiogenesis of embryonic stem cells with liquid marble micro-bioreactor. *Adv. Healthc. Mater.* **4**, 77–86 (2015).
10. Tian, J., Fu, N., Chen, X. D. & Shen, W. Respirable liquid marble for the cultivation of microorganisms. *Colloids Surfaces B Biointerfaces* **106**, 187–190 (2013).
11. Oliveira, N. M., Reis, R. L. & Mano, J. F. The Potential of Liquid Marbles for Biomedical Applications: A Critical Review. *Adv. Healthc. Mater.* **6**, 1–15 (2017).
12. Arbatan, T. & Shen, W. Measurement of the surface tension of liquid marbles. *Langmuir* **27**, 12923–12929 (2011).
13. Sreejith, K. R., Ooi, C. H., Dao, D. V. & Nguyen, N. T. Evaporation dynamics of liquid marbles at elevated temperatures. *RSC Adv.* **8**, 15436–15443 (2018).
14. Vadivelu, R. K., Kamble, H., Munaz, A. & Nguyen, N. T. Liquid marble as bioreactor for engineering three-dimensional toroid tissues. *Sci. Rep.* **7**, 1–14 (2017).

15. Buwalda, S. J. *et al.* Hydrogels in a historical perspective: From simple networks to smart materials. *J. Control. Release* **190**, 254–273 (2014).

16. Caliari, S. R. & Burdick, J. A. A practical guide to hydrogels for cell culture. *Nat. Methods* **13**, 405–414 (2016).

17. Green, J. J. & Elisseeff, J. H. Mimicking biological functionality with polymers for biomedical applications. *Nature* **540**, 386–394 (2016).

18. Lee, S. C., Kwon, I. K. & Park, K. Hydrogels for delivery of bioactive agents: A historical perspective. *Adv. Drug Deliv. Rev.* **65**, 17–20 (2013).

19. Pertici, V. *et al.* Degradable and Injectable Hydrogel for Drug Delivery in Soft Tissues. *Biomacromolecules* **20**, 149–163 (2019).

20. Moriyama, K., Minamihata, K., Wakabayashi, R., Goto, M. & Kamiya, N. Enzymatic preparation of a redox-responsive hydrogel for encapsulating and releasing living cells. *Chem. Commun.* **50**, 5895–5898 (2014).

21. Moriyama, K., Wakabayashi, R., Goto, M. & Kamiya, N. Enzyme-mediated preparation of hydrogels composed of poly(ethylene glycol) and gelatin as cell culture platforms. *RSC Adv.* **5**, 3070–3073 (2015).

22. Moriyama, K., Naito, S., Wakabayashi, R., Goto, M. & Kamiya, N. Enzymatically prepared redox-responsive hydrogels as potent matrices for hepatocellular carcinoma cell spheroid formation. *Biotechnol. J.* **11**, 1452–1460 (2016).

23. Wakabayashi, R., Ramadhan, W., Moriyama, K., Goto, M. & Kamiya, N. Poly(ethylene glycol)-based biofunctional hydrogels mediated by peroxidase-catalyzed cross-linking reactions. *Polym. J.* (2020) doi:10.1038/s41428-020-0344-7.

24. Ramadhan, W. *et al.* Enzymatically Prepared Dual Functionalized Hydrogels with Gelatin and Heparin To Facilitate Cellular Attachment and Proliferation. *ACS Appl. Bio Mater.* **2**, 2600–2609 (2019).

25. Langhans, S. A. Three-dimensional in vitro cell culture models in drug discovery and drug repositioning. *Front. Pharmacol.* **9**, 1–14 (2018).

26. Sant, S. & Johnston, P. A. The production of 3D tumor spheroids for cancer drug discovery. *Drug Discov. Today Technol.* **23**, 27–36 (2017).

27. Yuan, H., Xing, K. & Hsu, H. Y. Trinity of three-dimensional (3D) scaffold, vibration, and 3D printing on cell culture application: A systematic review and indicating future direction. *Bioengineering* **5**, 1–21 (2018).

28. Mirbagheri, M. *et al.* Advanced cell culture platforms: a growing quest for emulating natural tissues. *Mater. Horizons* **6**, 45–71 (2019).

29. Shamir, E. R. & Ewald, A. J. Three-dimensional organotypic culture: Experimental models of mammalian biology and disease. *Nat. Rev. Mol. Cell Biol.* **15**, 647–664

(2014).

30. Tibbitt, M. W. & Anseth, K. S. Hydrogels as extracellular matrix mimics for 3D cell culture. *Biotechnol. Bioeng.* **103**, 655–663 (2009).

31. Moriyama, K., Naito, S., Wakabayashi, R., Goto, M. & Kamiya, N. Enzymatically prepared redox-responsive hydrogels as potent matrices for hepatocellular carcinoma cell spheroid formation. *Biotechnol. J.* **11**, 1452–1460 (2016).

32. Moriyama, K., Minamihata, K., Wakabayashi, R., Goto, M. & Kamiya, N. Enzymatic preparation of streptavidin-immobilized hydrogel using a phenolated linear poly(ethylene glycol). *Biochem. Eng. J.* **76**, 37–42 (2013).

33. Moriyama, K., Wakabayashi, R., Goto, M. & Kamiya, N. Characterization of enzymatically gellable, phenolated linear poly(ethylene glycol) with different molecular weights for encapsulating living cells. *Biochem. Eng. J.* **93**, 25–30 (2014).

34. Ramadhan, W., Kagawa, G., Moriyama, K. & Wakabayashi, R., Minamihata K., Goto, M., Kamiya, N. Construction of higher-order cellular microstructures by a self- wrapping co-culture strategy using a redox-responsive hydrogel. *Sci. Rep.* **10**, 1–13 (2020).

35. Ramadhan, W. Ohama, Y., Minamihata K., Moriyama, K., Wakabayashi, R., Goto, M., Kamiya, N. Redox-responsive functionalized hydrogel marble for the generation of cellular spheroids. *J. Biosci. Bioeng.* (2020). https://doi.org/10.1016/j.jbiosc.2020.05.010

36. Sarker, B. *et al.* Fabrication of alginate-gelatin crosslinked hydrogel microcapsules and evaluation of the microstructure and physico-chemical properties. *J. Mater. Chem. B* **2**, 1470–1482 (2014).

37. Truong, V. X., Hun, M. L., Li, F., Chidgey, A. P. & Forsythe, J. S. In situ -forming click-crosslinked gelatin based hydrogels for 3D culture of thymic epithelial cells. *Biomater. Sci.* **4**, 1123–1131 (2016).

38. Kaufman, G., Nunes, L., Eftimiades, A. & Tutak, W. Enhancing the three-dimensional structure of adherent gingival fibroblasts and spheroids via a fibrous protein-based hydrogel cover. *Cells Tissues Organs* **202**, 343–354 (2016).

39. Li, Y. & Kumacheva, E. Hydrogel microenvironments for cancer spheroid growth and drug screening. *Sci. Adv.* **4**, 1–11 (2018).

40. Gionet-Gonzales, M. A. & Leach, J. K. Engineering principles for guiding spheroid function in the regeneration of bone, cartilage, and skin. *Biomed. Mater.* **13**, 034109 (2018).

41. Park, K. M., Lewis, D. & Gerecht, S. Bioinspired Hydrogels to Engineer Cancer Microenvironments. *Annu. Rev. Biomed. Eng.* **19**, 109–133 (2017).

42. Ye, S., Boeter, J. W. B., Penning, L. C., Spee, B. & Schneeberger, K. Hydrogels

for liver tissue engineering. *Bioengineering* **6**, 1–30 (2019).

43. Wang, C., Tong, X., Jiang, X. & Yang, F. Effect of matrix metalloproteinase-mediated matrix degradation on glioblastoma cell behavior in 3D PEG-based hydrogels. *J. Biomed. Mater. Res. - Part A* **105**, 770–778 (2017).

44. Liang, Y. *et al.* Enzyme-Induced Matrix Softening Regulates Hepatocarcinoma Cancer Cell Phenotypes. *Macromol. Biosci.* **17**, 1–9 (2017).

45. Mueller, S. Liver stiffness: a novel parameter for the diagnosis of liver disease. *Hepatic Med. Evid. Res.* **2**, 49–67 (2010).

46. Wang, L. S., Chung, J. E. & Kurisawa, M. Controlling fibroblast proliferation with dimensionality-specific response by stiffness of injectable gelatin hydrogels. *J. Biomater. Sci. Polym. Ed.* **23**, 1793–1806 (2012).

47. Davidenko, N. *et al.* Evaluation of cell binding to collagen and gelatin: a study of the effect of 2D and 3D architecture and surface chemistry. *J. Mater. Sci. Mater. Med.* **29**, 39 (2018).

48. Chen, J., Weihs, D. & Vermolen, F. J. A model for cell migration in non-isotropic fibrin networks with an application to pancreatic tumor islets. *Biomech. Model. Mechanobiol.* **17**, 367–386 (2018).

CHAPTER 5. CONCLUSIONS

5.1 Summary

In the last several years, the challenge of mimicking cellular environment and scaffold design is widening. As one of the excellent class of materials or platform for the development of cellular scaffolds which can better mimic the natural life form, hydrogel serve biocompatibility and mild and tunable reaction conditions that could altered with desirable properties. Among the possible crosslinking reaction, enzymatic crosslinking especially horseradish peroxidase (HRP)-catalyzed has led to significant advancements in the fabrication of hydrogel. HRP offers cytocompatibility for the in situ and *in vitro* formation of hydrogels because of its fast and easy processability and reactivity toward a variety of substrates. Although the HRP would then widely employ in the variety range of substrate and polymer, PEG was selected as the most prominent synthetic polymer in the fabrication of biofunctional-HRP hydrogel.

In the viewpoint of cell cytocompatibility, this HRP hydrogelation system required the exogenous H_2O_2 as an oxidant. Evidently, the use of H_2O can be removed by the presence of thiol and the inclusion of thiol moieties in the hydrogelation system[1] as the requirement of environmental standard. HRP-mediated hydrogelation reactions using phenol and thiol showed much slower reaction kinetics toward thiolated substrates than toward phenolated substrates, while in the presence of phenolic small compounds as additives, cross-linking between thiolated polymers was promoted, leading to the formation of redox-responsive hydrogels without the aid of hydrogen peroxide. However, as described in Chapter 1, the main polymer of this system is synthetic polymers where it does not present inherent biochemical cues or binding sites for bioactive molecules especially for the cellular signaling. Herein, to increase performance of PEG hydrogel in this HRP-phenol based system, the development of

HRP-mediated hydrogelation for further functionalization with other biofunctional molecules, such as gelatin, heparin, and growth factors, was introduced as an approach to approximate the properties of the natural ECM. Moreover, the live cell sheets are not only success enables the rapid fabrication on redox responsive hydrogel but also it can be utilized to wrap another biological entity, resulting the complex and the heterogenous cellular structure. Last, the hydrogel system was employed to fabricate a compartmentalized spheroid bioreactor in the marble form.

In Chapter 2, biologically active artificial scaffolds for cell seeding are developed by mimicking extracellular matrices using synthetic materials. A feasible approach employing biocatalysts to integrate natural components, that is, gelatin and heparin, into a synthetic scaffold, namely a polyethylene glycol (PEG)-based hydrogel is developed. Initiation of horseradish peroxidase-mediated redox reaction enabled both hydrogel formation of tetra-thiolated PEG, via disulfide linkage and incorporation of chemically thiolated gelatin (Gela-SH) and heparin (Hepa-SH) into the polymeric network. I found that the compatibility of the type of gelatin with heparin was crucial for the hydrogelation process. Alkaline-treated gelatin exhibited superior performance over acid-treated gelatin to generate dual functionality in the resultant hydrogel originating from the two natural biopolymers. The Gela-SH/Hepa-SH dual functionalized PEG-based hydrogel supported both cellular attachment and binding of basic fibroblast growth factor (bFGF) under cell culture conditions, which increased the proliferation and phenotype transformation of NIH3T3 cells cultured on the hydrogel. Inclusion of bFGF and a commercial growth factor cocktail in hydrogel matrices effectively enhanced cell spreading and confluency of both NIH3T3 cells and HUVECs respectively, suggesting a potential method to design artificial scaffolds containing active growth factors.

In Chapter 3, a strategy for constructing three-dimensional (3D) cellular architectures comprising viable cells is presented. The strategy uses a redox-responsive hydrogel that degrades under mild reductive conditions, and a confluent monolayer of cells (i.e., cell sheet) cultured on the hydrogel surface peels off and self-folds to wrap other cells. As a proof-of-concept, the self-folding of fibroblast cell sheet was triggered by immersion in aqueous cysteine, and this folding process was controlled by the cysteine concentration. Such folding enabled the wrapping of human hepatocellular carcinoma (HepG2) spheroids, human umbilical vein endothelial cells and collagen beads, and this process improved cell viability, the secretion of metabolites and the proliferation rate of the HepG2 cells when compared with a two-dimensional culture under the same conditions. A key concept of this study is the ability to interact with other neighboring cells, providing a new, simple and fast method to generate higher-order cellular aggregates wherein different types of cellular components are added. The method of using a cell sheet to wrap another cellular aggregate the ‘cellular Furoshiki’ was designated. The simple self-wrapping Furoshiki technique provides an alternative approach to co-culture cells by microplate-based systems, especially for constructing heterogeneous 3D cellular microstructures.

Chapter 4 focused on the adaptation of HRP hydrogelation system to another shape so that it can be used for other applications is a necessary step to improve and advance the hydrogelation technique. In this context, the potential of our hydrogel system as a compartment for spheroid bioreactor is explored. Recently, liquid marbles (LMs) have shown a great promise as microbioreactors to construct self-supported aqueous compartments for chemical and biological reactions. However, the evaporation of the inner aqueous liquid core has limited their application, especially in studying cellular functions. Hydrogels are promising scaffolds that provide a spatial

environment suitable for three-dimensional cell culture. the fabrication of redox-responsive hydrogel marbles (HMs) as a three-dimensional cell culture platform was described. The HMs are prepared by introducing an aqueous mixture of a tetra-thiolated polyethylene glycol (PEG) derivative, thiolated gelatin (Gela-SH), horseradish peroxidase, a small phenolic compound, and human hepatocellular carcinoma cells (HepG2) to the inner aqueous phase of LMs. Eventually, HepG2 cells are encapsulated in the HMs then immersed in culture media, where they proliferate and form cellular spheroids. Experimental results show that the Gela-SH concentration strongly influences the physicochemical and microstructure properties of the HMs. After 6 days in culture, the spheroids were recovered from the HMs by degrading the scaffold, and examination showed that they had reached up to about 180 μm in diameter depending on the Gela-SH concentration, compared with 60 μm in conventional HMs without Gela-SH. After long-term culture (over 12 days), the liver-specific functions (secretion of albumin and urea) and DNA contents of the spheroids cultured in the HMs were elevated compared with those cultured in LMs. These results suggest that the developed HMs can be useful in designing a variety of microbioreactors for tissue engineering applications.

5.2 Future prospects

Future studies should assess the efficacy of the cell sheet system for other therapeutic human cells as regenerative medicine models. While, although the main focus and the initial goal of this cellular Furoshiki is to investigate the potential of a confluent cell monolayer in a self-wrapping co-culture technique, a possible application of this technique either in the development of *in vitro* disease model for the drug screening application and or the tissue engineering for the prevention of the rejection of immunosuppression in transplantation is envisioned. Future challenges

include the design of tissue-like structures by integration of the cellular Furoshiki presented herein with other cell lines toward practical applications in biomedical fields. Notably, induced pluripotent stem cells (iPSCs), or mesenchymal stem cells as the main cell for the cellular Furoshiki system may represent an ideal condition to generate organoid model for the application in tissue engineering field.

Last, the HRP-mediated hydrogelation also was employed and succeeded to fabricate a compartmentalized or smaller compartment namely hydrogel marble for spheroid bioreactor. Future plans would be utilization of the hydrogel marble as a small compartment in the cryopreservation of multicellular spheroids.

In addition, the hydrogel state generated by the present HRP-mediated system are not limited to use in the bulk gel system but can be incorporated into a variety of biomedical application and integrated with advanced instruments for cultivation, screening and delivery of biofunctional molecules, as well as with diagnostic and therapeutic materials.

ACKNOWLEDGEMENTS

Firstly, I would like to express my utmost gratitude to my supervisor Prof. Noriho Kamiya, for his guidance and support throughout PhD course in Kyushu University, particularly for his inexhaustible drive in improving my life through science in chemical system and engineering. Under his mentorship, I have learned the good and the systematic approaches for doing the experiment and writing a scientific article. What's more, his earnest attitude and modest character concurrently along with humble and wise personality have deeply impressed me and given me a lot of great influence. Then, I also would like to thank Prof. Masahiro Goto, who served as my co-advisor and thesis committee, for his encouragement and continuous support throughout PhD course and for invaluable advice and suggestion during the lab meetings and on my PhD thesis. I am extremely proud and fortunate to become a member of the Goto-Kamiya (GK) Lab. I also would like to express my deep appreciation and gratitude to Prof. Satoru Kidoaki for become to be one of my PhD thesis committee. I really appreciate for his advice and constructive comment on my PhD thesis.

I am indebted to many people who have contributed to my completion in Kyushu University. I gratefully acknowledge Assistant Prof. Kosuke Moriyama from National Institute of Technology, Sasebo, Nagasaki and Genki Kagawa as a former member of GK lab, my nice tutor and 'senpai' who introducing me the hydrogel experiments. I also thank to another GK lab. member who always teaching me the technical knowledge of instrument in campus, Yuki Ohama, Komada Takuya, Kozaka, Hiroki Obayashi, Hamada, Sato Ryo, Imatani Rino, Hanada, and all members that I cannot mention in here. Without their expertise and support, this work would not have been possible.

I would like also to thank Assistant Prof. Rie Wakabayashi for helping me in many aspects of my research. Thank you for involves me in many aspects during my PhD course such as contributing the managerial aspect in laboratory, guiding a new student in their research as well as inviting me to write a focus review paper in the last year of my study. From your dedication to keep working hard, despite the hard time for taking care of family, inspires me to work harder and do better in my study. I would like to thank to Assistant Prof. Kosuke Minamihata for always giving me a brilliant idea, as a good learner he motivated me to learn many aspects in the bioengineering field. I would also to thank with Assistant Prof. Fukiko Kubota for her help and advice throughout my study in Kyushu

University. Also, I would thank to all staffs GK Lab for their kindness and help in many moments during my study in Kyushu University.

I would like to appreciate the support from the Support Center of Faculty of Engineering, particularly to Mrs. Yasura Oiwa and Mrs Chiem. I gratefully acknowledge the financial support provided by the Ministry of Education, Cultures, Sports, Science and Technology (MEXT) of Japan scholarship. Special thank also goes to Assoc. Prof. Uju for introducing the GK lab, as well as my former supervisor; Prof. Joko Santoso, Assoc. Prof. Wini Trilaksani and Assoc. Prof. Winarti Zahiruddin and all staffs in Department of Aquatic Product Technology, for their support towards my academic career in IPB University, Indonesia

I am grateful to Indonesian GK lab members (Dr. Alif Razi, Dr. Safrina Hardiningtyas, Dr. Lutfi Firmansyah, Dr. Patmawati, Dani Permana, Jessica, Adroit, Pugoh, and Ghazy) for their help and support and our togetherness. Thank for all international lab mates (Ms. Czarina D.R. Rodriguez, Dr. Qingliang Kong, Dr. Md. Moshikur Rahman, Dr. C. Md Raihan, Mr. Md Rafiqul Islam, Mr. Ali Md Korban, Mr. Uddin Shihab, Mr. Islam MD Shimul, Ms. Nguyen Minh Thi Hong, Mrs. Maha M. Sharaf, Ms. Xiao Wei, Ms. Jiang Shuhan, and others) for their help, friendship, and pleasant moments. I would like also to appreciate PPIF – BSOB for their excellent support and togetherness during my stay in Fukuoka.

I would like to thank my family, my father, my mother, my brothers and sisters also my father-in-law and my mother-in-law for their unconditional love and support. Especially, I am truly grateful to my wife, Lia Astriani for her unconditional love and support. I am immensely grateful for her devotion and sacrifices in parenting our two children, Ahsan Sabiq Abhipraya and Aratarei Dzikra Abhinaya during my long absence in the normal daily life. They have been my best supporters and partners in every aspect of my life. To you all, I dedicate this thesis. Lastly, Alhamdulillah I praise and thank to the Almighty God Allah SWT for guiding and giving me strength to complete this study, without his blessing this work would not have been possible.

Wahyu Ramadhan, Fukuoka, 11 July 2020